NUREG/CR-3638
SAND84-0060
R3
Printed February 1985

Hydrogen-Steam Jet-Flame Facility and Experiments

Joseph E. Shepherd

Prepared by
Sandia National Laboratories
Albuquerque, New Mexico 87185 and Livermore, California 94550
for the United States Department of Energy
under Contract DE-AC04-76DP00789

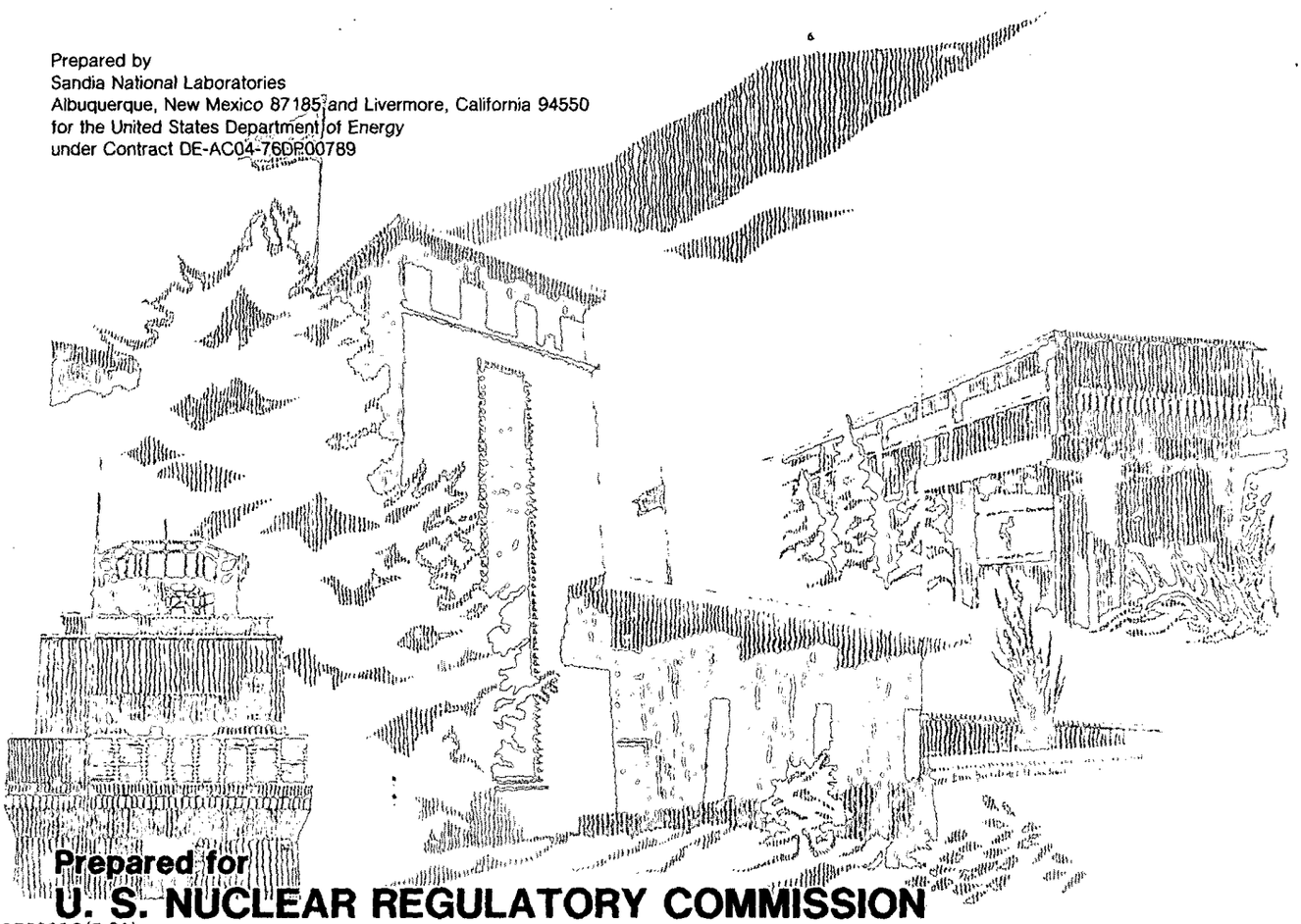

Prepared for
U. S. NUCLEAR REGULATORY COMMISSION

SF2900Q(8-81)

Available from

GPO Sales Program
Division of Technical Information and Document Control
U.S. Nuclear Regulatory Commission
Washington, D.C. 20555

and

National Technical Information Service
Springfield, Virginia 22161

NUREG/CR-3638
SAND84-0060
R-3

Hydrogen-Steam Jet-Flame Facility and Experiments

Joseph E. Shepherd

October 1984

Sandia National Laboratories
Albuquerque, New Mexico 87185
Operated by
Sandia Corporation
for the
U. S. Department of Energy

Prepared for
Division of Engineering Technology
and
Division of Accident Evaluation
Office of Nuclear Regulatory Research
U. S. Nuclear Regulatory Commission
Washington, DC 20555
Under Memorandum of Understanding DOE-40-550-75
NRC Fin Nos. A1246, A1336

Abstract

This report provides results from an in-depth analysis of twenty-one of the twenty-four premixed large-scale combustion experiments sponsored by the U. S. Nuclear Regulatory Commission (NRC) and the Electric Power Research Institute (EPRI) and conducted by EG&G at the Nevada Test Site (NTS). These experiments were performed in a 2048 cubic meter spherical vessel (hydrogen dewar) with mixtures of hydrogen, steam, and air ignited by glow plugs or heated resistance coils. Hydrogen concentrations ranged from 5 to 13% (by volume) and steam concentrations from 4 to 40%. Several tests also incorporated spray systems and/or fans which enhanced the combustion rate and significantly altered the postcombustion gas cooling.

In this work, data provided by EPRI from instrumentation designed to characterize the thermal environment in the dewar during and following combustion have been evaluated. The data reduction package SMOKE has been used to process data from thin-film gauges, Gardon and Schmidt-Boelter heat flux gauges, capacitance calorimeters, gas and wall thermocouples, and pressure sensors. Local measurements of the heat transfer are provided from the calorimetry, and global averages are inferred from the pressure. Instrumentation "goodness" for each test is assessed based on the raw data and on comparisons of local and global results. Graphical and tabular results are provided for each test, and trends observed from the results are reported. This information should be useful for benchmarking existing computer codes used in modeling nuclear containment and associated safety-related equipment response to degraded-core accidents and for improving combustion and heat transfer models currently used in these computer simulations.

Contents

List of Figures

List of Tables

Tables in Appendix A

Acknowledgments

O. B. Crump, Jr. (SNLA) was responsible for constructing the apparatus and performing many of the experiments described in this document. M. Berman (SNLA) and J. C. Cummings (SNLA) were the project leaders at Sandia. The NRC project managers were J. Larkins and P. Worthington. Many Sandians contributed to the success of the experimental effort, particularly the staff of the laboratory shops. Credit for the excellent text formatting is due to B. Fredlund and TEX.

Nomenclature

Symbols

A	Dewar surface area	[m^2]
C_v	Gas specific heat at constant volume	[J/kg-K]
F_c	Correction factor for sapphire (Eq.(3))	
P	Gas pressure	[kPa]
q	Heat flux	[W/cm^2]
Q	Energy deposition	[J/cm^2]
R	Gas constant	[kPa-m^3/kg-K]
t	Time	[s]
Δt	Time interval	[s]
T	Temperature	[K]
$T_{1/2}$	Temperature threshold = $(T_m + T_0)/2$	[K]
V	Dewar volume	[m^3]
x	Depth into dewar wall	[m]

Greek

α_g	Gas absorptance	
α_w	Dewar wall thermal diffusivity	[m^2/s]
ϵ	Emittance	
ρ	Gas density	[kg/m^3]
σ	Stefan-Boltzmann constant	[W/m^2-K^4]
τ	Transmittance	

Subscripts

all	Pertaining to the entire test
AIC	Pertaining to adiabatic isochoric combustion
c	Sapphire cover
C	Convective component
g	Gas
m	Maximum condition
mp	Pertaining to time interval between time of peak pressure and time of the measured maximum
off	Baseline value
P	Pertaining to peak pressure
ref	Reference condition
R	Radiative component
RU	Uncorrected radiative component
q_T	Pertaining to time of pressure-inferred peak total flux
T	Total
$T_{1/2}$	Pertaining to the temperature threshold
w	Dewar wall
0	Initial precombustion condition

1 Introduction

A large portion of the recent research on hydrogen combustion[1] during degraded core accidents in light-water reactors has focused on volume combustion in a premixed hydrogen-air-steam atmosphere within the reactor containment. The primary threat to containment integrity in that case is due to overpressurization. However, another serious problem may be the formation of diffusion flames at the point-of-release of the hydrogen-steam mixture into the containment. The jet of steam and hydrogen will entrain and mix with the containment atmosphere, and possibly burn as a turbulent diffusion flame. The ignition source could be accidental (arcing switch contacts) or deliberate (glow plugs), and, if the jet mixture is hot enough, spontaneous ignition could occur (autoignition). The primary threat from diffusion flame combustion will be the high thermal loads imposed by the flame on safety-related equipment.

In this report we do not attempt to determine scenarios under which flame jets will exist during light-water reactor accidents or discuss the probability of such accident sequences. Accepting that such flame jets are a possibility, our goal has been to investigate the physical characteristics of these flames and attempt to determine the controlling parameters. To this end, we have constructed a small-scale facility to study the combustion of high-temperature hydrogen-steam jets in air.

The present report is primarily a discussion of that facility and the experiments carried out in it. These include studies of autoignition, flame stability, flame-length dependence on jet mixture, and heat transfer to various objects placed within or above the flame. These results are specific to the steam-hydrogen-air system, but whenever possible, we have tried to show how they are related to generally accepted ideas in combustion science.

Burning steam-hydrogen jets may not only originate from accidentally-ignited breaks or stuck-open valves, but also from deliberately-ignited, controlled releases from the primary system to the containment. Intentional burning from a known location, *i.e.*, a high-point vent, could be used to rid the primary system of accident-produced hydrogen in a controlled way. This has been termed "deliberate flaring" in analogy to the common practice in the chemical processing industry of flaring unwanted combustible by-products. The problems associated with and the practicability of deliberate flaring are discussed in the last section of this report.

The remainder of this introductory chapter is devoted to giving an overview of the combustion science and fluid mechanics of jets and diffusion flames. This material will serve as a background for much of the discussion in the rest of the report. Chapter 2 is a discussion of the experimental facility and its instrumentation. Chapter 3 is a discussion of our experiments and the current theoretical understanding of flame-length scaling and stability. Chapter 4 is a discussion of our experiments and analyses on heat transfer from hydrogen-air-diluent flames. Chapter 5 presents our conclusions on the threat of diffusion flames and proposed direction for future research. The problem of deliberate flaring is discussed and possible engineering solutions for the removal of combustion-generated heat are proposed.

1.1 Jets, Plumes, and Diffusion Flames

Jets, plumes, and diffusion flames all have a number of common features which are relevant to the present discussion. The character of a diffusion flame will be determined by the basic flow field, which will be either a jet or a plume. We distinguish between jets and plumes on the basis of the role of buoyancy in the flow. In jet-like flows, any buoyancy-induced momentum is dominated by the initial momentum of the jet. In plume-like flows, the initial momentum is negligible compared to that induced by buoyancy.

Accidental releases (*e.g.*, stuck-open relief valves) from Pressurized-Water Reactors (PWRs) will probably occur through small diameter openings (2-10 cm). These will result in momentum-dominated jets of hydrogen and steam, driven initially by very high pressure (1000-2000 psia), and expanding into a containment at or near atmospheric pressure. A typical calculation[†] of the steam and hydrogen flow rates and reactor vessel pressure during the course of an accident is shown in Figures 1-1, 1-2, and 1-3. Note the large ratio of steam to hydrogen flow rates for the majority of the flow.

These jets have a rich structure which includes supersonic flow, shock waves and mixing layers between streams of disparate density. For large volume fractions of steam, the flow will have condensed water present in some portions, introducing the additional complexity of two-phase flow.

[†]This calculation was done by Eric Haskins of SNLA using the MARCH code with a Watts Bar configuration for an S_2D break scenario. Break size was 5 cm diameter for the case shown.

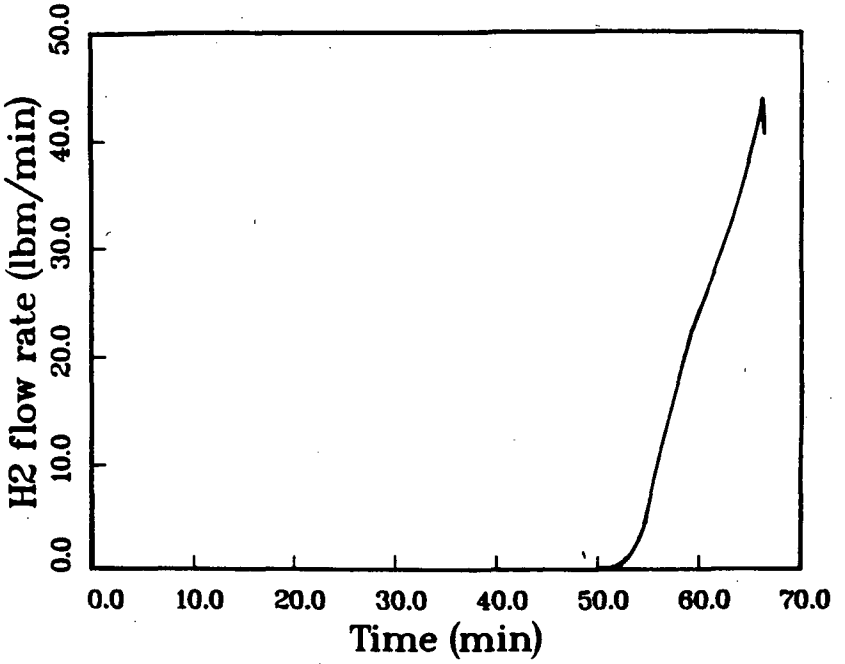

Figure 1-1. Hydrogen mass flow rate from an S_2D break in an Ice Condenser reactor.

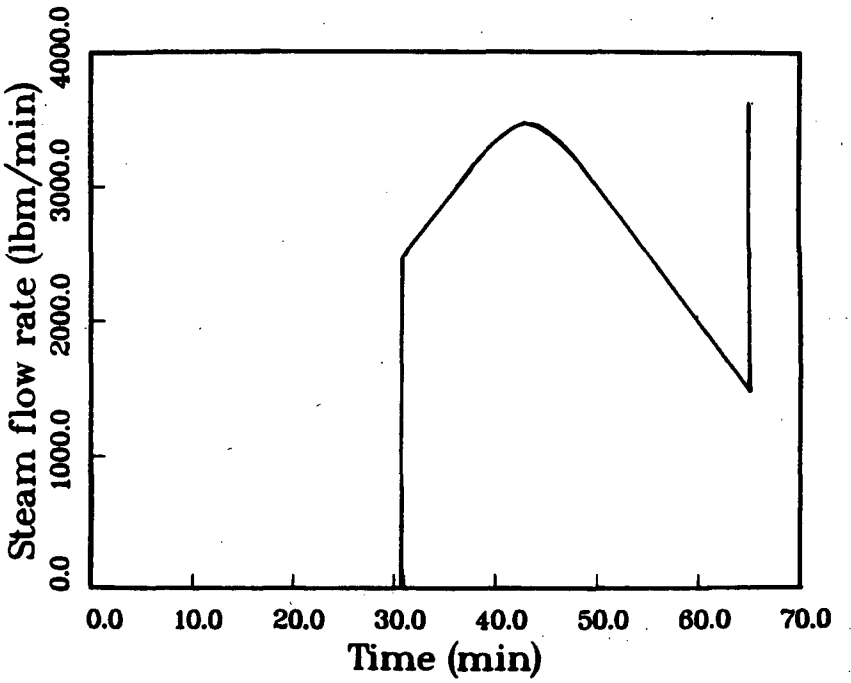

Figure 1-2. Steam mass flow rate from an S_2D break in an Ice Condenser reactor.

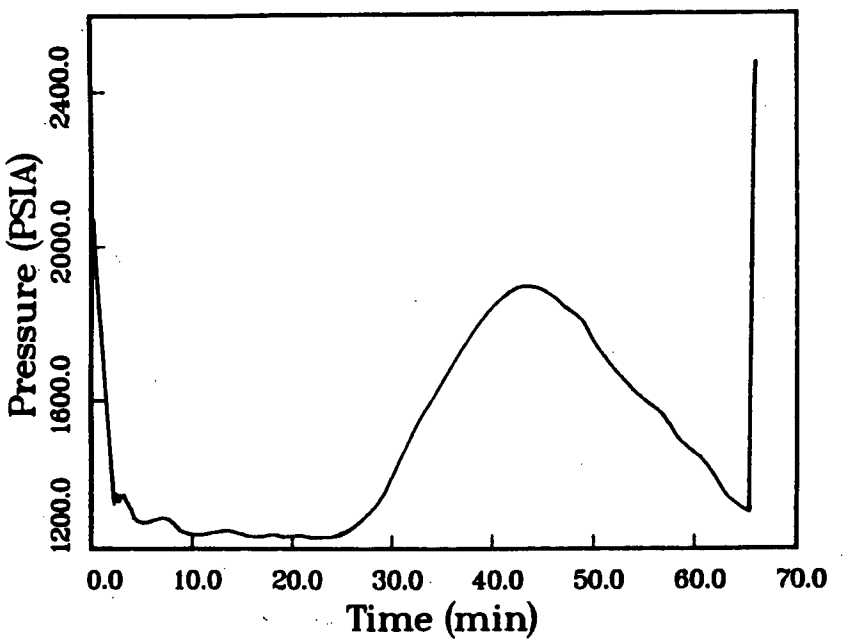

Figure 1-3. Reactor vessel pressure as a function of time during an S_2D break in an Ice Condenser reactor.

On the other hand, releases from Boiling-Water Reactors (BWRs) will probably come from the spargers in the suppression pool. These flows will be at low pressure, spread over a relatively large area (3 m diameter) and have a small steam content relative to the PWR cases. The basic flow is buoyancy dominated and similar types of fires have been thoroughly studied[2] over the last 20 years. However, the influence of the peculiar nature of the source in this case (a bubbly flow of hydrogen and steam through a free surface) has not been studied.

Between the extremes of these two cases, a wide range of behavior can exist. We cannot possibly cover all the cases, but we will attempt to describe the basic features of each type of flow. First, we will discuss the dominant features of subsonic, noncombusting jets and plumes. Second, we will describe the unique features of underexpanded jets. Finally, we will summarize the available information on combusting flows of each type.

1.1.1 Jets

A turbulent jet in a homogeneous atmosphere is characterized by a linear spreading rate and a constant momentum flux.[3] Variation of the average properties with downstream distance can be deduced from these facts and a simple similarity hypothesis. That is, all mean and some fluctuating properties of any jet can be described by a set of universal functions of the reduced variables x/D (downstream distance divided by the jet diameter) and y/b (cross-stream distance divided by the local jet width). Spreading rates and the basic scaling laws for planar and axisymmetric jets have been abstracted from Reference 3 and presented in Table 1-1.

Of particular interest are axisymmetric jets, since the flame jets studied in the present work were all of this type. As shown in Figure 1-4, the centerline velocity decreases inversely with downstream distance from the jet exit. The total mass flow within the jet, which is equal to the original mass flow plus entrained atmosphere, increases linearly with downstream distance. Strictly speaking, these rules only apply to "fully-developed" flows, which occur at some distance (typically 5-10 exit diameters) downstream from the jet exit.

1.1.2 Plumes

Plumes are distinguished from jets by having a nonconstant momentum flux. The momentum of a fluid element in the flow changes continuously as it moves downstream, due to the acceleration of gravity and the local density difference between the plume fluid and the surrounding atmosphere. Eventually, mixing between the plume fluid and the surroundings will eliminate the density difference and the flow will cease. A variety of configurations can exist depending on the initial density difference between the plume and the atmosphere, the existence of stratification in the atmosphere and the direction of the flow relative to gravitational acceleration.

Of the many possible configurations which could exist during a reactor accident, we will select the simplest flow to illustrate the plume physics. The simplest case is a low-density, low-momentum flow directed vertically upward into a homogeneous atmosphere of higher density. This flow has been extensively studied for both infinite and finite atmospheres[3,4] and is the type examined in the present work. For a discussion of the other possibilities, see Turner's book[4] and the recent review by List.[5]

Table 1-1. Properties of Turbulent Jets

	Planar	Axisymmetric
Spreading rate, s b = sx	0.11	0.086
Centerline Velocity $\frac{U}{U_o}$	$2.4\left(\frac{\rho_o}{\rho_\infty}\right)^{1/2}\left(\frac{D}{x}\right)^{1/2}$	$6.2\left(\frac{\rho_o}{\rho_\infty}\right)^{1/2}\frac{D}{x}$
Normalized centerline concentration or temperature	$2.\left(\frac{\rho_o}{\rho_\infty}\right)^{1/2}\left(\frac{D}{x}\right)^{1/2}$	$5.\left(\frac{\rho_o}{\rho_\infty}\right)^{1/2}\frac{D}{x}$
Entrainment rate $\frac{dM}{dx}$	$0.407\left(\frac{J\rho_o}{2x}\right)^{1/2}$	$0.282(J\rho_o)^{1/2}$
Momentum Flux, J	$\int_{-\infty}^{\infty}\rho U^2 dy$	$\int_o^{\infty}\rho U^2 2\pi r dr$
Mass flux, M	$\int_{-\infty}^{\infty}\rho U dy$	$\int_o^{\infty}\rho U 2\pi r dr$
Range of applicability	$2 < F^{2/3}\left(\frac{\rho_o}{\rho_\infty}\right)^{1/3}\frac{D}{x}$	$2 < F^{1/2}\left(\frac{\rho_o}{\rho_\infty}\right)^{1/4}\frac{D}{x}$

Froude number, F = $\frac{\rho_o U^2}{g(\rho_o-\rho_\infty)D}$

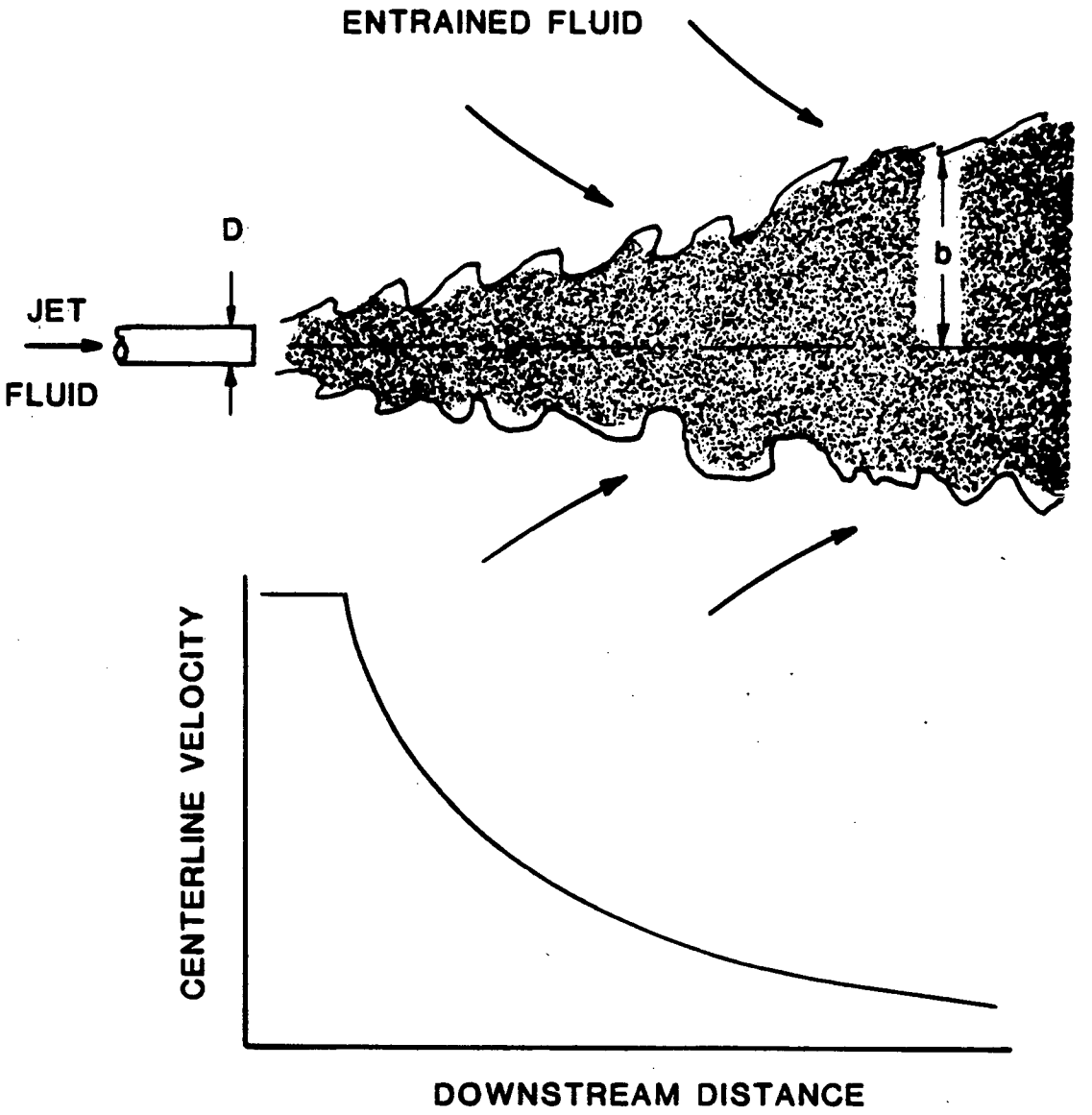

Figure 1-4. Schematic of momentum-dominated jet velocity development.

Like the turbulent jet, the plume is observed to spread at a linear rate and the flow has simple similarity or "self-preserving" structure. In place of the jet's constant momentum flux, the invariant for the plume is the "buoyancy" or thermal flux. However, this simple picture is valid[6] only as long as the buoyancy is weak, *i.e.*, the density difference between the plume and the atmosphere is small.

Spreading rates and scaling laws for weak plumes have been abstracted from Reference 3 and presented in Table 1-2. Note that the downstream variation of the mean properties depends only on the buoyancy flux, initial density ratio and the downstream distance. As expected, the results are independent of the momentum flux and more surprisingly, the diameter of the source. We shall find below that these ideas also seem to apply to plume-like fires.

The fundamental parameter which characterizes the difference between turbulent jets and plumes is the Froude number, F,

$$F = \frac{\rho_o U^2}{g(\rho_o - \rho_\infty)D} \tag{1}$$

where U is the characteristic jet velocity at the exit, ρ_o is the jet exit density, ρ_∞ the ambient density, g the acceleration of gravity, and D the jet diameter. The Froude number is essentially the ratio of inertial forces associated with the flow momentum to the buoyancy forces associated with the initial density difference. In plumes, the local Froude number will vary throughout the flow. However, the flow can be characterized in an overall way by the value of the Froude number at the source of the plume.

A Froude number of zero corresponds to a pure plume flow and a Froude number of infinity corresponds to a pure jet flow. For intermediate cases, expressions corresponding to those in Tables 1-1 and 1-2 can be formulated with the initial Froude number as a parameter.[3] Approximate limiting Froude numbers for the pure jet or pure plume cases can be computed for density ratios near one. For axisymmetric (planar) jets, the initial Froude number must be greater than 40,000 (3,000) for the flow to be momentum dominated until 100 diameters downstream. For an axisymmetric (planar) plume, the initial Froude number must be less than 4 (2.8) for the flow to be buoyancy dominated after 10 diameters downstream.

Table 1-2. Properties of Turbulent Plumes

	Planar	Axisymmetric
Spreading rate, s (radians)	0.12	0.11
Centerline Velocity U	$1.9\left(\frac{W}{\rho_\infty}\right)^{1/3}$	$3.5\left(\frac{W}{\rho_\infty x}\right)^{1/3}$
Normalized centerline concentration or temperature	$2.4\left(\frac{W}{\rho_\infty}\right)^{2/3}\frac{1}{gx}$	$9.35\left(\frac{W}{\rho_\infty x}\right)^{2/3}\frac{1}{gx}$
Entrainment rate $\left(\frac{dM}{dx}\right)$	$0.53\left(\frac{J\rho_\infty}{x}\right)^{1/2}$	$0.48(J\rho_\infty)^{1/2}$
Buoyancy Flux, W	$\int_{-\infty}^{\infty} g(\rho_\infty - \rho_o)U^2 dy$	$\int_o^{\infty} g(\rho_\infty - \rho_o)U\pi r dr$
Range of applicability	$0.2 > F^{2/3}\left(\frac{\rho_o}{\rho_\infty}\right)^{1/3}\frac{D}{x}$	$0.2 > F^{1/2}\left(\frac{\rho_o}{\rho_\infty}\right)^{1/4}\frac{D}{x}$

1.1.3 Underexpanded Jets

As mentioned above, for many PWR accidents the pressure inside the reactor vessel can be 100-200 times the containment atmosphere pressure. A jet driven by such a large pressure ratio is referred to as "highly underexpanded," since the flow must undergo a large volume increase before the jet fluid pressure is reduced to the ambient pressure. This volume increase occurs through a diverging supersonic flow followed by a series of shock waves and expansions referred to as "shock bottles" or "shock cells" (see Figure 1-5).

Some variation of this type of flow field will always occur if the jet pressure at the exit is higher than the ambient pressure. Generally, the flow at the minimum or "throat" of an area contraction (*i.e.*, the smallest area cross section in the flow path to the containment atmosphere) will be "choked" or "sonic" if the

pressure ratio is greater than a critical value. Another way of stating this is that the ratio of the jet stagnation pressure (*i.e.*, reactor vessel pressure) to the ambient pressure must be greater than about 2. This fact is a direct consequence of one-dimensional compressible fluid flow theory.[7]

Although the conditions at the sonic point alone determine the mass flow rate, the jet geometry will be influenced by the flow path between the sonic point and the point-of-release into the containment atmosphere. A large number of configurations exist depending on the amount of dissipation involved, the net amount of expansion or contraction in the flow path cross-sectional area, and the shape of the exit. For simplicity, we will concentrate on the case where the flow is sonic at the release point, *i.e.*, the exit and the throat coincide.

Much of the work on this problem has been done in connection with rocket flight in the atmosphere. This body of work is not directly applicable since the rocket exhaust is hot, quite supersonic, and exits into a supersonic co-flowing stream. However, some of the computational methods and codes[8,9] developed for rocket plume chemistry modeling could be adapted to the present problem.‡

Drawing upon the experimental work of References 10 and 11, we now present a description of the main features of the flow field of an underexpanded jet exiting at Mach 1 into a homogeneous atmosphere at a lower pressure. We will concentrate on the flow near the exit for two reasons. First, for slightly underexpanded jets, the flow is quasi-periodic in the downstream direction (see Figure 1-6a) and the basic features of all shock cells are similar. Second, for highly underexpanded jets, the first shock is quite strong and generates a unique structure (see Figure 1-6b) which dominates the downstream flow, a set of weak, oblique shock waves. The crossover between the two cases occurs at a jet exit to ambient pressure ratio of about 2.

To reduce the jet pressure to atmospheric at the jet boundary, an expanding flow develops at the exit. This expansion occurs through an initially self-similar flow known as an expansion fan in gas dynamics. The mathematical characteristic lines of this flow are sketched as the radial spokes emanating from the nozzle lip in Figure 1-6. The expansion is so severe that an oblique intercepting shock is required to bring the pressure back to ambient for most of the expanding flow.

---

‡The author would like to thank John Boccio of Brookhaven National Laboratories for bringing this to his attention.

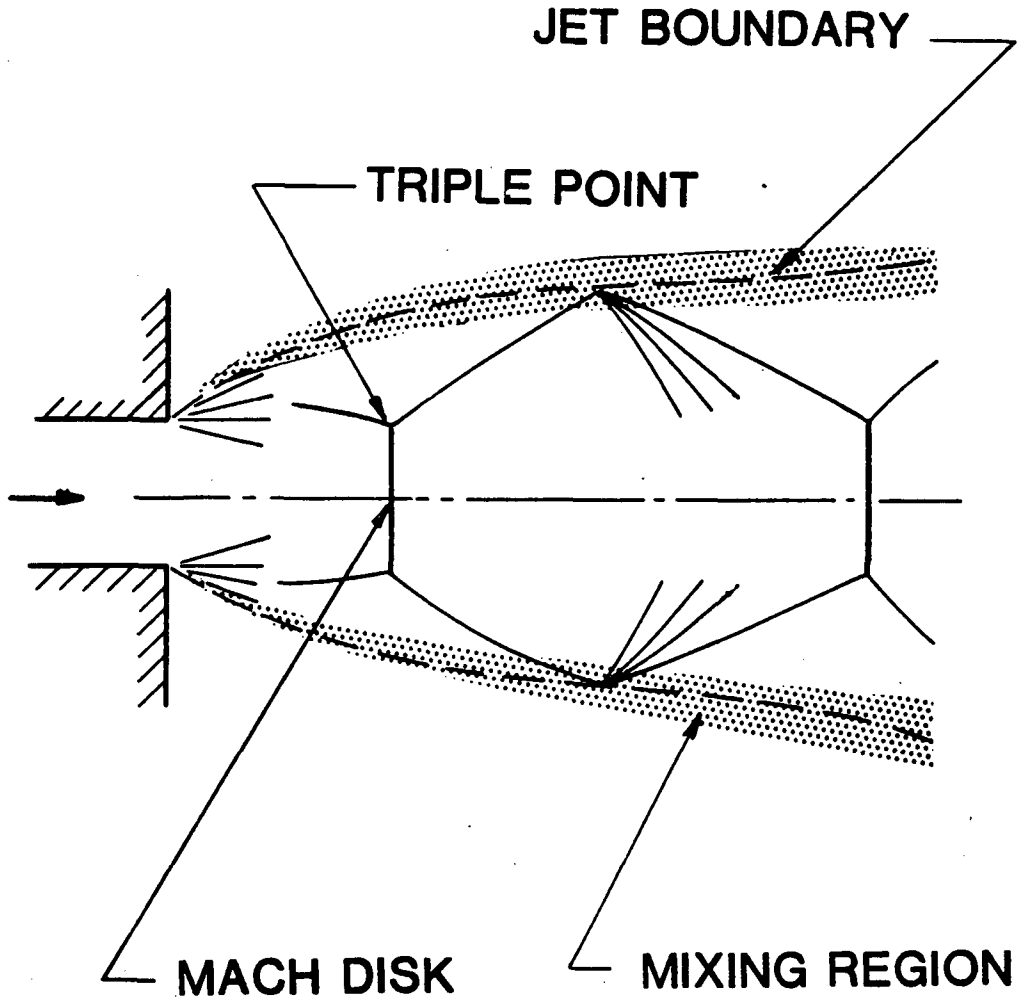

Figure 1-5. Schematic of the flow produced by an underexpanded jet exhausting into a stagnant atmosphere.

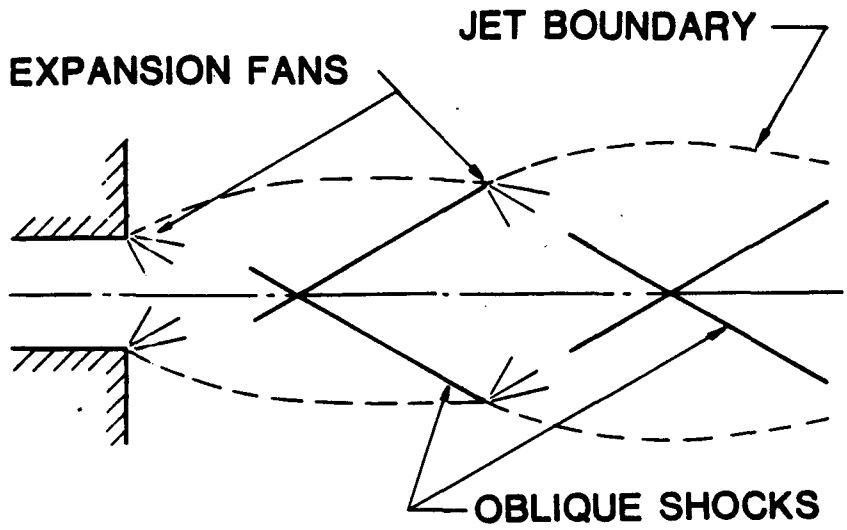

(a)

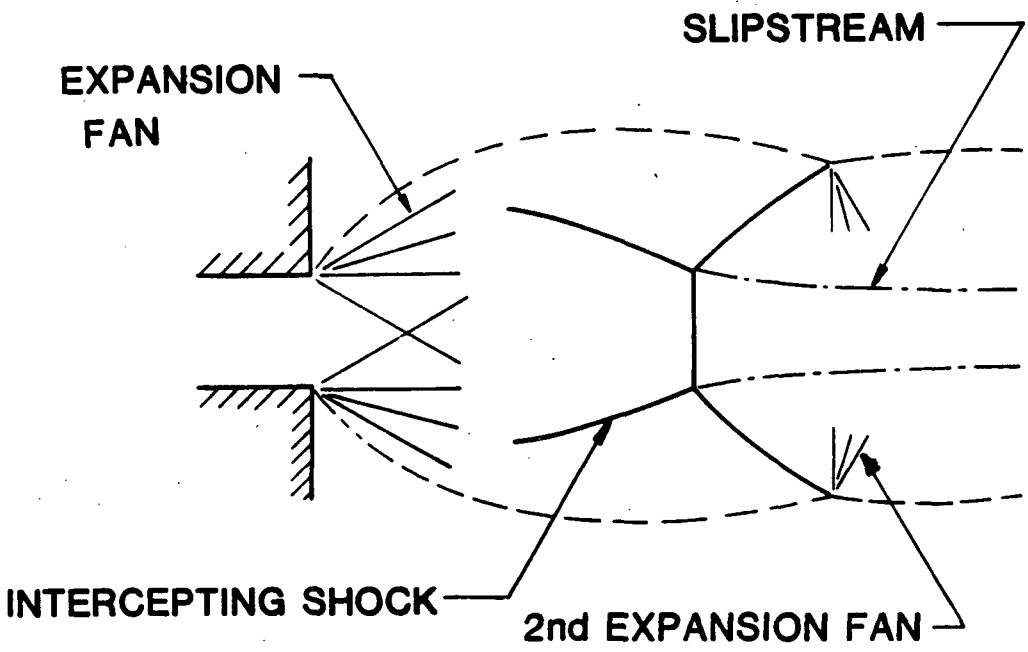

(b)

Figure 1-6. (a) Details of the first shock cell for a slightly underexpanded jet. (b) Details of the first shock cell for a highly underexpanded jet.

For an axisymmetric jet, the intercepting shock takes the form of a cone converging on the jet axis. At the apex of the cone, the shock surface converges smoothly for a slightly underexpanded jet (Figure 1-6a) or results in the formation of a normal shock (shown as the "Mach disk" on Figure 1-6b) for highly underexpanded jets. The shocks emerging from the convergence or branching off from the Mach disk extend to the jet boundary where they reflect as expansion waves. This expansion accelerates the flow and generates a new shock cell.

Mixing between the jet fluid and the atmosphere occurs in the shear layer formed at the jet boundary between high-velocity jet fluid and the stagnant atmosphere. Until the shock-expansion structure in the central or "core" region reaches ambient pressure, all combustion will occur in the annular shear-layer region. Following the decay of the core region (after 10-15 diameters), the remainder of the jet begins to mix and a transition to the subsonic jet structure takes place. Combustion downstream of the transition will presumably be similar to that observed in subsonic jets. Eventually, if the jet density differs appreciably from ambient, the flow will take on plume-like characteristics.

1.1.4 Diffusion Flames

The difference between combusting and noncombusting plume or jet flows is due to the effects of chemical reaction. There are two main effects: heat release due to the exothermicity and the change of thermophysical properties due to the composition change upon reaction. Of these, heat release has the strongest effect on the flow.

Heat released by combustion alters the thermodynamic state by raising the temperature of the fluid and since the process usually occurs at constant pressure (for subsonic flows), the specific volume increases. The chemical reaction and heat release occurs at the interface between the jet and atmosphere fluid. The topology of this interface is quite complex for turbulent flows and its character is very different for plumes than for jets.

At low Reynolds numbers (laminar flow), the reaction interface or "flame sheet" has a smooth shape which takes the form of a cylindrical surface aligned with the direction of the jet. One "base" of the cylinder is near the jet exit and the other is near the flame tip as shown in Figure 1-7.

As the Reynolds number is increased, the flame sheet becomes more and more unsteady due to the intrinsic instability of the jet flow itself. Low-Froude-number (buoyancy-dominated) flames are highly unsteady and exhibit a low-frequency puffing, apparently due to the roll-up of the flame sheet into large vortices.[12] High-Froude-number (momentum-dominated) flames exhibit a much higher frequency and smaller scale unsteadiness.

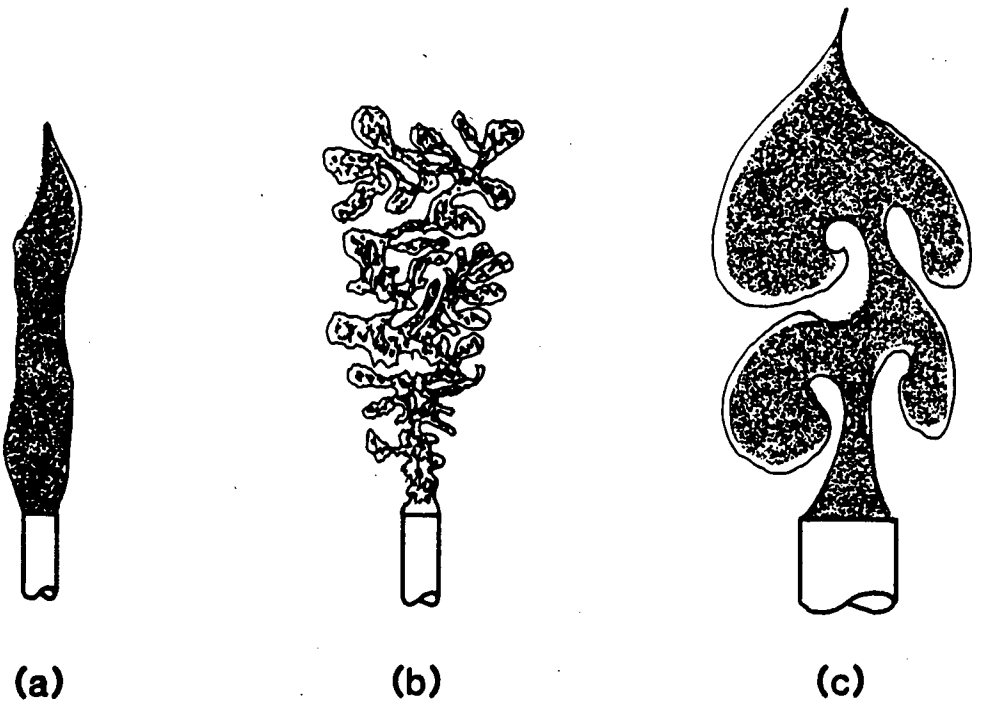

Figure 1-7. (a) Laminar flame-sheet geometry. (b) Turbulent flame-sheet geometry, momentum-dominated flow. (c) Turbulent flame-sheet geometry, buoyancy-dominated flow.

While no simple technique exists to calculate the flame-sheet area (or more importantly, the reaction rate) as a function of position in a turbulent jet flame, the reaction can be quantified to some extent. An extensive review and discussion of the various approximate techniques which have been used to calculate diffusion flame structure can be found in References 13 and 14. For hydrogen-air diffusion flames, a relatively simple extension of the methods used for non-reacting boundary layer flows has been fairly successful in predicting the gross features of the flow.

The characteristic temperature of the products of reaction can be estimated by calculating the temperature that an adiabatic, stoichiometric mixture of atmosphere and jet fluid will reach under constant-pressure conditions. This temperature will depend on the amount of diluent present in both the jet fluid and atmosphere and also on the initial temperature of the mixture. Results of a representative calculation are shown in Figure 1-8. These are appropriate for a hydrogen jet diluted with either nitrogen or steam and then mixed with room-temperature air. These results will be used frequently in our discussion of flame structure and heat transfer (Chapters 3 and 4 of this report).

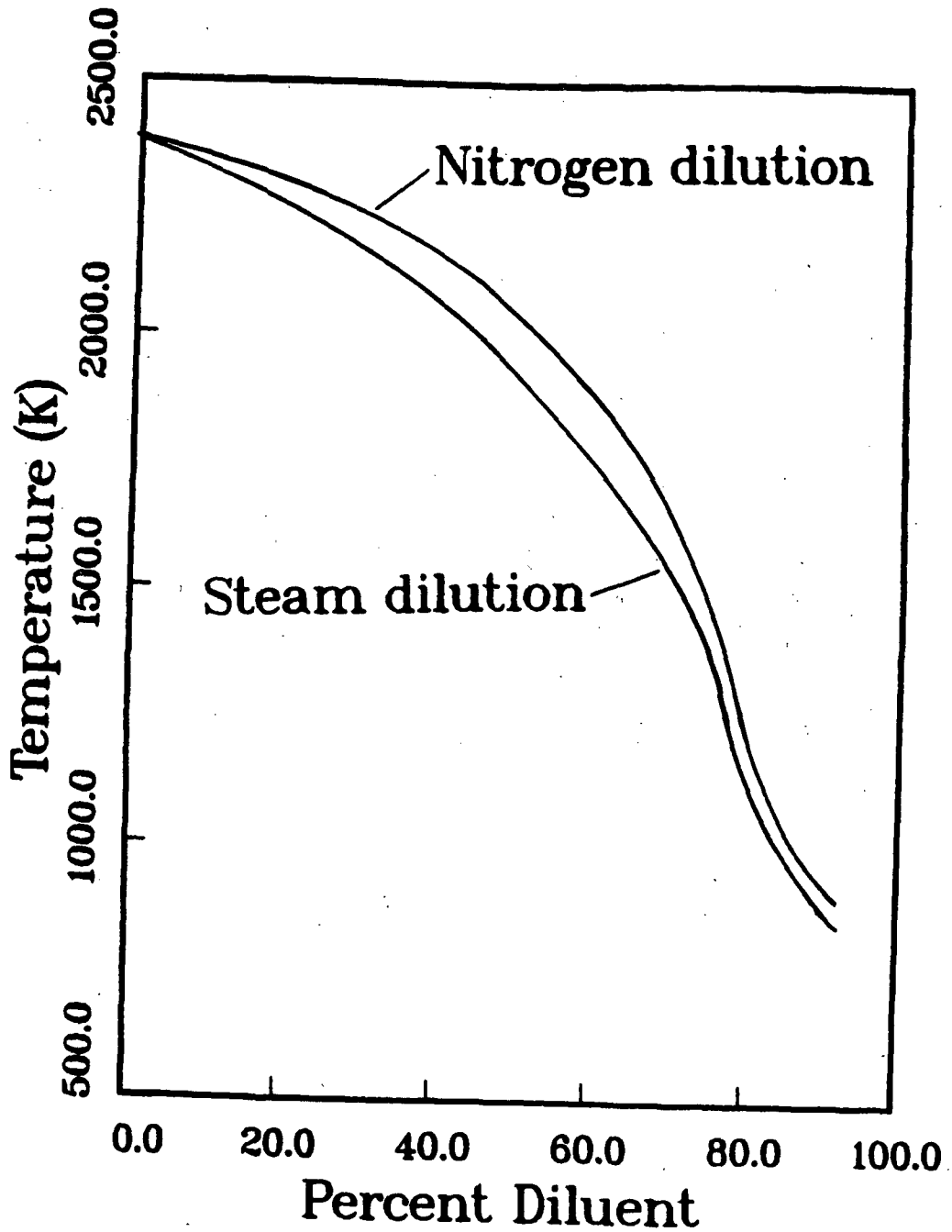

Figure 1-8. Adiabatic flame temperature for hydrogen jets diluted with either steam or nitrogen and then mixed with room-temperature air.

1.2 Scaling

An important consideration for hazard evaluation is the parameter range that hypothesized reactor fires will occupy. One method of parameterizing diffusion flames is to plot the expected range of conditions on a burner (release opening) size *vs.* flow rate diagram. Such a diagram is shown in Figure 1-9. Of course, several other parameters such as fuel type, diluent fractions and pressure ratio can be important. The main purpose of Figure 1-9 is to demonstrate the qualitative behavior of the postulated accident conditions.

The shaded regions in Figure 1-9 are regimes in which either the limiting case of a jet-like or plume-like fire will occur. For large-area or low-flow-rate fires, the behavior will be plume-like; this corresponds to the upper left-hand portion of the plot. For small-area or high-flow-rate fires, the behavior will be jet-like; this corresponds to the lower right-hand corner of the plot.

Lines parallel to the boundaries of the shaded regions can be thought of as lines of constant Froude number. These boundaries are somewhat arbitrary and will depend on the particular release geometry, jet fluid and atmosphere composition and temperature. Shown in Figure 1-9 are boundaries for a pure hydrogen jet at 200°C exhausting vertically upward into a cold air atmosphere.

While more qualitative than quantitative, this plot does demonstrate that the majority of postulated reactor accidents fall in the intermediate regime between jet and plume fires. For more realistic PWR jet conditions (*i.e.*, with more steam in the jet fluid), the conditions will be much more jet-like than shown here. On the other hand, the fires postulated to occur in the wetwell of the BWR Mark III nuclear plants will be much more plume-like.

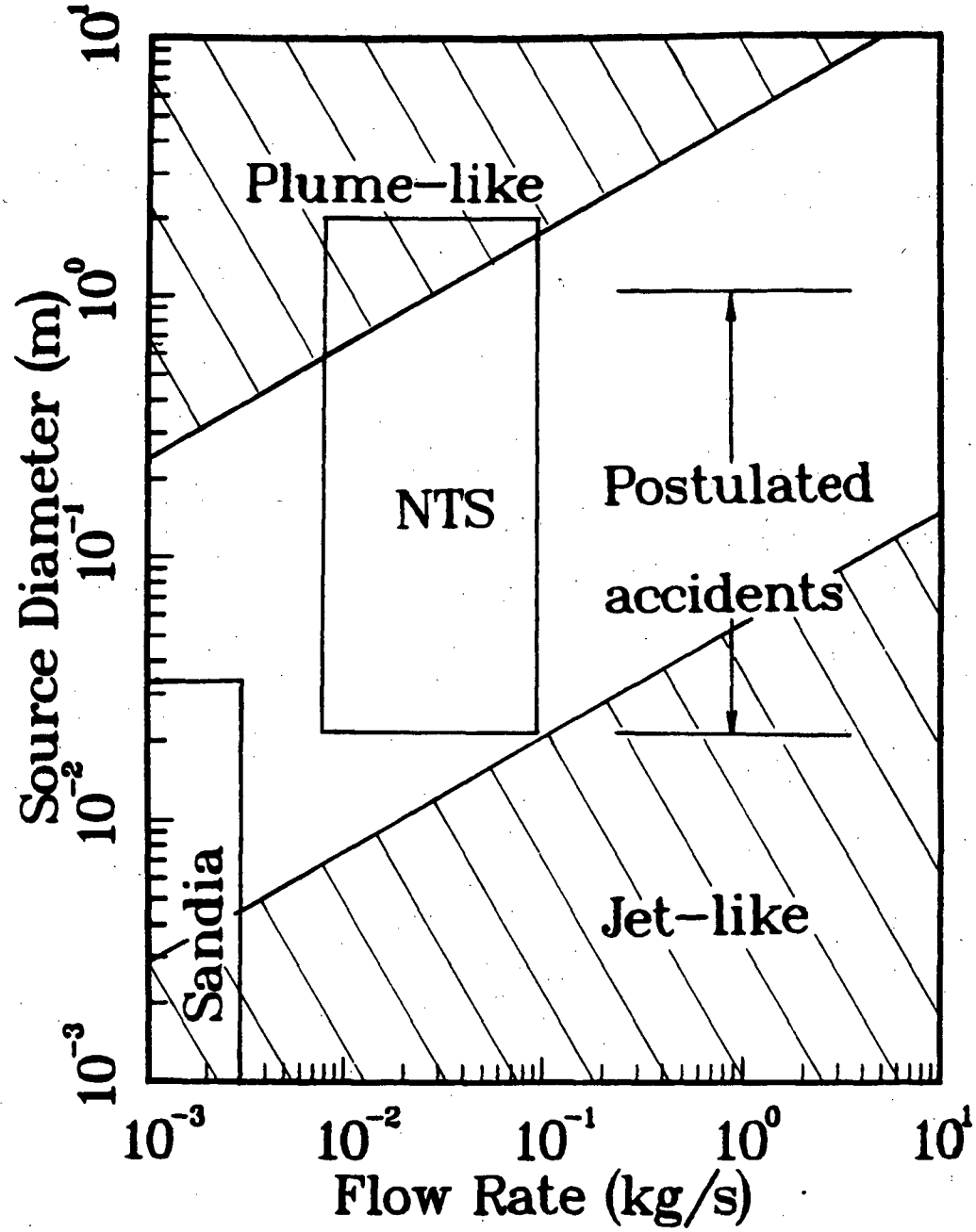

Figure 1-9. Parameter space for the combustion of a pure hydrogen jet at 200°C in cold air. The capabilities of both the present facility at Sandia and the dewar experiment at NTS are shown in relation to postulated accident conditions.

References

1. M. Berman and L. Thompson, **Proceedings of the Second International Workshop on Hydrogen Behavior in Light Water Reactors,** available as Sandia National Laboratory Report SAND82-2456 (1982).
2. H-Z. You and G. M. Faeth, *Buoyant Axisymmetric Turbulent Diffusion Flames in Still Air,* Combustion and Flame **44,** 261-275 (1980).
3. C. J. Chen and W. Rodi, **Vertical Turbulent Buoyant Jets,** Pergamon Press, NY (1980).
4. J. S. Turner, **Buoyancy Effects in Fluids,** Cambridge University (1973).
5. E. J. List, *Turbulent Jets and Plumes,* Annual Review of Fluid Mechanics **14,** Annual Reviews, Inc., 189-212 (1982).
6. M. A. Delichatsios, *Strong Turbulent Buoyant Plumes,* Combustion Science and Technology **24,** 191-195 (1981).
7. P. A. Thompson, **Compressible Fluid Dynamics,** McGraw-Hill, NY (1976).
8. S. Dash, H. S. Pergament, and R. D. Thorpe, *The JANAF Standard Plume Flowfield Model: Modular Approach, Computational Features and Preliminary Results,* **Proceedings of the JANAF 11th Plume Technology Meeting, CPIA Publication 306,** 345-442 (1979).
9. J. Boccio, S. Dash, and G. Weilerstein, *A Computational System for the Prediction of Low Altitude Rocket Plume Flow Fields,* Volumes I and II, General Applied Science Laboratories, GASL-TR-239 (1976).
10. E. S. Love and C. S. Grigsby, **Some Studies of Axisymmetric Free Jets Exhausting from and into Supersonic Streams,** NACA RM L54L31 (1955).
11. C. Dup. Donaldson and R. S. Snedeker, *A Study of Free Jet Impingement. Part 1. Mean Properties of Free and Impinging Jets,* Journal of Fluid Mechanics **45,** 281-319 (1971).
12. E. E. Zukoski, T. Kubota, and B. Cetegen, *Entrainment in Fire Plumes,* Fire Safety Journal **3,** 107-121 (1980).
13. R. W. Bilger, *Turbulent Jet Diffusion Flames,* Progress in Energy and Combustion Science **1,** 109-131 (1976).
14. H. Eickhoff, *Turbulent Hydrocarbon Jet Flames,* Progress in Energy and Combustion Science **8,** 159-168 (1982).

2 Facility Description

In this section we describe the facility constructed at Sandia National Laboratories to study high-temperature, hydrogen-steam flame jets. The facility is located at an isolated test site used for explosive experimentation. It consists of a remotely-controlled gas supply and flow-control system, a gas temperature control system, the jet itself and the associated instrumentation. Each of these components are described separately below.

2.1 Gas Supply System

Steam is supplied by a small (23 kg/hr) electrically-fired boiler located outside and about 5 m away from the experiment. Hydrogen and nitrogen are supplied by a bottle farm located about 10 m from the experiment. The output pressure is set by standard two-stage regulators. One nitrogen supply can be used as a diluent in place of steam; the other is used to power the flow-control system.

All gases flow through stainless-steel tubing to the jet. Air-operated ball valves are used to control the hydrogen flow and, for safety, three separate sets of valves are used. The air-operated valves are actuated by electro-pneumatic (EP) valves connected to the nitrogen supply. Electric power to the EP valves is low-voltage (28 VDC) and controlled through an interlocked, key-operated panel in the control room.

Hydrogen sensors, manufactured by General Monitors, are located above the bottle farm, in the control room and at several locations near the flame jet. The sensors are connected to alarm circuits which are actuated if the hydrogen concentration rises above 4% by volume. If any of the alarm circuits are actuated, the hydrogen supply is automatically shut off and the hydrogen lines to the jet purged with nitrogen.

Gas flow rates to the jet are regulated by Taylor Instruments orifice-plate flow meters connected by a pneumatic feedback circuit to needle valves. In addition there is a Matheson electronic flow meter and regulator which can be used for low (less than 100 slpm) hydrogen flows and a Teledyne-Hastings electronic flow meter for hydrogen flow rates up to 700 slpm. The orifices in the

Taylor Instruments flow meters can be changed from 0.76 to 8.4 mm diameter to allow a wide range of flow rates.

Rather than use the calibrations supplied by the manufacturer, we used the ASME standard calibrations[1] for the orifice plates. The upstream pressure, temperature, and the pressure drop across the orifice plate were all measured. A simple computer program was then used to compute the flow rate from an analytical representation of the empirical correction factors. Calibration is only dependent on the pressure transducers, which could easily be calibrated against a standard Wallace and Tiernan mechanical gauge.

2.2 Superheaters and Jet Manifold

The jet itself is situated inside an existing explosives test chamber. The chamber is a steel box open on one side and constructed of 5 cm thick plate; the box dimensions are 4.0 m long, 3.5 m wide, and 2.3 m high. Only the jet, associated diagnostics and the superheaters are located in the chamber (see Figure 2-1). The remainder of the experimental system was located outside or in the adjacent building.

Steam and hydrogen pass through separate control systems and superheaters before being mixed at the jet manifold. Each superheater consists of a coil of stainless steel tubing mounted inside of a 50 kW electric furnace. There are approximately 50 turns of tubing on a 10 cm diameter form that is about 60 cm long. Furnace temperature is regulated by an electrical feedback circuit. Gas temperature can be increased up to 700°C by this method.

After passing through the superheaters, the gases flow through heated lines to the jet manifold. The gases flow coaxially into the plenum as shown in Figure 2-2. The hydrogen stream is divided into a number of small jets which are directed into the steam, transverse to main flow direction. To enhance mixing and promote more uniformity in the flow, a coarse baffle (3 mm diameter holes) and a section of honeycomb (15 cm long with 0.5 mm diameter channels) are located between the plenum and the jet exit.

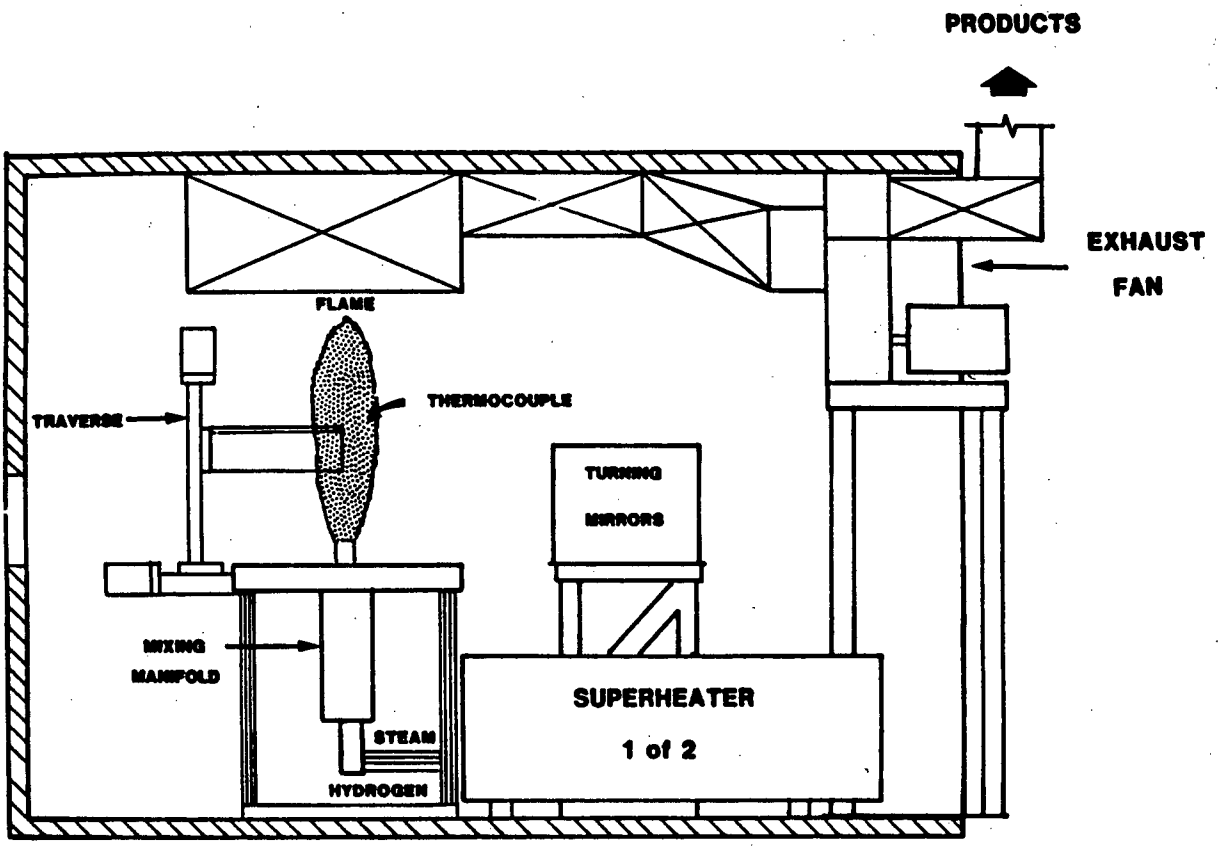

Figure 2-1. Layout of equipment inside the test chamber.

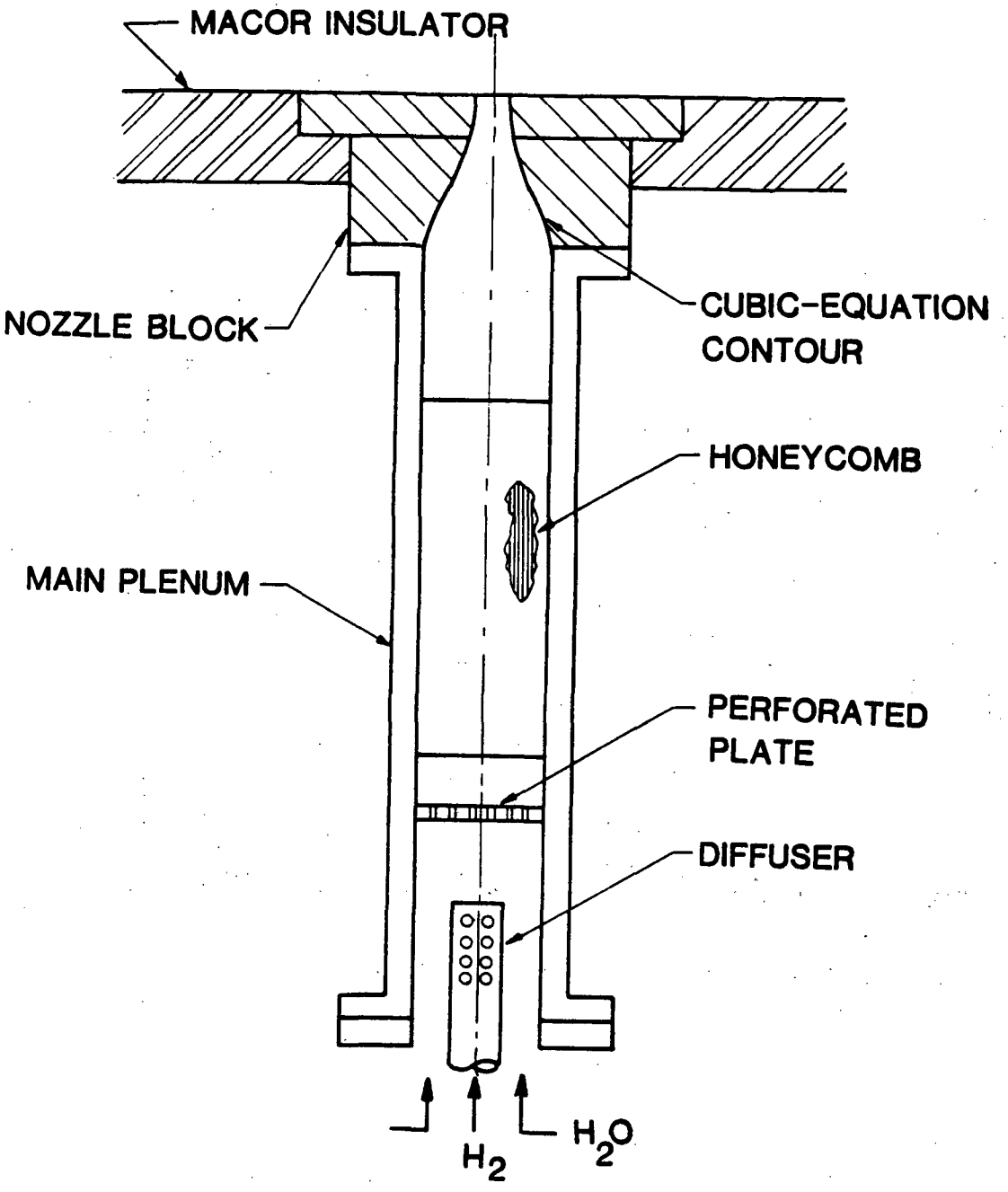

Figure 2-2. Cross section of jet plenum and nozzle.

An interchangeable, flanged nozzle is located at the exit of the jet manifold. Smooth, cubic-equation nozzles with areal contraction ratios of 4, 9, or 36 (exit diameters of .635, 1.27, or 1.8 cm) were used for most of the testing. The effective nozzle size was increased by add-on fixtures for some experiments; these are described later in the sections dealing specifically with those experiments.

The jet exhausts vertically upward and the gases are drawn into a duct by a high-temperature blower. The blower exhausts outside the chamber through a 1m stack. If the jet does not spontaneously ignite as it emerges into the atmosphere, an electrical ignitor, either a spark or a glow plug, is used to initiate burning. Our standard ignitor is a repetitive spark discharge which is remotely inserted and retracted by an air-driven hydraulic cylinder.

2.3 Instrumentation

Data recording, processing, and experiment control are accomplished with a CAMAC[2] system interfaced to a DEC LSI 11/23 minicomputer. Analog-to-digital convertor, temperature monitors, AC switch controllers, and indicators are mounted in the CAMAC crate and connected to the various instruments and control panels used in the experiments. Much of the effort on this project was in developing and integrating the software needed to effectively operate the experiment under computer control.

In addition to the flow rate, pressure and temperature instrumentation needed to operate the jet, there were several specialized diagnostics for the flame jet itself. All of these diagnostics depended on a remotely-controlled X-Y traverse system to position the measuring instrument accurately in the flame. The traverse could be positioned either manually or under computer control. A computer program was developed to automatically move the traverse on a prescribed pattern through the flame and to record average and instantaneous data at specified points.

Examples of instruments used on the traverse are: a platinum-rhodium thermocouple; a false ceiling equipped with a Gardon gauge for stagnation-point heat flux; a water-cooled tube for cylinder cross-flow heat transfer measurements; and a water-cooled pitot probe. Detailed descriptions and results from these devices are presented later.

References

15. H. S. Bean (ed.), **Fluid Meters, Their Theory and Application,** The American Society of Mechanical Engineers, NY (1971).

16. P. Clout, **CAMAC Primer,** Los Alamos National Laboratory Report LA-UR-82-2718 (1982).

3 Flame Size and Stability

In this section we discuss the variation of flame size and stability with dilution and burner geometry. Both our experimental results and those of others are discussed. Some simple theoretical ideas about the role of diluents are presented and the predictions of models based on those ideas are discussed. In particular, two methods for predicting the relationship between blowoff velocity and burner diameter are compared.

Flame length, while not a fundamental or well-defined quantity, is of interest for several reasons. The physical volume occupied by the flame will be needed for models which treat the flame as a separate entity or "compartment," this volume can be estimated from the flame length. Models for the heat flux from flames depend on whether the object of interest is located above or in the flame. Finally, the variation of flame length with dilution can be easily measured and used as a simple test of combustion models.

The blowoff velocity of a diffusion flame appears to be more well-defined than the flame length, however, the temperature of the nozzle or burner can have a large effect. If the temperature of the orifice from which the jet originates is not controlled, then the combustion-generated heat of the flame will cause the nozzle temperature to change with time. This will almost certainly be the case for flame jets generated in reactor accidents. This fact should be kept in mind when applying data derived from laboratory experiments to reactor situations.

3.1 Flame-Length Scaling

Flame length is essentially a measure of the distance at which all the jet fluid has mixed and reacted with the atmosphere. Therefore, both the chemistry of the reactants and the fluid-mechanical processes governing entrainment and mixing are important. Of these two factors, the entrainment rate is by far the most important for turbulent flames. A common way to express this idea is to say that "the reaction rate in turbulent combustion is mixing limited."

Typically, the reaction rates between fuel and oxidizer are sufficiently fast that the detailed chemical kinetics of the reaction are unimportant. The only exception to this circumstance we will consider is the case of flames near the

blowoff or blowout limit. For our purposes, then, the chemistry of the fuel-oxidizer system can be completely characterized by the heat of reaction and the stoichiometry, *i.e.*, the quantity of atmosphere required to completely oxidize a unit quantity of jet fluid. For the hydrogen-oxygen system, water is the only product we will consider to be important; the heat of reaction is 57.5 kcal/mole, and one-half mole of oxygen is required to completely oxidize each mole of hydrogen.

Entrainment and mixing are not only more important processes than the chemical reaction but also much more complex. The turbulent character of the flow and the added complexity of reacting fluids make this problem an area of intense current research.[1] Many of the ideas used in turbulent reacting flow analysis are taken unmodified from the corresponding nonreacting flow. For example, the entrainment rate of a reacting jet is frequently assumed to be identical to that of a nonreacting jet with the same momentum flux.

Our discussion of entrainment and mixing can be naturally divided between jet-like flows and plume-like flows as was done in the introduction. While our understanding of entrainment and mixing is greater for jet-like flows without heat release, plume-like fires have been much more extensively studied than jet-like fires. For this reason, we will be compelled to use arguments based on flows without heat release for much of the flame jet discussion.

3.2 Temperature Profiles and Photographs

In this subsection, we present measurements and photographs that demonstrate the effect of steam dilution on flames. For comparison, some data obtained with jets diluted by nitrogen are also shown. These data are presented so that the reader will gain some familiarity with the type of flames we are studying, and also for comparison to some of the theories discussed below.

Photographs of the flame jets were taken with a 4" x 5" view camera and Polaroid film (3000 ASA). The camera was positioned about 1 meter from the flame and a 135 mm focal-length lens was used. In order to obtain sufficient intensity to record an image, a small amount of commercial window cleaner was sprayed near the base of the flame. Radiation from the sodium in the entrained cleaner rendered the flame visible. Actually, it is the region where the flow is hot enough to cause chemiluminesence that is visualized, not just the region where combustion is occurring.

Table 3-1. Jet Parameters for Photographs

Case	Q_{H_2} (slpm)	Q_{H_2O} (slpm)	U (m/s)	R	F (K)	T_f
1	44.0	0.0	51.5	1.05×10^3	2.0×10^3	2381.
2	109.2	0.0	127.7	2.61×10^3	1.2×10^4	2381.
3	100.7	28.3	150.9	6.59×10^3	5.2×10^4	2288.
4	28.3	113.2	165.5	1.80×10^4	2.2×10^4	1151.

Q_X = flowrate of component X of the jet fluid

U = Jet exit velocity

R = UD/ν, Reynolds number of jet exit flow

F = $\rho U^2/g\Delta\rho D$, Froude number of jet exit flow.

T_f = temperature of a stoichiometric mixture of jet and atmosphere fluid burned under adiabatic, constant-pressure conditions.

Nominal ambient pressure 630 torr, nominal ambient temperature 300 K, jet exit diameter $D = 0.635$ cm, nominal jet temperature 500 K for all cases

Our initial interest in photography was to obtain time-exposure photographs in order to determine the flame length. As discussed in the next section, this technique was found to be unsuitable and more reliable techniques based on centerline temperature profiles were used. However, the photographs are very useful to illustrate the changes that occur in the flow as diluents (steam or nitrogen) are added.

Reproductions of a selection of short- and long-duration photographs of flames with various amounts of steam dilution are shown in Figures 3-1 through 3-4. All of these flames were from jets with an initial diameter of 0.635 cm and an exit temperature of 200°C. The parameters (*i.e.*, flame temperature, Reynolds number, Froude number, *etc.*) characterizing these jet flames are given in Table 3-1.

Note the decrease in the flame height with increasing diluent fraction in the flow. This is due to the increased entrainment rate of the jet per unit flow

rate of the fuel (hydrogen). This phenomenon might be anticipated from the scaling laws presented in Table 1-1 of the first chapter and the fact that the flame length is proportional to the location of a stoichiometric ratio of fuel to oxidizer. However, we believe that this is the first demonstration of this effect in a jet flame. A quantitative discussion of this effect is presented in the next section.

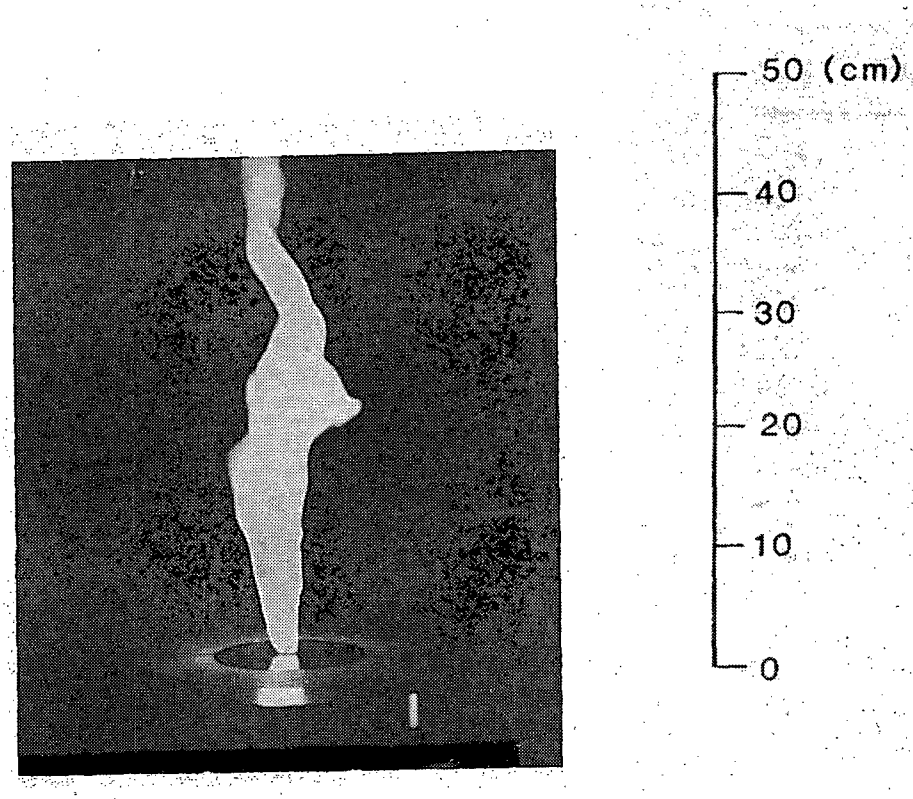

Figure 3-1. Reproduction of a short (4 ms) exposure photograph of a hydrogen flame jet. Case 1 of Table 3-1, 44 slpm hydrogen from a 0.635 cm diameter nozzle at a temperature of 200°C.

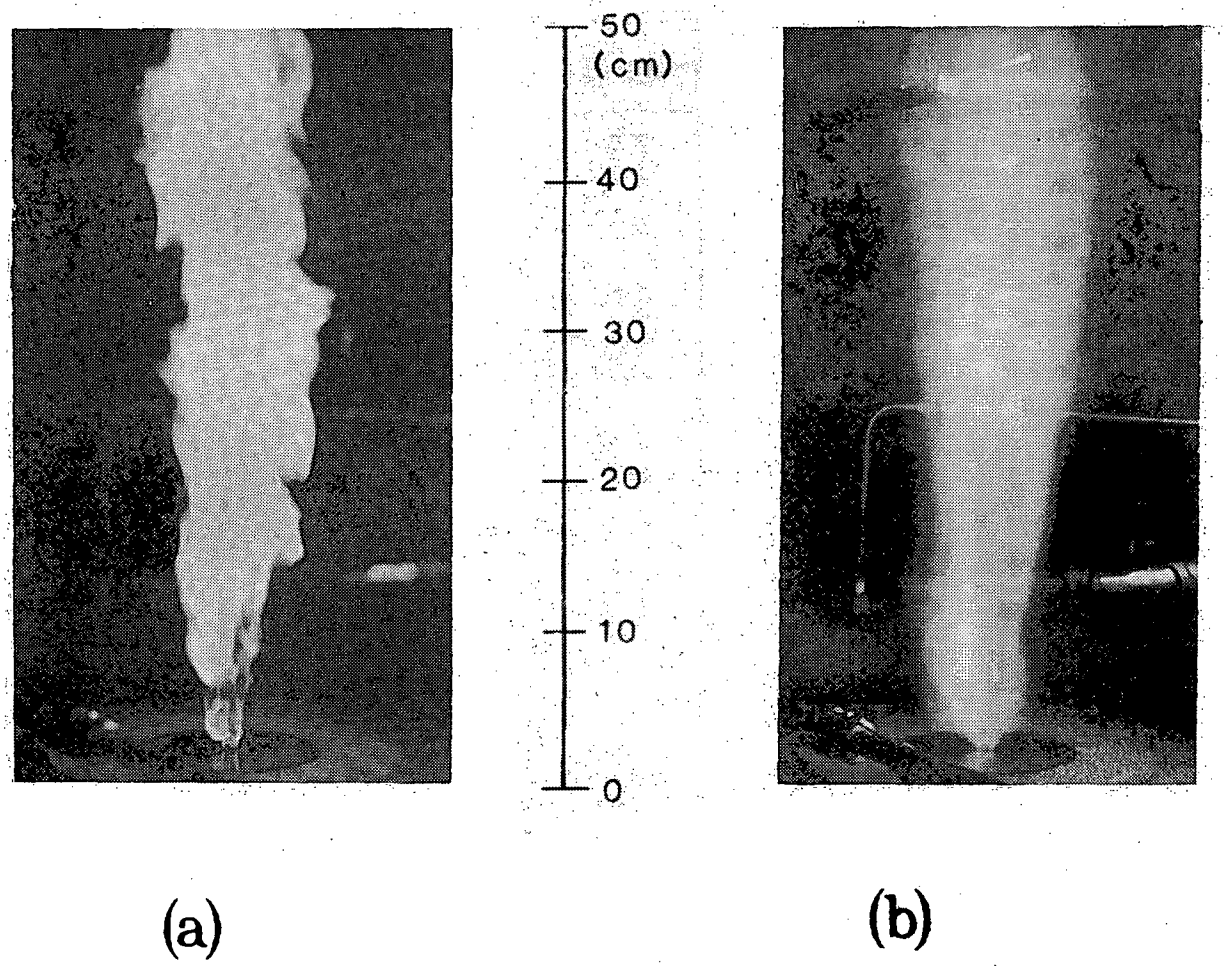

Figure 3-2. Reproduction of (a) short and (b) long (1 s) exposure photographs of a hydrogen flame jet. Case 2 of Table 3-1, 109 slpm hydrogen from a 0.635 cm diameter nozzle at a temperature of 200°C.

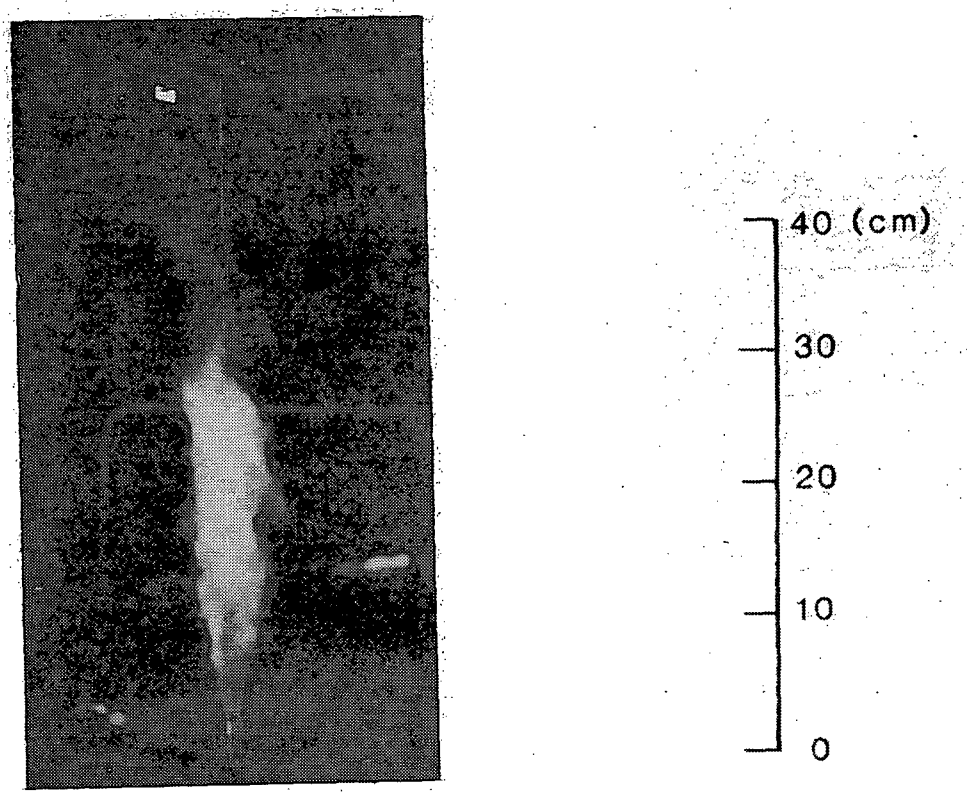

Figure 3-3. Reproduction of a short exposure photograph of a hydrogen-steam flame jet. Case 3 of Table 3-1, 100.7 slpm hydrogen and 28.3 slpm steam from a 0.635 cm diameter nozzle at a temperature of 200°C.

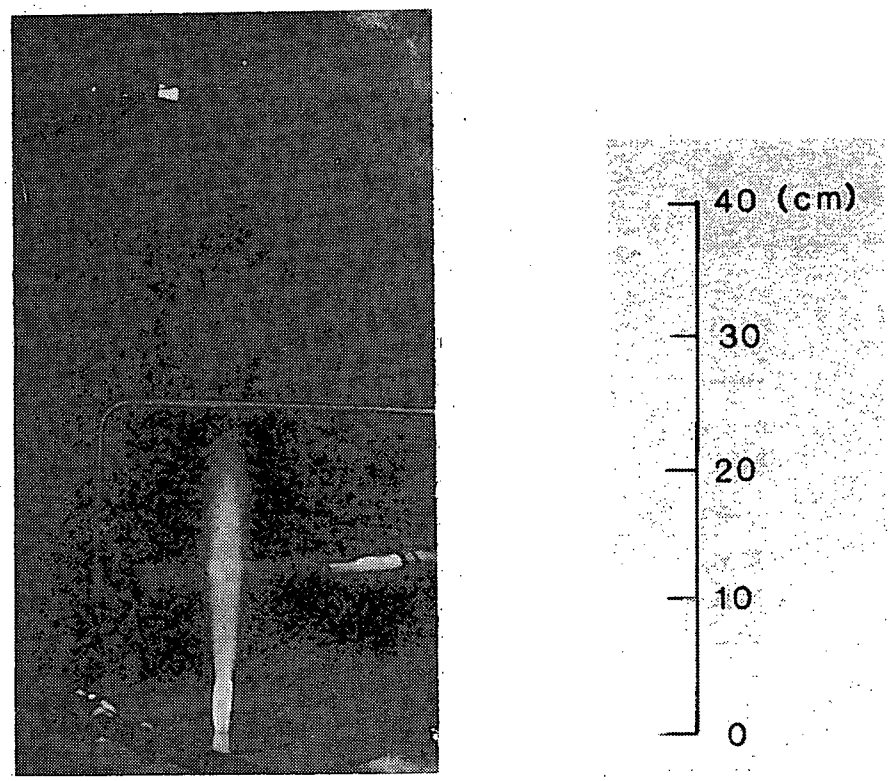

Figure 3-4. Reproduction of a short exposure photograph of a hydrogen-steam flame jet. Case 4 of Table 3-1, 28.3 slpm hydrogen and 113 slpm steam from a 0.635 cm diameter nozzle at a temperature of 200°C.

As the jet diluent fraction is increased, both the experimentally measured peak temperature and the calculated flame temperature decrease. This effect ultimately limits the maximum amount of steam that can be present in the jet before the flame becomes unstable and steady combustion ceases. The possibility of instability, *i.e.*, blowoff or blowout of the diffusion flame, is discussed in the last section of this chapter.

Centerline temperature profiles of several different jet flames are shown in Figures 3-5 through 3-7. Each curve is labeled with α, the ratio of diluent to hydrogen flow rate (molar). The temperature profile for an undiluted hydrogen jet is shown separately in Figure 3-5. Note that this profile is quite dissimilar to those shown in later figures. This is probably due to the importance of both buoyancy and viscosity in this flow; the Froude and Reynolds numbers for this jet are substantially lower than for the other cases.

Centerline temperatures for steam-diluted hydrogen jets are shown in Figure 3-6; data for nitrogen-diluted jets are shown in Figure 3-7. Both sets of data were obtained from a 0.635 cm diameter jet at an initial temperature of 200°C. Diluent fractions, flow rates and other parameters of these flows are given in Table 3-2. Temperatures were measured with an uncoated platinum-rhodium (type S) thermocouple traversed along the centerline of the flame.

Typically, several hundred individual measurements were averaged at each vertical station and stations were located every 1-2 cm. Since only an indication of the length of the flame and the characteristic temperature were desired, the thermocouple data shown have not been corrected for radiation and conduction losses. These are estimated to be on the order of 100-200°C (see Becker and Yamazaki[5] for the details).

The effects of dilution on the flame are quite obvious in these figures. Both the decrease in flame temperature and the flame shortening with increasing diluent fraction can be seen in Figures 3-6 and 3-7. Note that the temperatures are slightly higher if nitrogen diluent is used in place of steam, due to the lower heat capacity of nitrogen. This effect is clearly shown in the flame temperature calculations presented in Figure 1-8. The nitrogen-diluted flames are also slightly shorter than the equivalent flow with steam dilution. This is due to the higher molecular weight and hence, higher entrainment rate of nitrogen at the same flow rate (molar) as steam.

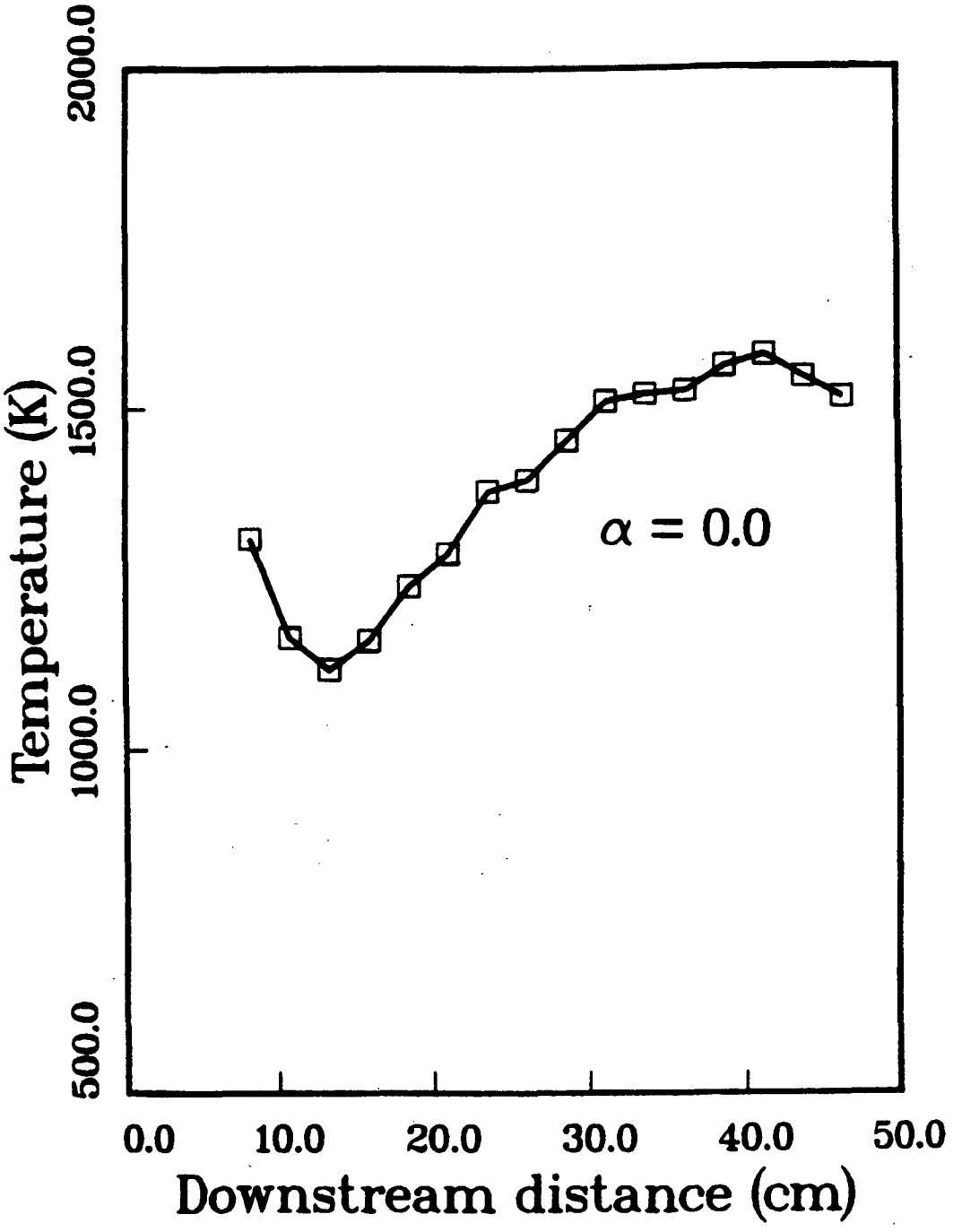

Figure 3-5. Centerline temperature profile for a pure hydrogen jet flame. Jet initial diameter was 0.635 cm and the initial temperature was 200°C. The parameters for this flow are given in Table 3-2.

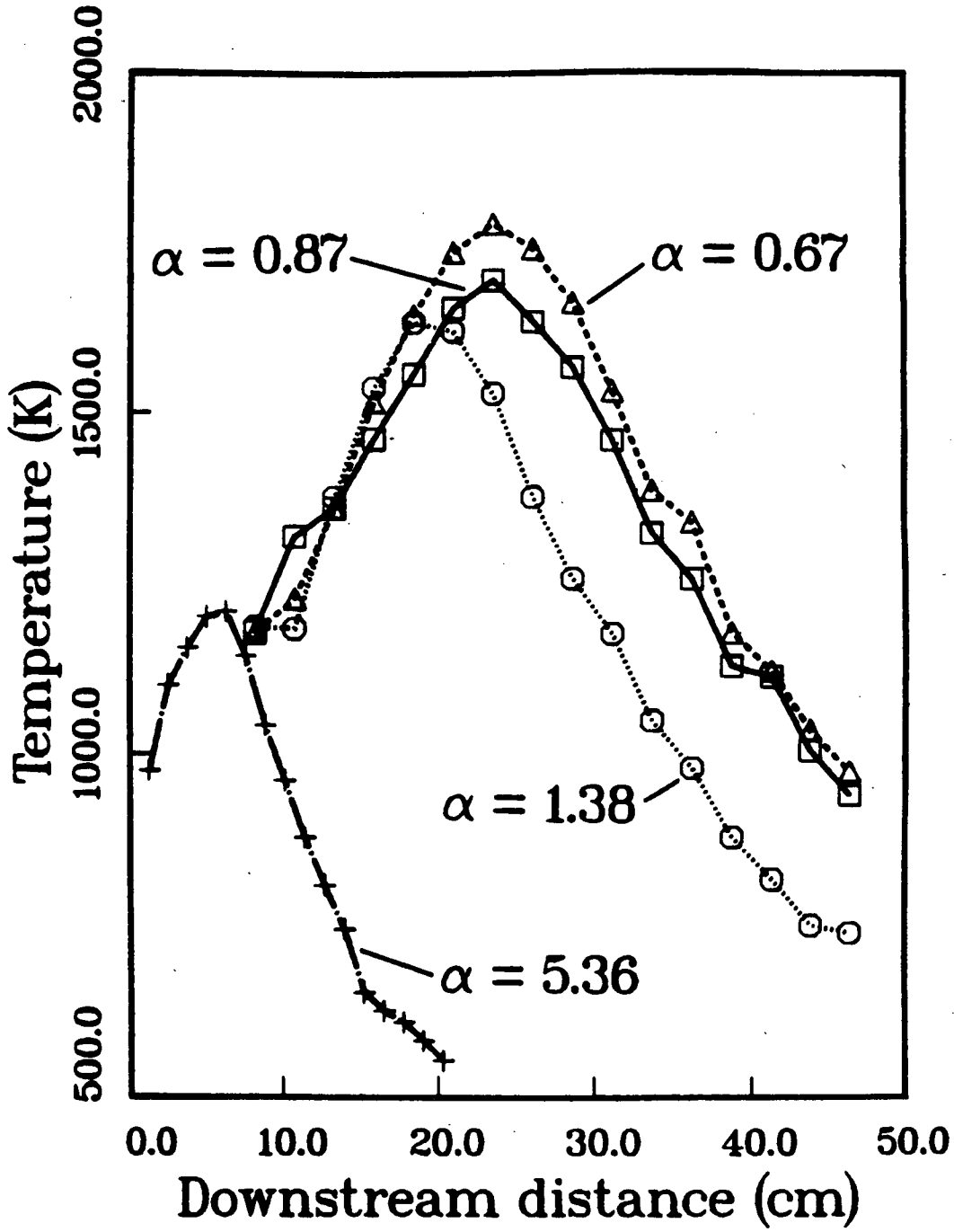

Figure 3-6. Centerline temperature profiles for hydrogen jet flames diluted with steam. Jet initial diameter was 0.635 cm and the initial temperature was 200°C. The molar ratio of steam to hydrogen is shown above each set of data; other parameters are given in Table 3-2.

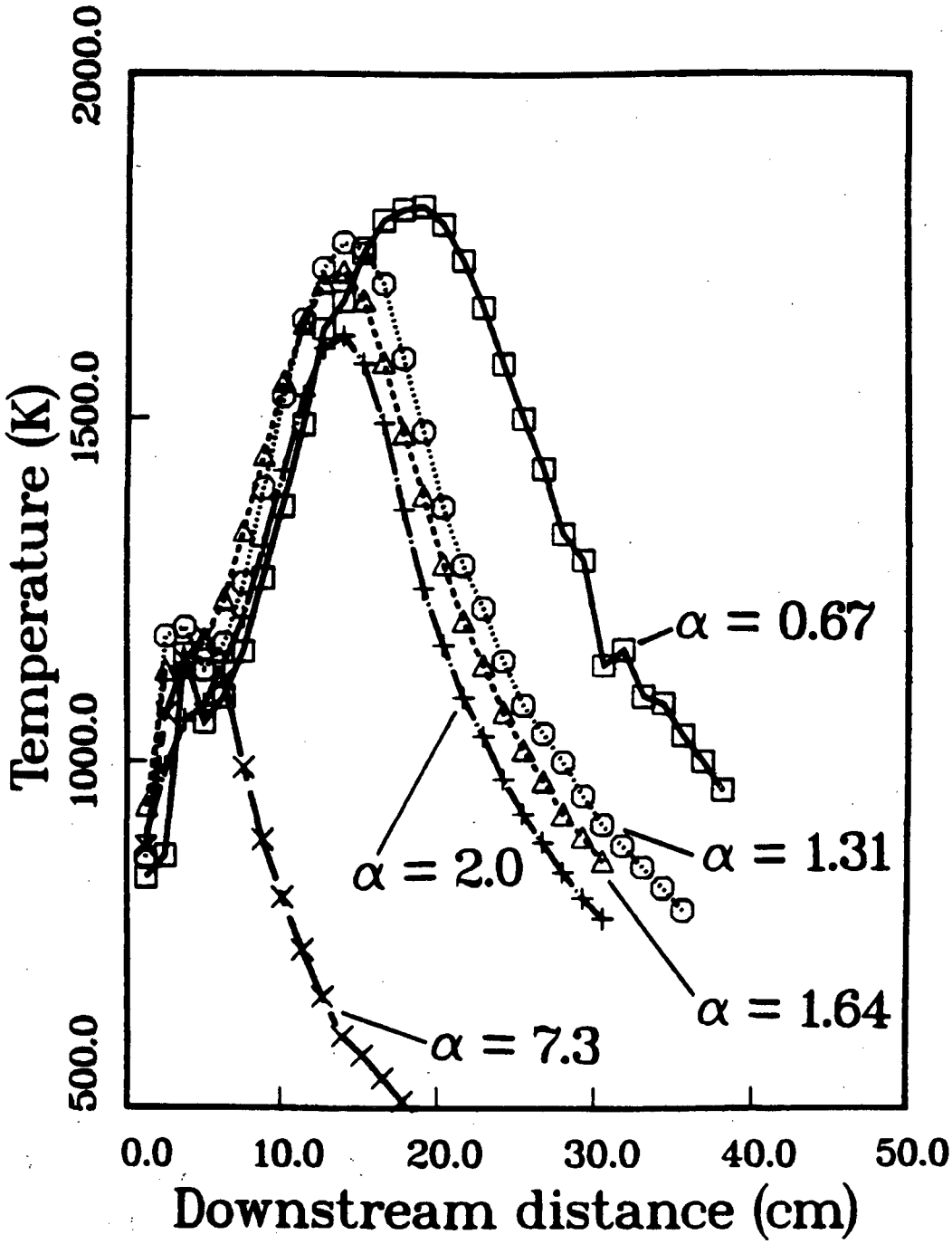

Figure 3-7. Centerline temperature profiles for hydrogen jet flames diluted with nitrogen. Jet initial diameter was 0.635 cm and the initial temperature was 200°C. The molar ratio of steam to hydrogen is shown above each set of data; other parameters are given in Table 3-2.

Table 3-2. Jet Parameters for Centerline Temperature Measurements

α	T_o (K)	U (m/s)	R	F	T_f (K)
			Pure hydrogen		
0	490.	68.4	1.5×10^3	3.6×10^3	2381
			Steam dilution		
0.67	498.	115.8	7.4×10^3	5.1×10^4	2060
0.87	483.	205.4	1.5×10^4	1.9×10^5	2000
1.38	489.	162.6	1.4×10^4	1.5×10^5	1800
5.36	485.	80.3	9.8×10^3	5.8×10^4	980
			Nitrogen dilution		
0.67	495.	116.0	8.1×10^3	8.6×10^4	2138
1.31	487.	159.7	1.5×10^4	2.6×10^5	1900
1.64	483.	180.8	1.8×10^4	3.8×10^5	1830
2.0	482.	134.5	1.4×10^4	2.4×10^5	1720
7.3	482.	102.0	1.4×10^4	2.3×10^5	990

$\alpha =$ ratio of moles of diluent to moles of hydrogen in the jet.

$T_o =$ Jet exit temperature

$U =$ Jet exit velocity

$R =$ UD/ν, Reynolds number of jet exit flow

$F =$ $\rho U^2/g\Delta\rho D$, Froude number of jet exit flow.

$T_f =$ temperature of a stoichiometric mixture of jet and atmosphere fluid burned under adiabatic, constant-pressure conditions.

Nominal ambient pressure 630 torr, nominal ambient temperature 300 K, jet exit diameter $D = 0.635$ cm

Note that the Froude number can also have a dramatic effect on the temperature profiles. The lower the Froude number, the higher the entrainment rate for a given source flow rate. This results in lower temperatures and shorter flames for given jet-atmosphere parameters (composition, flow rate, and source size). A convenient measure of the magnitude of this effect is the ratio of the amount of atmosphere entrained by the flame (*i.e.*, the entrained atmosphere flow rate at the end of the flame) to that required for complete combustion of the jet fuel. This quantity can be estimated for jets from the scaling laws presented in Chapter 1 and direct measurements are available for plume fires.[7] For a laminar diffusion flame, this ratio is one; for turbulent jets ($Fr \geq 10^4$), the ratio is about 3; for buoyant plumes ($Fr \leq 4$), the ratio has been measured to be 10-15. The large value of this ratio for buoyant flows is consistent with the scaling laws for plumes and measured flame heights. An important implication is that the maximum average temperature increase at the top of a plume fire will be a factor of 3-5 lower than the temperature rise in the equivalent jet flame.

A final example of what can be obtained by combining temperature measurement and photography is shown in Figure 3-8. The temperature was recorded at about 200 points on a rectangular grid covering a planar, vertical cross section of the flame. This array of measurements was then interpolated to produce the contour plot of the isotherms shown in Figure 3-8. The sampled region covered an area 35 cm long by 5 cm wide with the left-hand boundary located at the centerline of the flame jet and the bottom located 2.54 cm above the jet exit. A mirror image of the contours was produced on the plot to aid the viewer in visualizing the temperature field. An outline of a time-exposure flame recorded by the method described previously is superimposed on the isotherms.

This particular flame was obtained from a jet with a hydrogen flow rate of 71 slpm and a steam flow rate of 37 slpm through a contoured nozzle 0.635 cm in diameter at the exit. The gases and piping were at a temperature of 540°C and the flame was ignited externally by a spark source. At this temperature, the flow was just below the autoignition limit and would reignite spontaneously if the flow was restarted immediately after being shut off. Apparently, the nozzle heated up above the autoignition temperature due to heat transfer from the flame. However, if the flow was left off for a longer period of time (greater than 1 minute), spontaneous reignition would not occur since the nozzle would have time to cool below the autoignition limit. The subject of autoignition is discussed further in Appendix B.

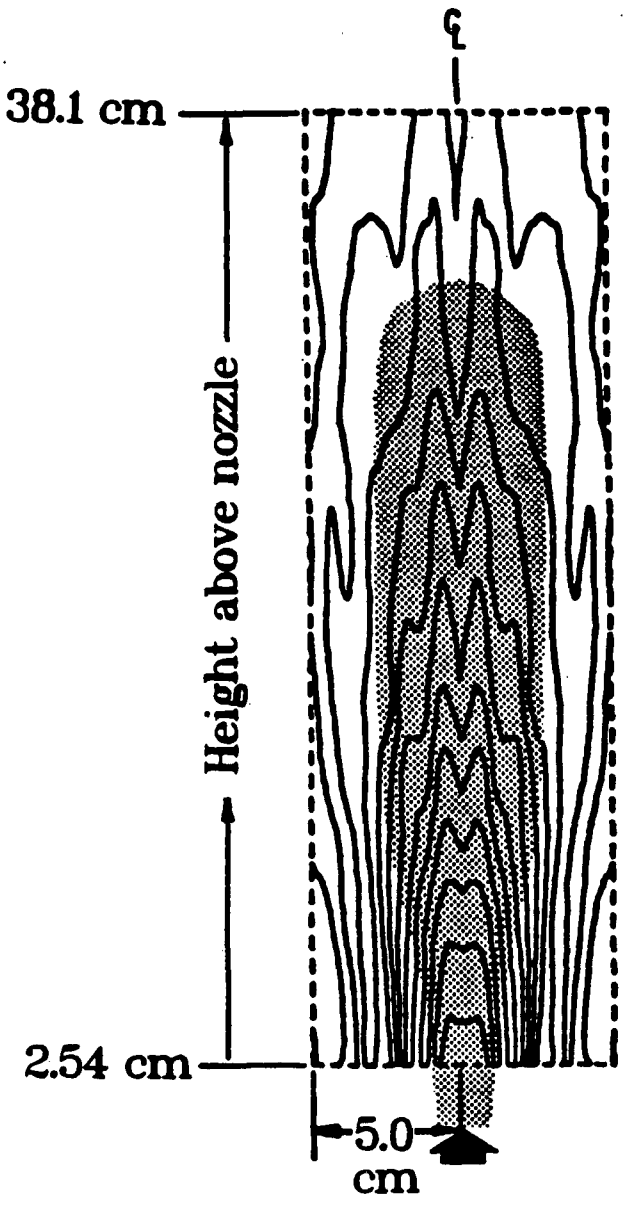

Figure 3-8. Comparison of visually determined flame shape to average temperature profile determined by thermocouple probe measurements. Isotherms are 100°C apart and start at 1400°C closest to the nozzle. The jet was at 540°C and was composed of 34% steam and 66% hydrogen. The exit velocity was 203 m/s, Reynolds number 1.6×10^5, and Froude number 7.7×10^4.

3.3 Jets

The basis for all flame-length expressions for jets is that at any given downstream location, a constant fraction of the entrained fluid has been molecularly mixed and reacted with the original jet fluid. This observation was first made by Hottel[1] and has recently been extended by Dimotakis, *et al.*[2] Irrespective of whether the flow is combusting or not, this idea appears to apply to all reacting flows in which the reaction kinetics are sufficiently fast.

A particularly simple correlation for the flame length has been deduced from data on many types of reacting flows.[3] After correcting for the effects of the virtual origin of the jet, the flame length is found to be linearly proportional to the product of the equivalence ratio ϕ and the effective jet exit diameter, $(\rho_o/\rho_\infty)^{1/2}D$,

$$L = 10\phi\left(\frac{\rho_o}{\rho_\infty}\right)^{1/2} D \qquad (3-1)$$

Here, the equivalence ratio ϕ is defined to be the mass ratio of air to jet fluid in a stoichiometric mixture. For example, pure hydrogen jets exiting into cold air have a value of ϕ equal to 35 and the square root of the density ratio is equal to 0.26. Inserting these values into Eq. (3-1) results in a predicted flame length of 90 jet diameters. Typical visual lengths, observed in our experiments with a 0.635 cm diameter nozzle and a flow rate of 75 slpm were about 80 diameters. The difference is due to the imprecise method of determining flame lengths by visual observation and the effect of buoyancy on pure hydrogen flame jets at this flow rate.

Variation of flame length with jet and atmosphere dilution can also be calculated with this model. The simplest case is an atmosphere consisting of a mixture of air and steam (this will occur at the beginning of an experiment or burn inside a containment), with the ratio of moles of steam per mole of air defined to be δ. If the ratio of moles of diluent to moles of hydrogen in the jet fluid is α, then the equivalence ratio is

$$\phi = \left(\frac{34.3 + 1.19 M_D \delta}{1. + 0.5 M_D \alpha}\right) \qquad (3-2)$$

where M_D is the diluent molecular weight. If the flame is inside a closed vessel, the atmosphere will become vitiated as the burn proceeds, and the variation of

the gas composition will have to be accounted for by introducing an additional parameter (for example, the nitrogen/oxygen mole ratio) in Eq. (3-2).

The density ratio will also depend on the dilution parameters α and δ and the ratio of jet and atmosphere temperature. For subsonic jets,

$$\frac{\rho_o}{\rho_\infty} = \frac{M_o T_\infty}{M_\infty T_o} \qquad (3-3)$$

where M is molecular weight, T is temperature (absolute), the subscript 0 denotes jet exit conditions, and the subscript ∞ denotes atmosphere conditions. The jet molecular weight can be calculated from

$$M_o = \frac{M_{H_2} + \alpha M_D}{1+\alpha}. \qquad (3-4)$$

The atmosphere molecular weight can be calculated by a similar formula,

$$M_\infty = \left(\frac{M_{air} + \delta M_D}{1+\delta}\right). \qquad (3-5)$$

Substituting Eqs. (3-2) through (3-5) into Eq. (3-1), we obtain the complete flame-length expression for hydrogen-diluent jet flames in an air-diluent atmosphere:

$$\frac{L}{D} = 23.8\sqrt{\left(\frac{T_\infty}{T_o}\right)\left(\frac{1+\delta}{1+\alpha}\right)\left(\frac{M_{air} + \delta M_D}{M_{H_2} + \alpha M_D}\right)} \qquad (3-6)$$

Normalized flame lengths (L/D) predicted by Eq. (3-6) are shown below in Figures 3-9 and 3-10. In Figure 3-9, the variation of flame length with both jet temperature and jet dilution (with steam) are shown for fixed conditions in the atmosphere, $T_o = 300$ K and pure air. Variation of flame length with dilution in the atmosphere is shown in Figure 3-10 for fixed jet conditions, $T_o = 300$ K, and pure hydrogen.

Both effects of flame shortening with jet dilution and flame lengthening with atmosphere dilution have been observed in experiments at NTS and in the small-scale facility at SNLA. Our initial attempt (reported in Reference 4)

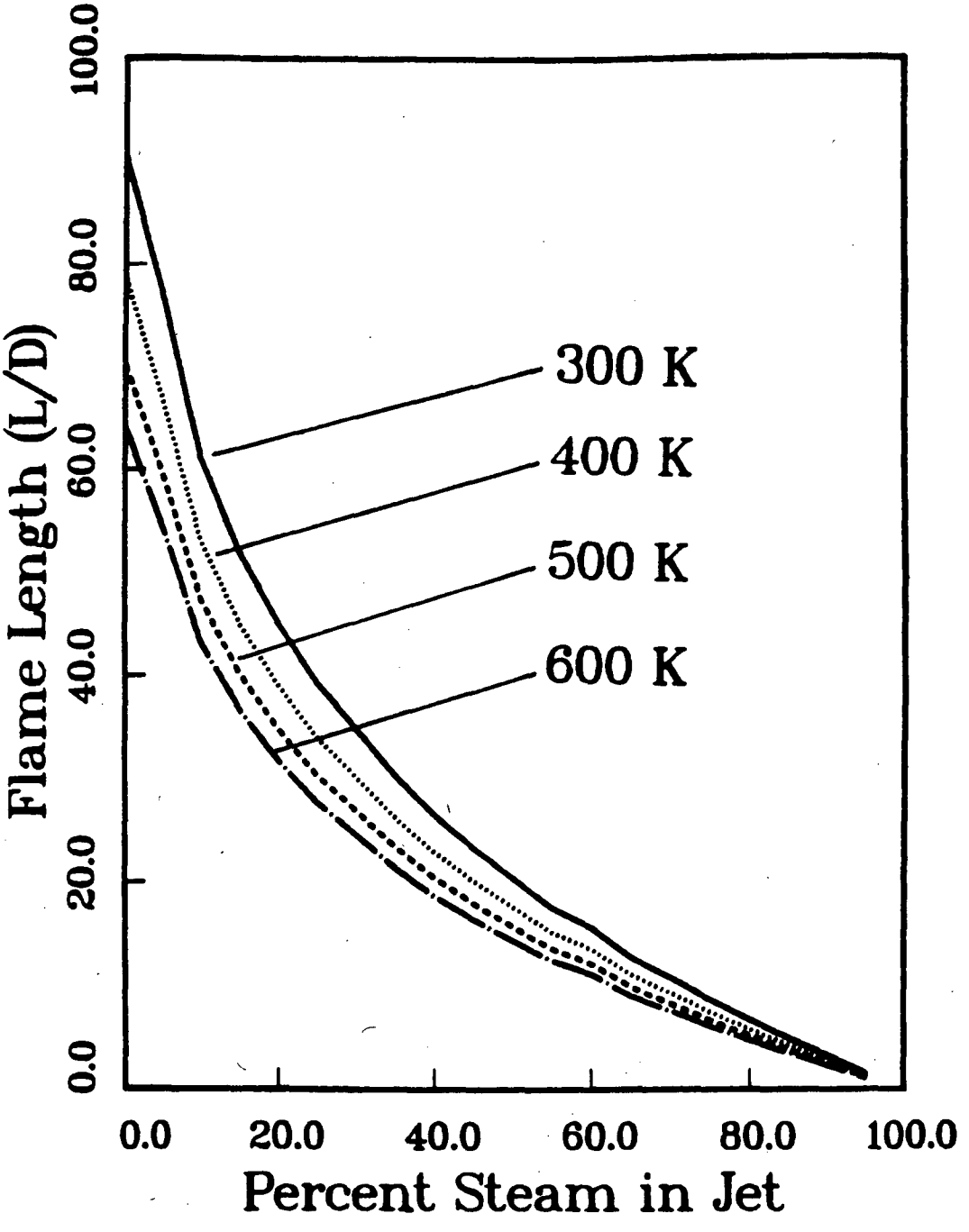

Figure 3-9. Predicted variation in flame length with jet dilution for hydrogen-steam jets in an air atmosphere at 300 K. The four curves shown correspond to jet temperatures of 300, 400, 500, and 600 K, respectively from top to bottom.

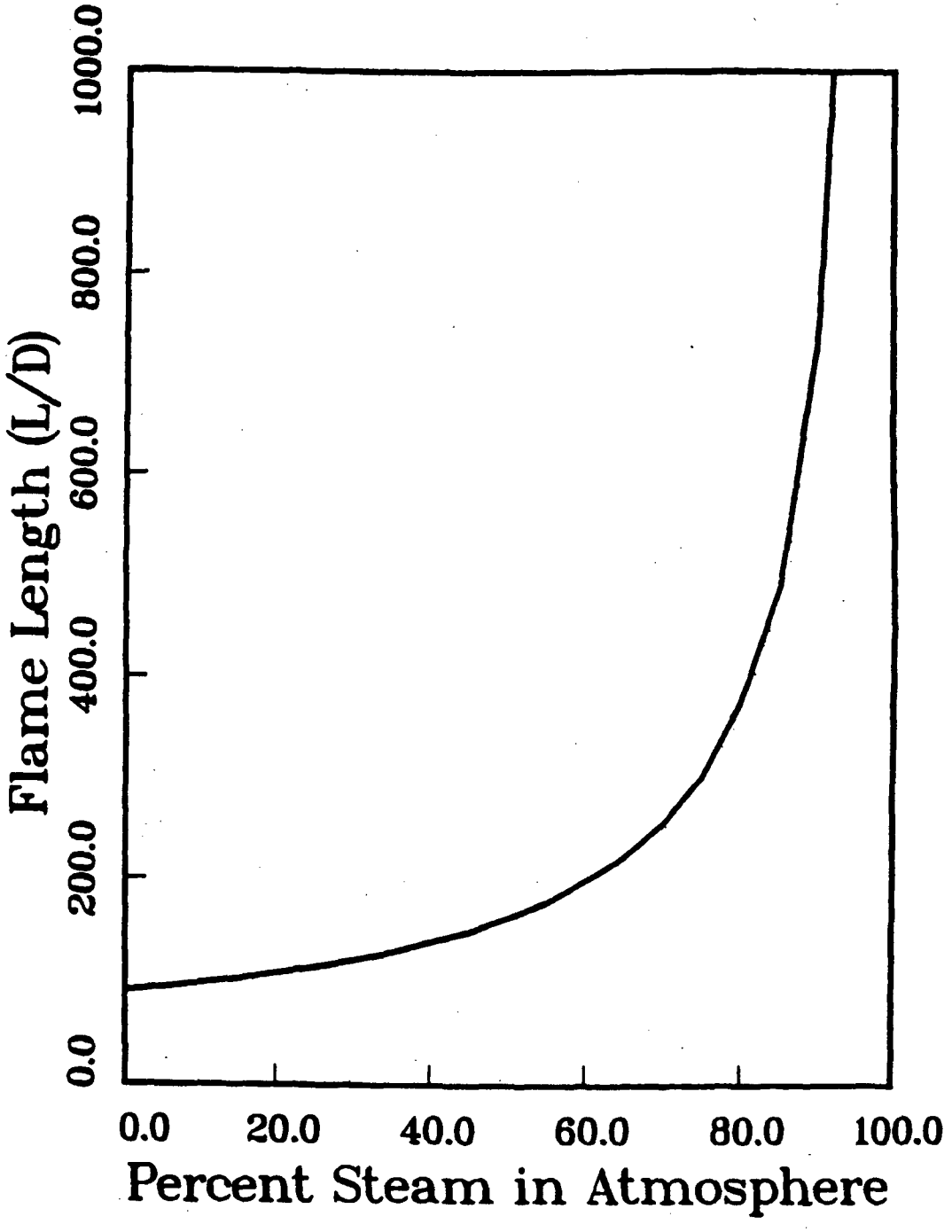

Figure 3-10. Predicted variation of flame length with the dilution of the atmosphere with steam. The jet is pure hydrogen and both jet and atmosphere are at 300 K.

to determine flame length was from time-exposure photographs taken with the method described in the previous section. In order to obtain sufficient luminosity to record an image, the jet was seeded by spraying a small amount of commercial window cleaner near the base of the flame. Unfortunately, the seeding technique was not reproducible enough to obtain reliable data. Later on, we found that infrared-sensitive television cameras could be used to directly visualize the hotter flames without seeding. However, all techniques based on visualization of steam luminosity or radiation from impurities (the two main sources of visible or infrared radiation in these flames) suffer a common deficiency. The flame length defined by these methods does not indicate the actual point where the chemical reaction ceases but rather the point where the average temperature drops below a certain value.

To avoid the problems associated with visual methods of flame length determination, a more quantitative technique based on centerline temperature profiles was used. This technique is based on the results of Becker and Yamazaki[5], who showed that the distance from the jet exit to the peak in the centerline flame temperature was proportional to the visual flame length.

Using the data shown in Figures 3-5 and 3-6, we have evaluated the flame length as determined by the temperature maximum in the flow. These data are plotted together with the theory discussed above in Figure 3-11 (for steam dilution) and Figure 3-12 (for nitrogen dilution). The trend shown with increasing dilution is correctly predicted; the quantitative discrepancy may be due to our method of determining flame length.

An empirical correlation for flame length was developed by Becker and Liang[6] to account for the effects of both buoyancy (Froude number) and viscosity (Reynolds number). For high Froude and Reynolds numbers, their expression reduces to one quite similar to Eq. (3-1). The difference is that their expression is multiplied by a factor β

$$\beta = \sqrt{\frac{M_\infty T_S}{M_S T_\infty}}, \qquad (3-7)$$

where T_s and M_s are the temperature and molecular weight of a stoichiometric mixture of jet and atmosphere fluid. Their expression also has a slightly different dependence on the stoichiometric coefficient,

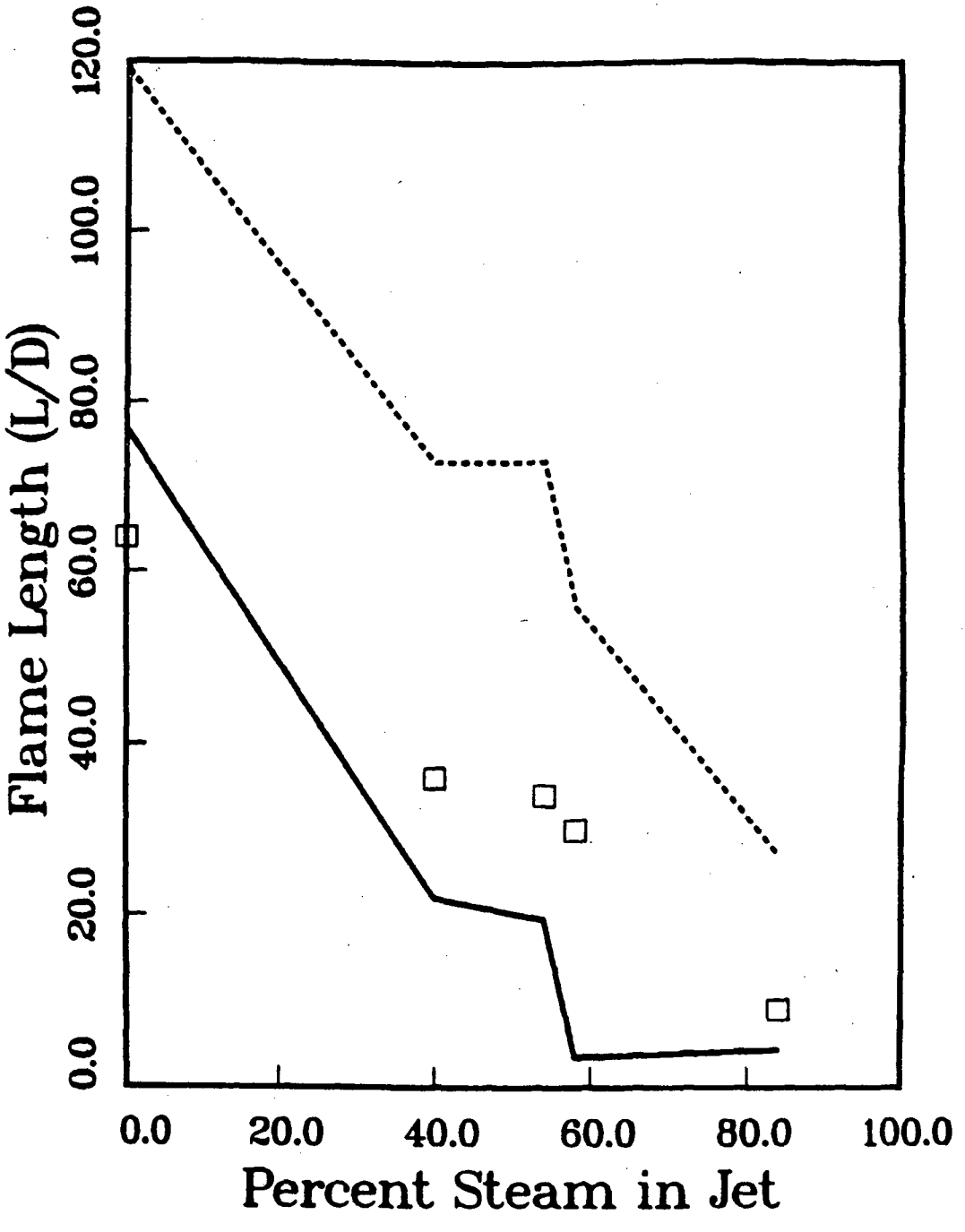

Figure 3-11. Comparison of thermal flame lengths (from Figure 3-6) with the simple theory (solid line) and the correlation of Becker and Liang (dotted line).

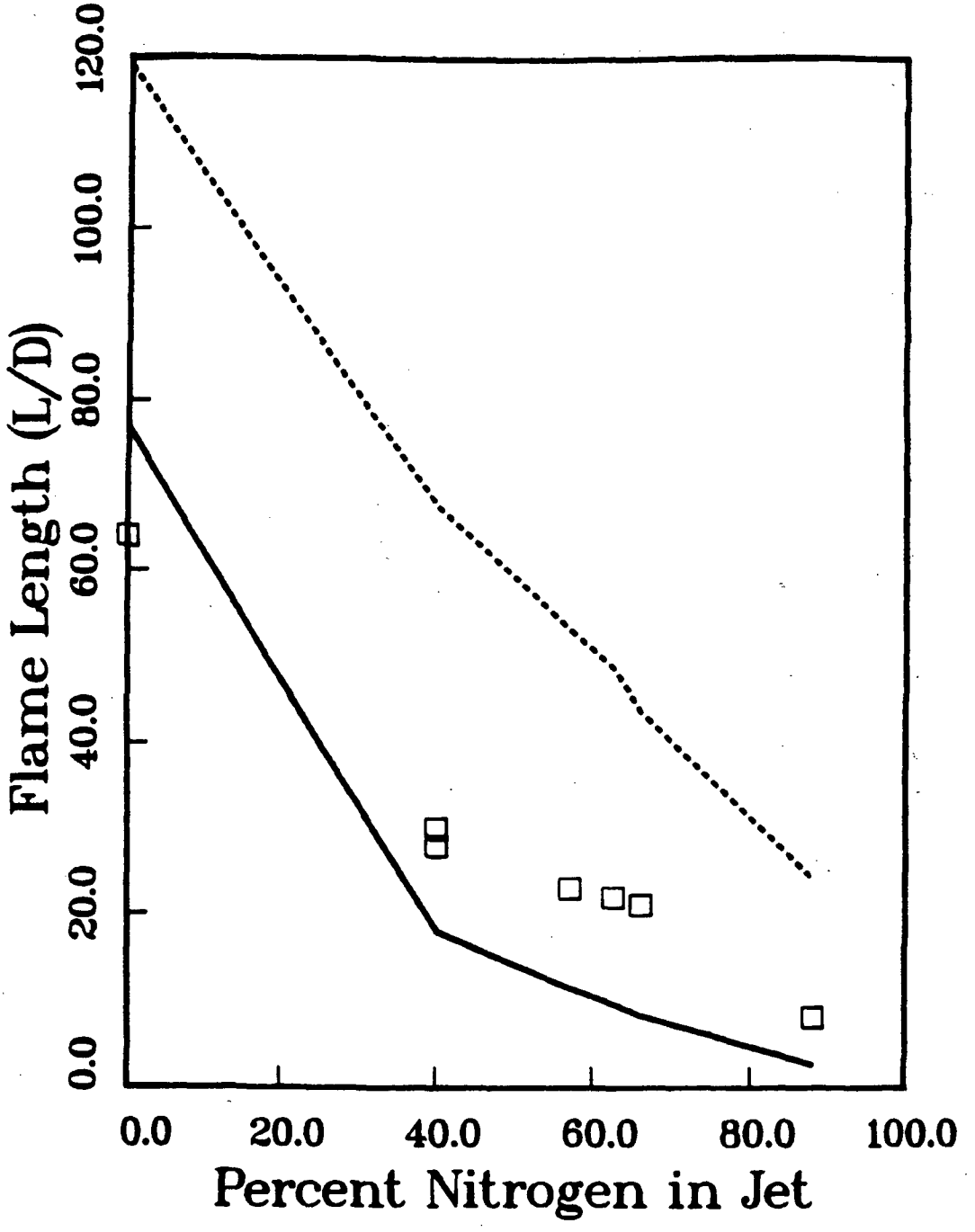

Figure 3-12. Comparison of thermal flame lengths (from Figure 3-7) with the simple theory (solid line) and the correlation of Becker and Liang (dotted line).

$$L_\infty = 13(1+\phi)\left(\frac{\rho_o}{\rho_\infty}\right)^{1/2}\beta D. \qquad (3-8)$$

Typical values of β vary between 1 and 3 depending on the amount of dilution in the jet. This results in predicted flame lengths which are proportionally larger than those predicted by Eq. (3-1). Becker and Liang explain this on the grounds that all previous investigations have not been truly in the forced convection regime. The figure of merit that they propose for determining the relative importance of buoyancy is denoted ξ_L and is defined by

$$\xi_L = \frac{L}{D}F^{-1/3}. \qquad (3-9)$$

Using data from a number of sources, they have developed a composite empirical expression for flame length. For values of ξ_L less than 20 (intermediate to forced convection regime), they recommend the approximate relation

$$L = \frac{L_\infty}{(1+0.12\xi_L)^{3/2}}. \qquad (3-10)$$

The values of L given by Eq. (3-10) are appropriate for visually-determined flame lengths. As discussed in Becker and Yamazaki, flame lengths based on the peak centerline temperature are about one-half the value of those determined visually. To account for this difference, the values predicted by Eq. (3-10) are divided by two before plotting in Figures 3-11 and 3-12. The agreement with the data is somewhat better than the previously discussed theories. However, this may be fortuitous, and the only strong conclusion we can draw from these results is that the influence of buoyancy should be carefully considered. Equation (3-10) is probably not the definitive flame-length expression and this problem continues to be an active area of research.

3.4 Plumes

The flame length of plume fires has a completely different scaling than that for jet fires. This is a consequence of the vast differences in the entrainment mechanisms and scaling laws for jets and plumes. Plume-like fires have a length which is independent of the fire diameter (for tall enough fires) and rate of diluent addition to the fuel flow.

For plume fires with heights greater than 4 times the source diameter, the flame length can be correlated with the heat release rate Q, by the following dimensional expression:

$$L = 0.18Q^{2/5}; \qquad (3-11)$$

where L is in meters and Q is in kW. This formula and the implied scaling has recently been verified for a wide range of fire strengths and diameters by Zukoski,*et al.*[7] While this is a dimensional expression, it does appear to correlate the data independent of the type of fuel. One difficulty in buoyant plume height theory is that there is no good theory or even empirical support for a nondimensional version of Eq. (3-11). However, the form of Eq. (3-11) yields the correct scaling with buoyant forces, *i.e.*, Froude scaling, a point discussed further below.

The lack of a nondimensional form for Eq. (3-11) limits our ability to predict several phenomena of interest. For example, Eq. (3-11) does not have any dependence on the diluent content of the atmosphere or the jet. Clearly, if the amount of dilution is large enough, there must be an effect. Experimental observations on this phenomena are sparse, what little exists (*cf.* Zukoski,*et al.*) suggests that diluents have a much weaker effect on plumes than on jets. One possible explanation (supported by studies of the fluid dynamics of plume fires) is that the fluid dynamics plays a much more important role in plume fires than in jet flames.

If the fire is too short, less than 4 diameters high, a dependence of flame height on source diameter is found. A simple expression for correlating data on flames in this regime is given by Zukoski:

$$L = 0.026\left(\frac{Q}{D}\right)^{2/3} \qquad (3-12)$$

where again, Q is the fire strength in kW and D is the source diameter. As in the previous case, there is no agreement on the appropriate method for presenting this correlation in nondimensional form. This expression is also consistent with Froude scaling. That is, for fires of different scales (physical dimensions) but at the same Froude number, the flame-length scales linearly with the geometric scale factor.

We have not carried out any experiments on hydrogen-steam-air plume fires with the specific intention of testing the relations presented above. At the present time, the only hypothetical accident in which plume fires would be the major form of combustion is a LOCA in a BWR Mark III nuclear plant. In this reactor, the hydrogen-steam mixture would probably be released through spargers located beneath the surface of the suppression pool. The gas mixture would bubble to the surface, mix with the containment atmosphere, and then possibly burn as a diffusion flame.

Preliminary experiments conducted by EPRI[8] indicate that under certain conditions, diffusion flames do indeed exist above the surface of the pool. These flames are highly unsteady and the surface of the pool is violently agitated by the gas bubbling to the surface. Visually, the flames appear to be quite different from the standard burner-produced plume fires. We believe that this is due to the distributed and unsteady nature of the source.

The containment atmosphere is probably entrained by each individual bubble of gas as it bursts at the pool surface. This localized entrainment is quite different than the entrainment that occurs at the outer edge of the burners used to produce the usual laboratory plume fires. For these reasons alone, we believe that the standard correlations Eqs.(3-11) and (3-12) are inadequate to predict the behavior of plume fires above the suppression pool in a BWR Mark III nuclear plants. There are other difficulties in applying the conventional plume correlations, due to the confining geometry of the region above the suppression pool.

3.5 Stability

For a fixed jet composition and nozzle diameter, a stable diffusion flame will exist only if the flow rate is less than a critical value. This effect has been known and studied extensively since the beginnings of combustion science; a general discussion can be found in Lewis and von Elbe.[9]

The existence of a stability boundary is due to the competing effects of chemical reactions and quenching processes. Quenching processes of importance

include: heat conduction and species diffusion to solid surfaces; "stretching" of the flame zone by velocity gradients in the flow; and, disruption of the flame zone by strong turbulent fluctuations. Any or all of these processes, if strong enough, can cause the chemical reactions to cease and the flame will no longer exist.

A simple method of quantifying the competition between chemical reactions and quenching processes is to compare the characteristic time scales.† For diffusion flame instability, referred to as blowoff or blowout, the quenching process is due to the rapid turbulent mixing of the cold, entrained atmosphere with the hot products of combustion. If the mixing occurs rapidly enough, the gas temperature will be reduced below the ignition temperature before the chemical reactions become self-sustaining.

The characteristic times for each process can be computed as follows. For chemical reactions, the simplest approach is to use the elementary burning velocity theory of Mallard and Le Chatelier.[10] The result of this theory is to relate burning velocity S to the thermal diffusivity κ and the characteristic reaction time T_r (which is identical to the reciprocal of the reaction rate):

$$S = \sqrt{\frac{\kappa}{T_r}}. \qquad (3-13)$$

Using the measured values of the burning velocity S and the known values of the thermal diffusivity, the characteristic reaction time can be determined. For the characteristic mixing time, a simple dimensional approach is used. If the local velocity is U and the characteristic flow dimension is B, then the characteristic time is

$$T_m = \frac{B}{U}. \qquad (3-14)$$

Fortunately, in jet-like flows, there exists a well-defined scale length (the local jet width) and scale velocity (the downstream component of the velocity on the centerline). The criterion for the stability boundary is that

---

†For this point of view and the origin of many ideas discussed below, I am indebted to Gene Broadwell of the California Institute of Technology.

$$T_r \approx T_m \qquad (3-15)$$

In the following section we will explore the implications of these ideas and compute the stability boundary for selected hydrogen-steam jet flames. These results will be compared to data and an empirical correlation of Kalghatgi.[11]

3.6 Blowout Diameter and Velocity

Experimentally, it is observed that for fixed jet and atmosphere composition, a diffusion flame from a given diameter source will remain stable until the jet velocity is increased beyond a certain point. For a fixed jet velocity, the flame is stable until the diameter is decreased below a certain value. This velocity-diameter relationship can be summarized as follows: For fixed jet and atmosphere compositions, the blowout (blowoff) velocity and diameter are linearly related as long as the flow is subsonic.

The instability of a diffusion flame can occur in two steps, hence the distinction is sometimes made between blowoff and blowout. The first step is called lift-off; as the jet velocity is increased, the base of the flame (the start of the chemical reaction) lifts off the burner and becomes fixed at some distance downstream. This distance to the base of the flame increases as the flow rate is increased until the blowout limit is reached. No stable diffusion flame can exist for velocities exceeding the blowout limit. If the burner diameter is small enough, the flame does not lift off, but directly blows off when the critical conditions (blowout limit) are exceeded.

There is also a hysteresis effect in the flame lift-off phenomena. If the jet flow rate is first increased and then decreased below the critical value for lift-off, the flow rate at which the flame base reattaches to the burner is different than the lift-off value. These phenomena and other experimental observations about diffusion flames are discussed in References 11, 12, and 13.

The preceding remarks are in reference to the behavior of subsonic jets and flames. However, as indicated in the introduction, most postulated accidents in PWR's involve highly underexpanded supersonic jets. Soviet scientists have shown that for supersonic jets, stability is restored if the pressure ratio at the jet exit is increased to a large enough value. [14]

In addition, they report the existence of a limiting nozzle diameter for blowoff. For jets with exit diameters greater than the limiting diameter, no

blowout was observed. In other words, the flame is absolutely stable if the jet exit diameter is larger than a certain size. The value of the critical diameter will depend on both the jet and atmosphere composition; for pure hydrogen jets in air, the critical diameter is about 1 mm. We consider the existence of a limiting diameter for blowoff to be exceedingly important to analyses of diffusion flames inside reactor containments. For this reason, we recommend (see Section 5.1 below) that this phenomenon be the subject of further study.

A schematic diagram of the stability boundaries of a diffusion flame is shown in Figure 3-13. This velocity-diameter plot is based on the ideas presented above and exhibits the major qualitative features of the stability problem. In order to make this presentation quantitative, a more detailed discussion of the material presented in the previous section is in order. First, we will discuss the determination of the slope of the velocity-diameter relation for subsonic jets.

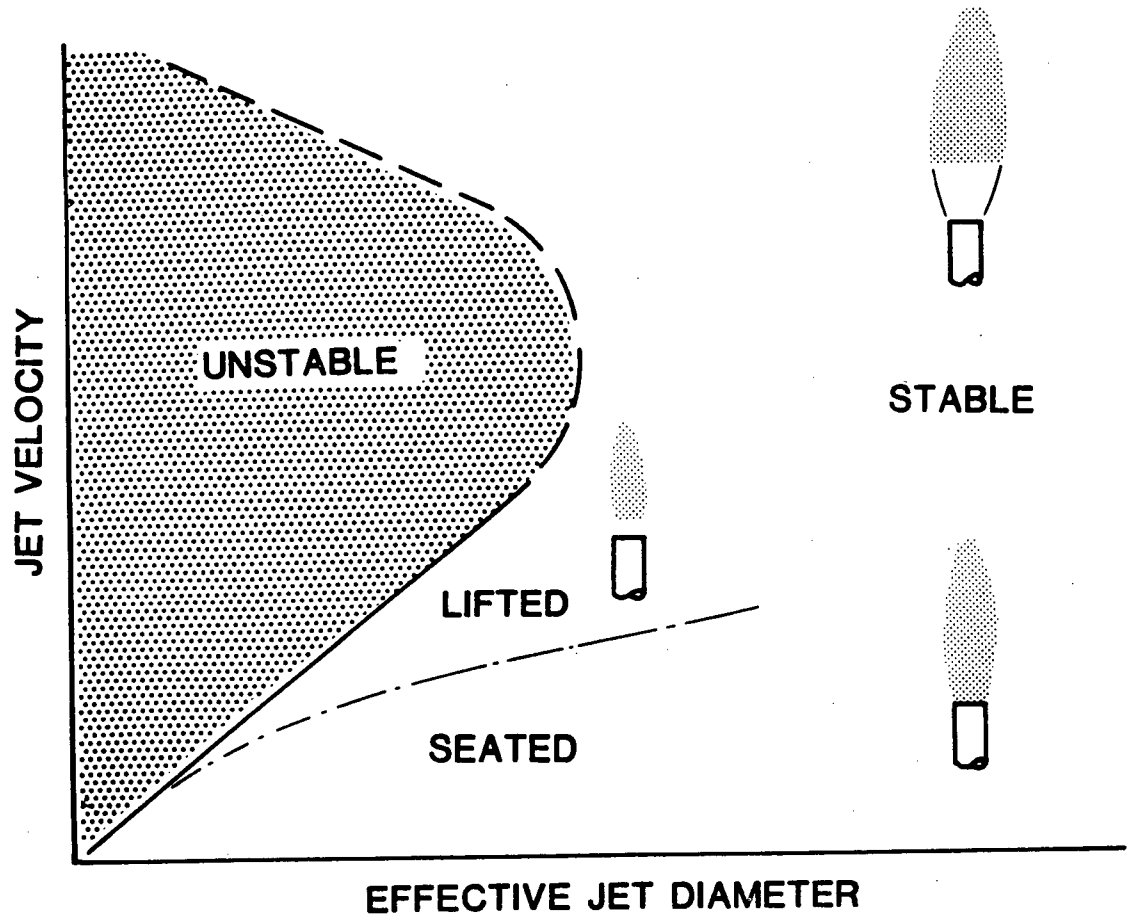

Figure 3-13. Schematic diagram of the region of instability (blowoff) for a turbulent diffusion flame.

The basic relation is given in Eq. (3-15), which states that at blowoff, the characteristic mixing time scale is of the same order as the chemical reaction time scale. Evaluation of these time scales for the specific case of hydrogen-air-steam diffusion flames is discussed below.

A characteristic jet velocity and width are needed to evaluate the mixing time scale. These values can be obtained from the standard jet scaling relations (*i.e.*, Table 1-1) if the location of the flame base at blowoff is known. Since it is not necessary to know this location exactly, we will only suppose that it is proportional to the flame height.

The characteristic chemical reaction time scale is calculated using the Mallard Le Chatelier burning velocity formula Eq. (3-13). While calculating the diffusivity is straightforward, determining the burning velocity is somewhat more involved. Lacking any experimental data at high steam concentrations, we employ a calculational technique developed by Smooke.[15] More details and results of these calculations are given in Appendix A.

After substituting the scaling relations for jet velocity and width (evaluated at the flame tip), the following formula is obtained for the ratio of jet velocity to exit diameter at blowoff:

$$\frac{U}{D} = C\frac{S^2}{\kappa}\phi^2\left(\frac{\rho_o}{\rho_\infty}\right)^{1/2} \qquad (3-16)$$

where C is an empirically-determined constant. Using the hydrogen-air blowoff data of Kalghatgi, the constant is found to be approximately 1. The critical straining rate $\left(\frac{U}{D}\right)$ at blowoff for hydrogen-air diffusion flames is found to be 2 x 10^6 sec^{-1}.

Note that Eq. (3-16) has the same form as that used to correlate the data on blowoff of laminar diffusion flames,

$$\frac{U}{D} = C'\frac{S^2}{\kappa} \qquad (3-17)$$

except that the constant C' has a value of about 1 for laminar flames and a value of 200 for turbulent flames. Also, there is no dependence of the constant C' on either the stoichiometry or the density ratio for the laminar case. In the case of laminar flames, the interpretation of the mechanism is also somewhat different.

The quenching occurs just downstream of the burner exit and is due to straining of the flame sheet by the velocity gradient in the gas flow near the burner wall.

A similar formula to Eq. (3-16) was derived by Kalghatgi,[11] but the functional dependence on equivalence and density ratios is different. Further, we feel that the arguments he uses to arrive at this result are less satisfying; the motivation being more in the nature of an empirical correlation than based on a physical model. In addition, he introduces the concept of a Reynolds number based on the flame length, an idea which probably has little relevance for the high-Reynolds-number flows under consideration in the present study.

The left-hand side of Eq. (3-16) is a function of the jet and atmosphere composition and thermodynamic state only. Therefore, once we are given these conditions, the critical straining rate at blowoff can be uniquely determined for any size jet. Using flame speeds for stoichiometric hydrogen-air-steam mixtures given in Appendix A, we have calculated the critical straining rates at 200°C for steam-diluted hydrogen jets into room-temperature air. The results of these calculations are presented in Figure 3-14.

For postulated reactor accidents, a more convenient way to present these data is to show the stability boundary for a fixed jet exit diameter as a function of the hydrogen and steam flow rates. Stability boundaries are shown in Figure 3-15 for a 5-cm diameter jet as a function of hydrogen and steam mass flow rates (kg/s). Note that in both Figure 3-14 and 3-15, the flame is shown to be absolutely unstable for diluent/hydrogen ratios of greater than 9:1 (molar). This effect is due to the very low flame temperature for these mixtures (less than 900 K), resulting in the reaction rate and flame speed becoming very small. In essence, the mixture has reached a "flammability limit" and self-sustaining combustion will cease at this point.

In order to calculate the exact location of this limit, it will be necessary to use a much more refined theory of turbulent quenching than given here. The limits shown in Figures 3-14 and 3-15 are therefore rather arbitrary and should not be taken too seriously. In fact, with a certain amount of care, diffusion flames can be produced in the laboratory with values of α greater than 9.

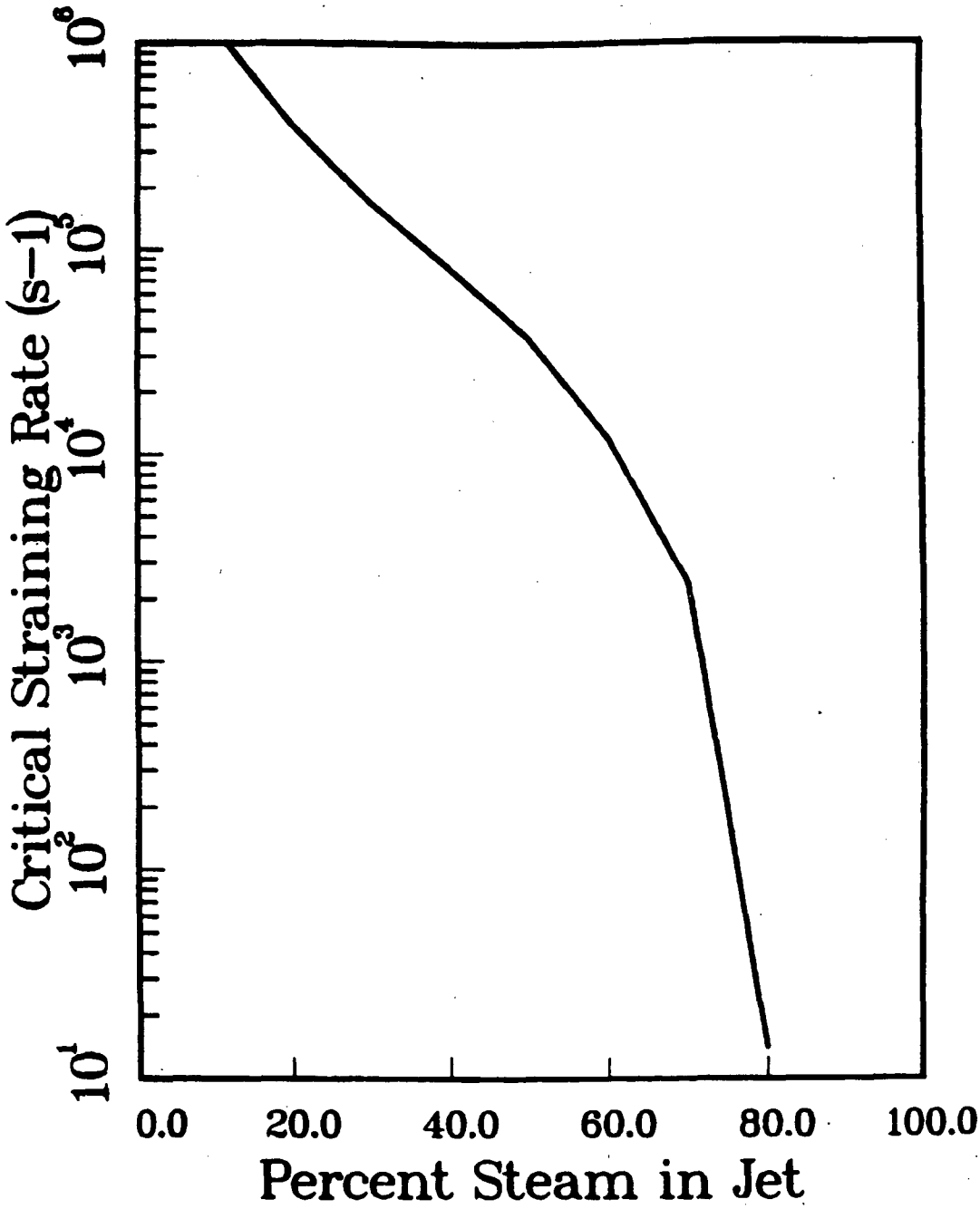

Figure 3-14. Calculated critical straining rate at blowoff (U/D) *vs* the steam mole fraction in the jet for 200°C hydrogen-steam flame jets in a room-temperature atmosphere.

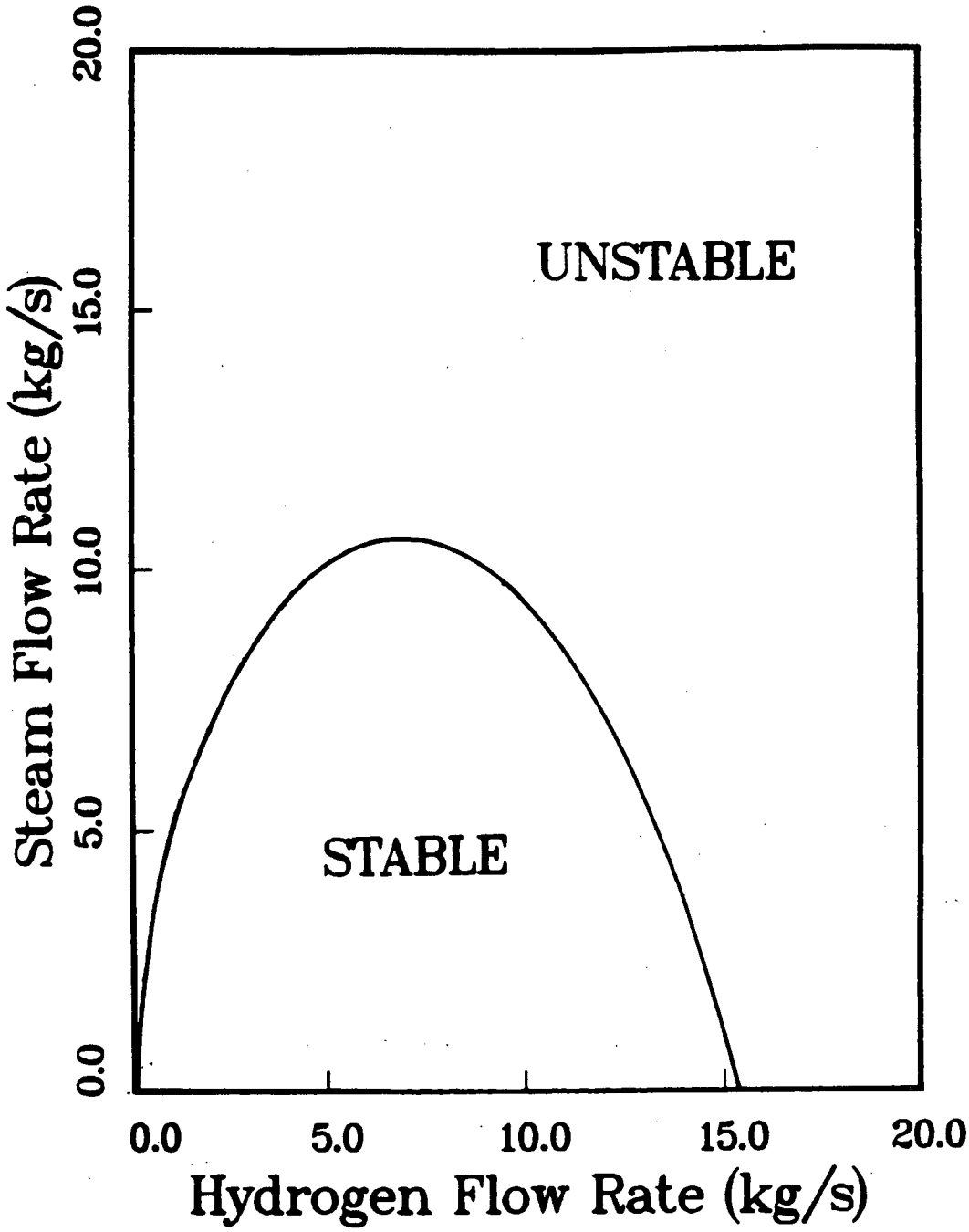

Figure 3-15. Calculated stability boundaries for a 5 cm diameter jet as a function of hydrogen and steam flow rates. Jet fluid is at 200°C, the atmosphere is air at room temperature.

References

1. H. C. Hottel, *Burning in Laminar and Turbulent Fuel Jets,* Fourth Symposium (International) on Combustion, **97** (1953).

2. P. E. Dimotakis, J. E. Broadwell, and R. D. Howard, *Chemically Reacting Turbulent Jets,* AIAA Paper 83-0474 (1983).

3. J. E. Broadwell, *A Model of Turbulent Diffusion Flames and Nitric Oxide Generation,* TRW final report, EERC contract No. PO 18889 (1982).

4. J. E. Shepherd and O.B. Crump, Jr., *Hydrogen-Steam Flame-Jet Experiments,* **Proceedings of the Second Workshop on the Impact of Hydrogen on Water Reactor Safety, Albuquerque, NM,** eds., M. Berman and L. Thompson, available as Sandia National Laboratories Report SAND82-2456 (1982).

5. H. A. Becker and S. Yamazaki, *Entrainment, Momentum Flux and Temperature in Vertical Free Turbulent Diffusion Flames,* Combustion and Flame **33,** 123-149 (1978).

6. A. Becker and D. Liang, *Visible Length of Free Turbulent Diffusion Flames,* Combustion and Flame **32,** 115-137 (1978).

7. E. E. Zukoski, T. Kubota and B. Cetegen, *Entrainment in Fire Plumes,* Fire Safety Journal **3,** 107-121 (1980).

8. Personal communication from John Hosler of EPRI.

9. B. Lewis and G. von Elbe, **Combustion, Flames and Explosions of Gases,** 2nd Edition, Academic Press, New York, NY (1961). See especially the discussion on p. 259.

10. I. Glassman, **Combustion,** Academic Press, New York, NY. See pp 66 and 101-104 (1977).

11. G. T. Kalghatgi, *Blow-Out Stability of Diffusion Flames: Part I: In Still Air,* Combustion Science and Technology **26,** 233-239 (1981).

12. D. A. Scholefield and J. E. Garside, *The Structure and Stability of Diffusion Flames,* **Third Symposium on Combustion, Flame and Explosion Phenomena,**102-110 (1949).

13. V. K. Baev and V. A. Yakasov, *Stability of a Diffusion Flame in Single and Mixed Jets,* Combustion, Explosion and Shock Waves **11,** 143-154 (1975).

14. Yu. M. Annushkin and E. D. Serdlov, *Stability of Diffusion Flames in Subsonic and Underexpanded Supersonic Gas-Fuel Streams,* Combustion, Explosion and Shock Waves **14,** 596-605 (1979).

15. M. D. Smooke, *Solution of Burner-Stabilized Pre-Mixed Flames by Boundary Value Methods,* Journal of Computational Physics **48,** 72 (1982).

4 Heat Transfer

The major effects of an unmitigated standing diffusion flame inside a reactor containment will be due to the high thermal load imposed on the structure and internal components. For example, a 1 kg/s hydrogen release rate is equivalent to 120 MW of thermal power. If all of this energy is directly deposited into the containment walls,† the average flux would be 1.7 W/cm^2 and the concrete surface temperature would rise 250°C in 15 minutes.

In fact, concrete may spall under these conditions[1] and bare electrical cables will pyrolize for fluxes above 2-4 W/cm^2 for these durations.[2] For components within or directly downstream of the flame, the fluxes could be an order-of-magnitude larger due to the convective transport from the high-velocity hot combustion products.

Heat transfer from a fire in an enclosure is a complex subject. Much of our current understanding is based on experiments to simulate fires within rooms of buildings or separate experiments designed to examine one particular aspect such as stagnation-point heat transfer from single, unconfined fires. Due to the motivation of these experiments, natural-convection dominated (plume-like) fires have been most extensively studied. By comparison, there is very little information available on flame jet heat transfer; although there is some fairly general information available on the associated problem of heat transfer from heated jets. We shall utilize some of this information in our discussion below.

We have identified three generic configurations which would produce the highest heat fluxes to the containment or internal components. In all of these configurations, the heat transfer is dominated by convection from the hot combustion products to an object (component) or structural element (ceiling, beam, *etc.*). As shown in Figure 4-1, these configurations are: grazing or side-on incidence of the fire; direct impingement or stagnation-point transfer to a flat surface; impingement on a pipe.

In addition to these configurations, there will always be an overall transfer of energy from the hot atmosphere to the boundaries (walls and other surfaces) of the containment. This large-scale convective heat transfer process is important in

†Simple models and experiments on room fires indicate that over 90% of the energy will be deposited in the walls after an initial transient.

determining the mean gas and wall temperatures and therefore the containment atmosphere pressure. In fact, the majority of the energy generated by combustion will be transported out of the gas by this process.

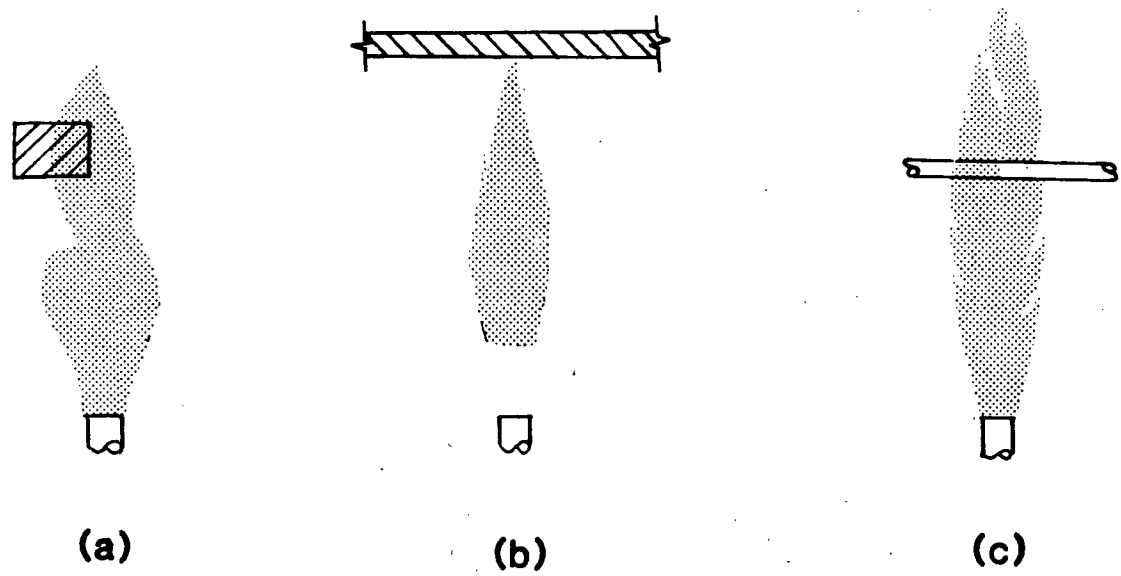

Figure 4-1. Generic configurations for direct heat transfer from diffusion flames: (a) side-on; (b) stagnation point; (c) cylinder cross flow.

While we recognize the importance of large-scale convective transport, our experimental experimental facility is not set up to address this problem. Other facilities such as the FITS tank at Sandia National Laboratories[3] or the dewar used in the EPRI/NRC tests at NTS[4] are better suited to that type of investigation. On the other hand, the studies described below should be representative of the most severe thermal environment that a component or surface directly in the flame would experience.

4.1 Jets

There have been several investigations of heat transfer from jet flames in the last two decades. Representative of these are: Anderson and Stresino,[5] who investigated flames impinging on flat and cylindrical surfaces; Connolly

and Davies,[6] who investigated heat transfer from premixed fuel-oxygen flames to a blunt body; and Kilham and Purvis,[7] who studied stagnation-point heat transfer from premixed hydrocarbon-oxygen flames. The last two investigations used transient calorimeters together with velocity measurements to correlate the heat transfer with a Stanton-Reynolds-number relationship. Primary emphasis in these studies was on the influence of chemical reactions (*i.e.*, recombination induced by the cool heat transfer probe) on heat transfer. Variation of the heat transfer with position in the flames was not considered in any detail.

Non-combusting jets have been investigated by Gardon and co-workers,[8,9,10] Huang,[11] and Donaldson, *et al.*[12] These studies used either heated jets impinging on cool surfaces or cool jets impinging on hot surfaces. Excellent correlations of Nusselt and Reynolds numbers have been developed in these studies, particularly in Donaldson, *et al.*[12] The relationship between those results and the results obtained in the present study is discussed below.

Due to the lack of general information on heat transfer in and above combusting jets, we have carried out a series of experiments on the different configurations described in Figure 4-1. Stagnation point heat transfer has been examined in the greatest detail and will be described first.

The stagnation point fixture consisted of an instrumented flat plate mounted on a bracket attached to the translation stage. The plate was oriented normal to the jet flow and could be translated from the jet exit to about 60 cm downstream. The plate was 36 cm × 36 cm and consisted of (see Figure 4-2) an asbestos layer 1 cm thick, an aluminum mounting bracket 0.635 cm thick and a water-cooled copper plate 0.317 cm thick. A water-cooled Gardon (circular-foil) gauge‡ was mounted in the center, flush with the asbestos front surface. The gauge cooling water was heated to 70°C in order to prevent condensation.

A Gardon gauge[13] consists of a thin constantan disk welded to a cooled copper body, see Figure 4-3. A small diameter copper wire is welded to the center of the back surface of the disk to form an intrinsic thermocouple. When the front of the gauge is heated, a radial temperature gradient is produced in the disk. The voltage developed between the wire and the body is proportional to the applied flux. The gauges used in the present study had disks about 3 mm in diameter and the entire front surface of the gauge (about 2.5 cm in diameter) was coated with a proprietary black finish of emissivity 0.95. Therefore, the sum of the convective and radiative fluxes was measured.

---

‡Model C-1301-A, manufactured by Hy-Cal Engineering, Santa Fe Springs, CA. The sensitivity of the particular gauge used here was 0.32 millivolt per W/cm^2.

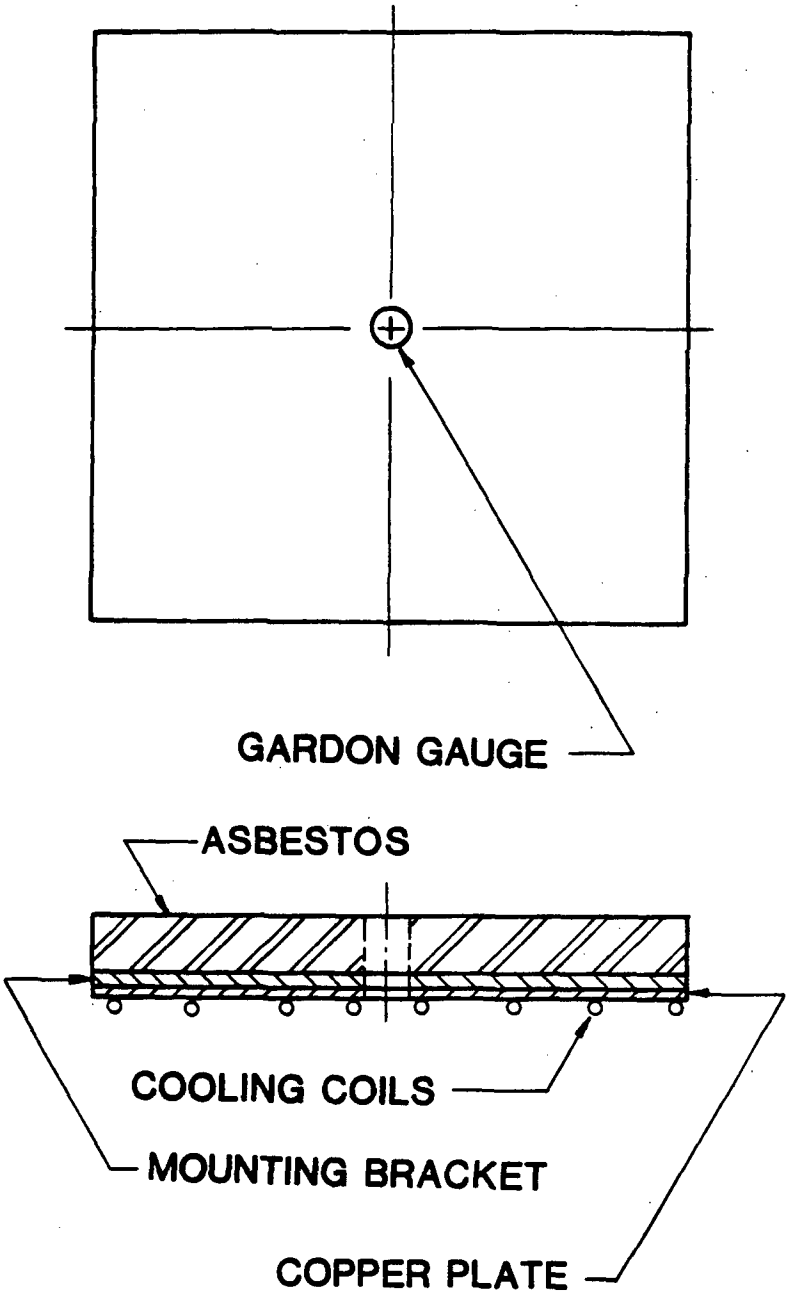

Figure 4-2. Stagnation-point heat flux fixture: (a) plan view; (b) cross section.

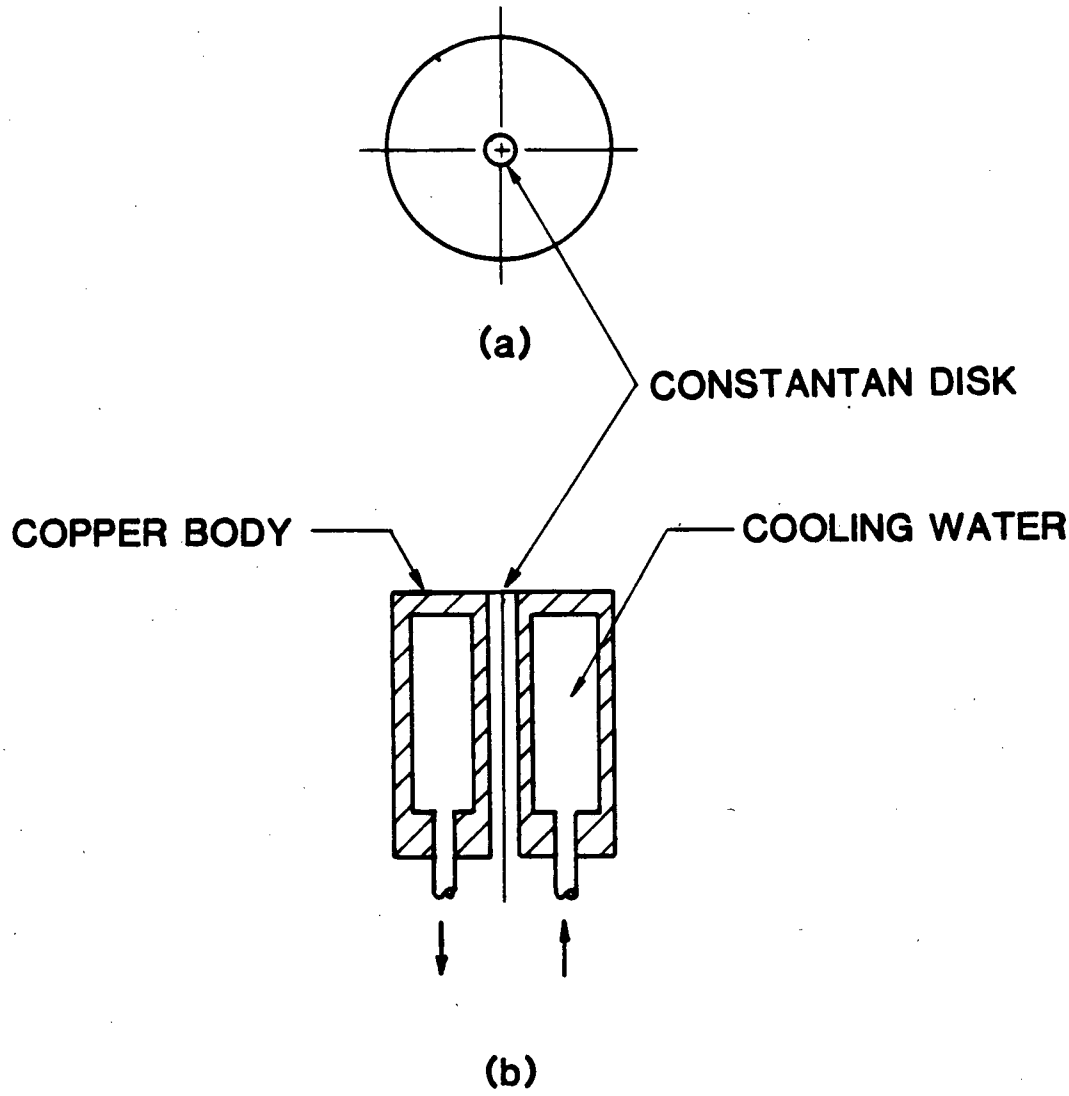

Figure 4-3. Gardon gauge: (a) plan view; (b) cross section.

A series of experiments was carried out at a fixed hydrogen flow rate of 75 slpm (0.11 g/s) and various steam or hydrogen flow rates from 0 to 140 slpm. The 0.635 cm diameter smooth nozzle was used throughout the tests. The gas was at a temperature of 200°C for all experiments; the nozzle, plumbing and superheaters were maintained at this temperature. The heat-flux gauge was positioned on the centerline of the jet and measurements were taken in increments of 2.54 cm from 10 to 60 cm downstream of the jet exit.

Parameters of the flows investigated are given in Table 4-1. Steam flow rates above 120 slpm were not used since the flame was highly unstable in that regime. The parameters were calculated from the measured flow rates, the jet exit pressure and temperature, and the thermophysical properties[14] of the gases. At the same molar dilution, jets diluted with steam had flame temperatures 5-10% lower than those diluted with nitrogen. Note that at the same molar flow rate, jets diluted with nitrogen will entrain 1.6 times as much atmosphere as jets diluted with steam due to the higher mass flow rate of nitrogen. Both steam and nitrogen dilution were investigated to determine if the added water from the steam dilution had any effect on the hydrogen oxidation. As discussed below, this does not appear to be the case.

Measured stagnation-point heat fluxes are shown in Figures 4-4 and 4-5 for steam and nitrogen dilutions respectively. The undiluted hydrogen jet, case 1, is also shown in Figure 4-5. Visual flame heights were estimated to be 20-30 cm except for the undiluted jet, which had a height in excess of 50 cm.

The trend is for heat flux to monotonically decrease with both downstream distance and dilution. Except for the undiluted jet (case 1), all cases are quite similar and seem to obey the same relation between heat flux and distance. That case 1 is exceptional is not surprising since, as pointed out above, the measurements are in the region of combustion for most of the traverse. In all other cases, the measurements are mostly above the region of combustion.

To gain further insight into the relationship between heat flux and downstream distance, the data have been replotted on a log-log graph in Figures 4-6 and 4-7. As shown, a linear relationship with the same slope for all cases (except Case 1) is obtained. This indicates that a power-law relation of the form

$$q = Ax^{-N} \qquad (4-1)$$

applies. Hand-fitting a straight line to several of the cases yields an exponent N of approximately 2.2 for both steam and nitrogen dilution. The exponent is close to a value of 2, which we might expect on the basis of the jet scaling laws presented in Chapter 1.

How can we explain or predict the simple form of Eq (4-1) and the values of N and A? One technique, which has been quite successful for both nonreacting jets[12] and plume fires,[15] is based on combining jet scaling laws (*i.e.*, Table 1-1) with stagnation heat transfer correlations developed for laminar flow.[16] This is a heuristic rather than a rigorous argument but is very useful for understanding the form of Eq. (4-1).

Table 4-1. Jet Parameters for Stagnation Heat Transfer Measurements

Case	α	T_o (K)	U (m/s)	R	F	T_f (K)
			Pure hydrogen			
1	0	505.	88.1	1.8×10^3	5.8×10^3	2381
			Steam dilution			
2S	0.4	535.	131.	5.9×10^3	4.4×10^4	2186
3S	1.0	542.	189.	1.2×10^4	1.5×10^5	1926
4S	1.33	530.	216.	1.6×10^4	2.3×10^5	1809
5S	1.6	509.	231.	1.9×10^4	3.0×10^5	1600
			Nitrogen dilution			
2N	0.4	526.	128.	6.5×10^3	6.7×10^4	2238
3N	1.0	511.	178.	1.4×10^4	2.4×10^5	2024
4N	1.33	507.	206.	1.8×10^4	4.1×10^5	1919
6N	1.87	507.	254.	2.4×10^4	7.5×10^5	1769

$\alpha =$ ratio of moles of diluent to moles of hydrogen in the jet.

$T_o =$ Jet exit temperature

$U =$ Jet exit velocity

$R =$ UD/ν, Reynolds number of jet exit flow

$F =$ $\rho U^2/g\Delta\rho D$, Froude number of jet exit flow.

$T_f =$ temperature of a stoichiometric mixture of jet and atmosphere fluid burned under adiabatic, constant-pressure conditions.

Nominal ambient pressure 630 torr, nominal ambient temperature 300 K, jet exit diameter $D = 0.635$ cm

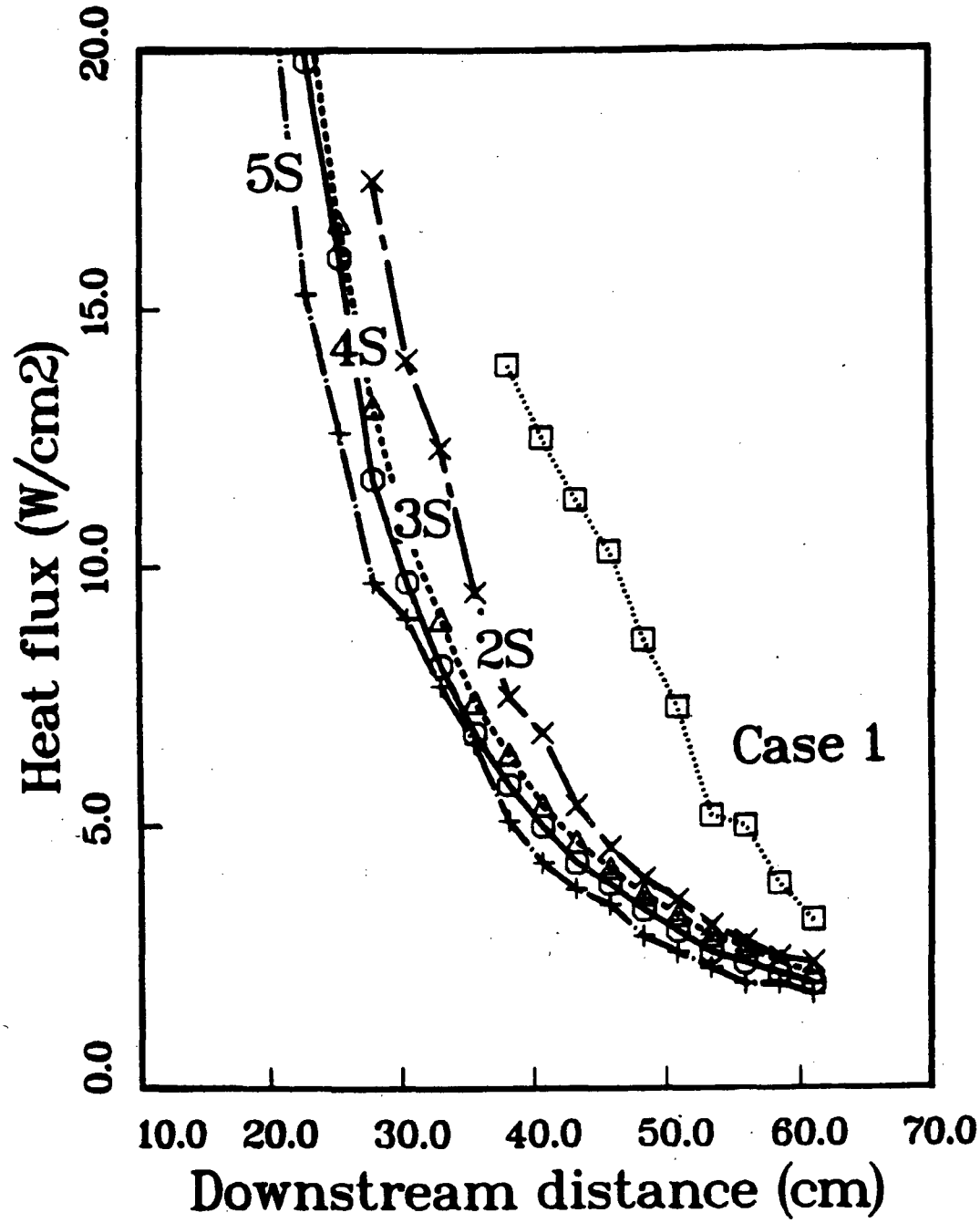

Figure 4-4. Stagnation-point heat flux data from steam-hydrogen jet flames in air. Conditions for the cases indicated are given in Table 4-1.

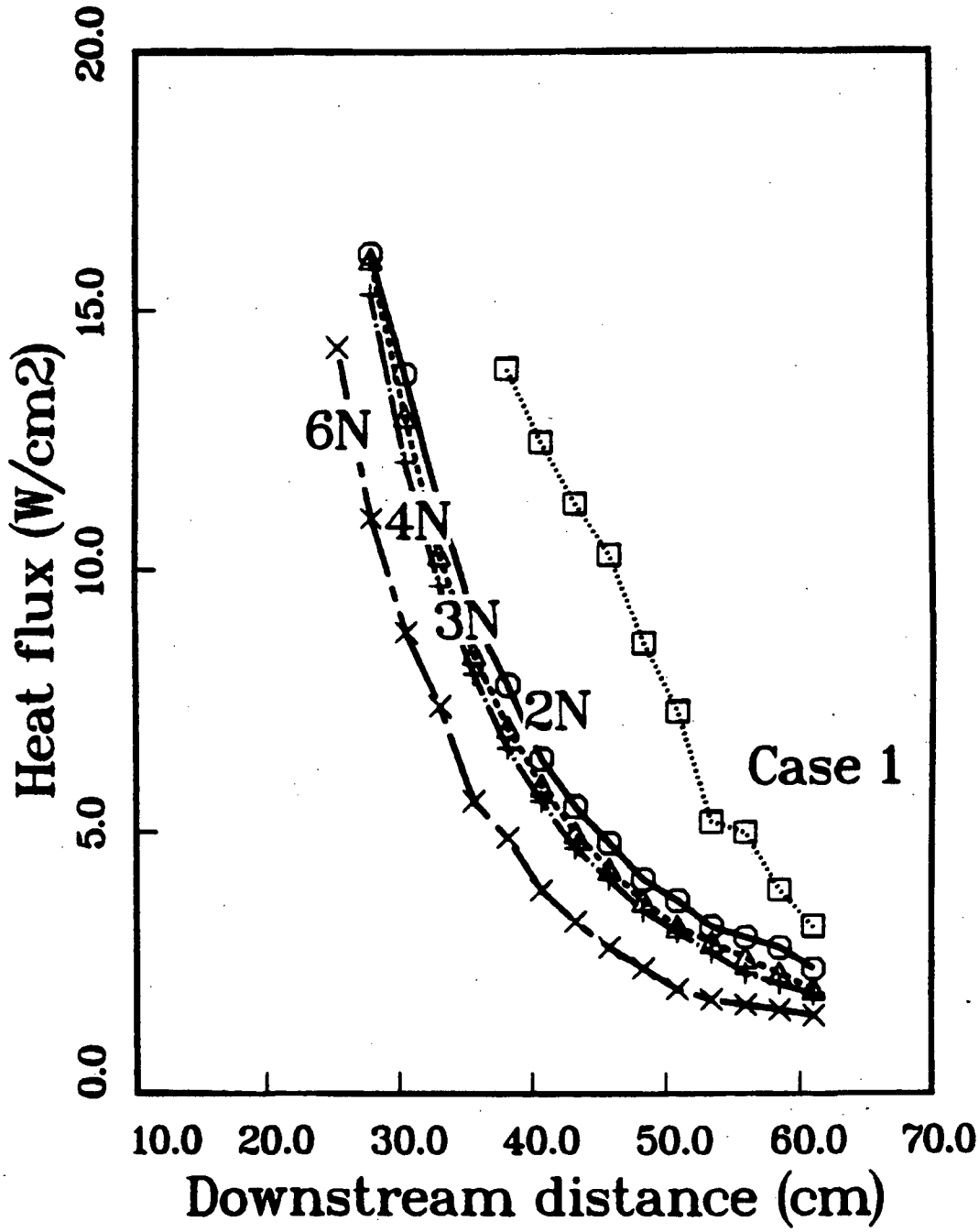

Figure 4-5. Stagnation-point heat flux data from nitrogen-hydrogen diffusion flame jets in air. Conditions for the cases shown are given in Table 4-1.

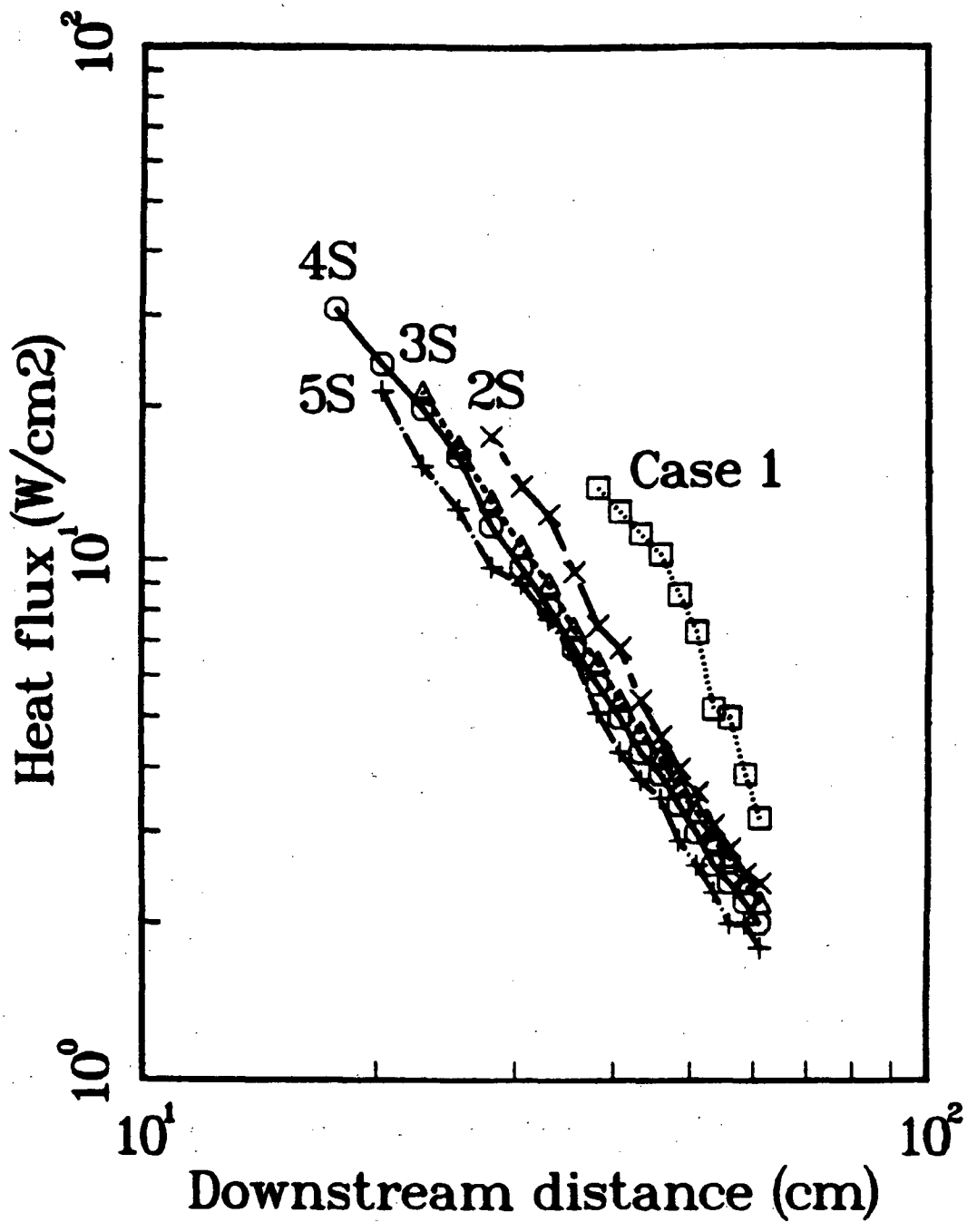

Figure 4-6. Heat flux *vs* distance data of Figure 4-4 replotted on a log-log scale.

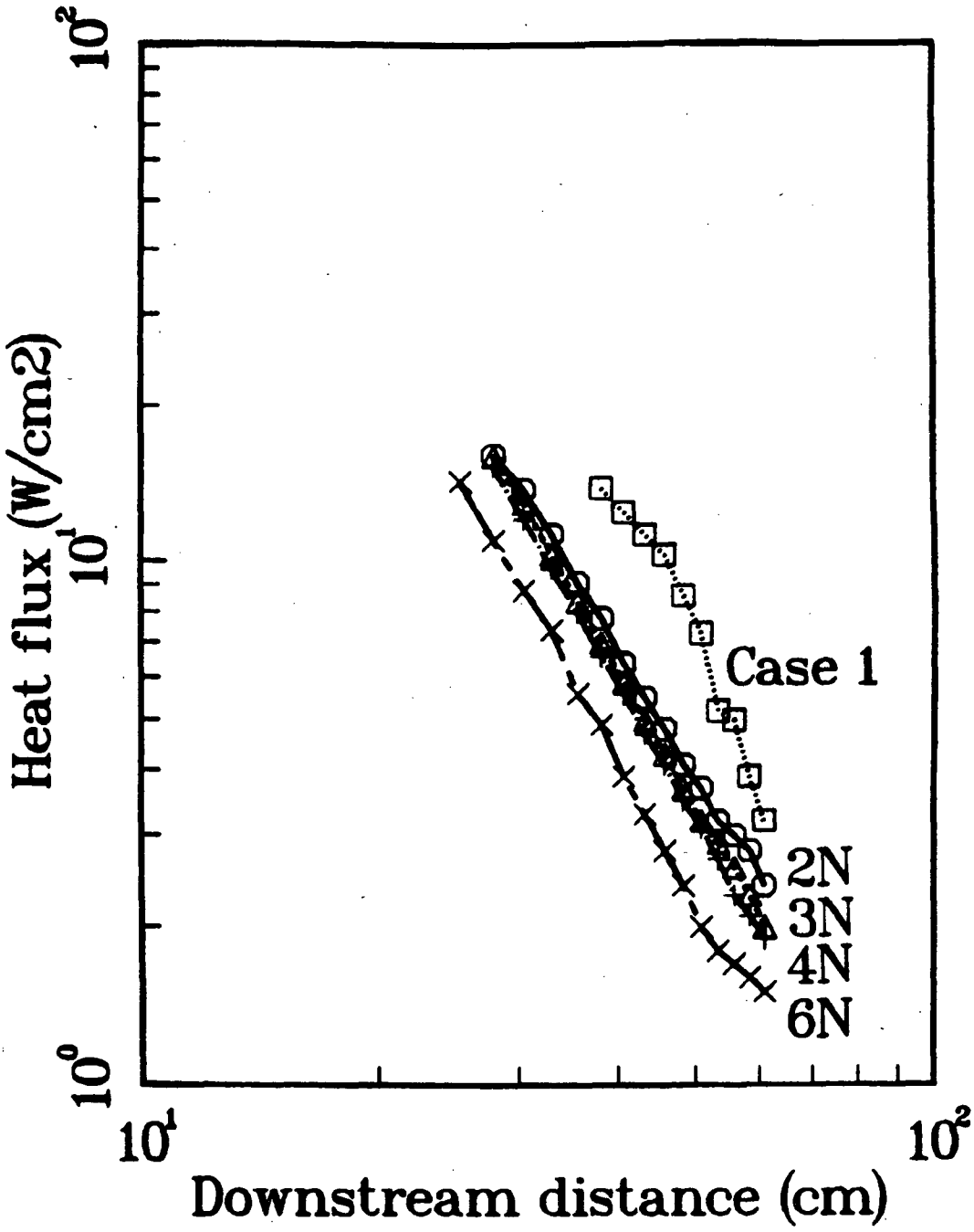

Figure 4-7. Heat flux *vs* distance data of Figure 4-5 replotted on a log-log scale.

In a stagnation point flow, the fluid velocity is zero at the center of symmetry and increases linearly with distance (to first order) along the stagnation surface (see Figure 4-8). The heat flux at the stagnation point is a function primarily of the velocity gradient K and the difference between the fluid enthalpy in the free stream and at the wall. For axisymmetric, laminar flow, the heat flux at the stagnation point is given by:

$$q = 0.763 Pr^{-0.6} (\upsilon_e K)^{1/2} \left(\frac{\upsilon_e}{\upsilon_w} \right)^{0.1} (h_e - h_w) \qquad (4-2)$$

where υ is the kinematic viscosity, h is the enthalpy, Pr is the Prandtl number, the subscript e represents evaluation at the free-stream conditions and the subscript w represents evaluation at the stagnation surface (wall) conditions.

In order to apply this to the present problem, we must correct for the presence of turbulence in the free-stream flow and determine the fluid enthalpy and velocity gradient K as a function of downstream distance in the flame jet. If this is to be applied within the flame, corrections for the effects of chemical non-equilibrium and surface-induced combustion may also have to be made.[6,7]

For a flow impinging on a flat plate, the gradient K is determined entirely by the free-stream velocity profile. Donaldson, *et al.*, have determined the values of K for noncombusting jets and obtained a unique relationship between K and the local jet centerline velocity U_c and half-width b,

$$K = 1.13 \frac{U_c}{b}. \qquad (4-3)$$

Using this value of K in Eq. (4-2), Donaldson, *et al.*, found that the calculated values of q were within a factor of two of the experimentally measured values.

Based on this success and the similar success of You and Faeth [15] in predicting heat transfer from fire-generated turbulent plumes, we will attempt to use this method on the present problem. To calculate the enthalpy as a function of position in the jet, a formula similar to that given for temperature in Table 1-1 will be used:

$$h_e - h_a = (h_o - h_a) 4 \frac{D}{x} \qquad (4-4)$$

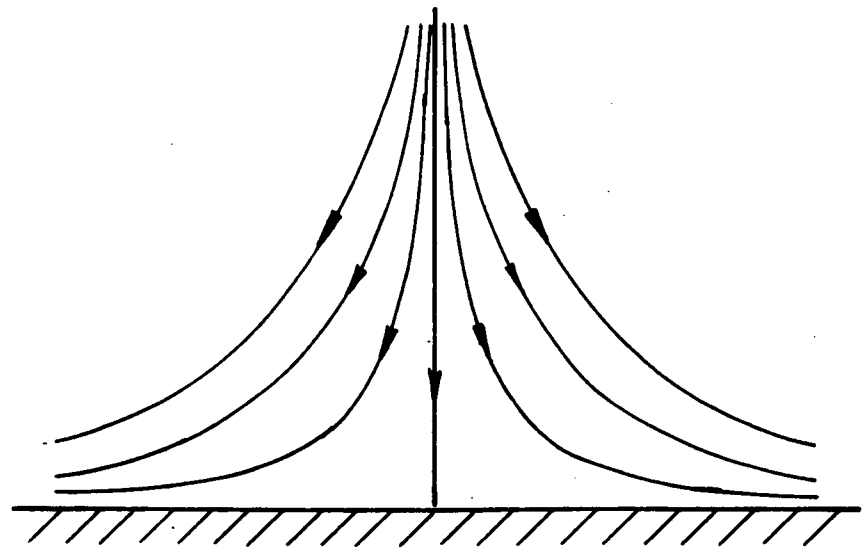

(a)

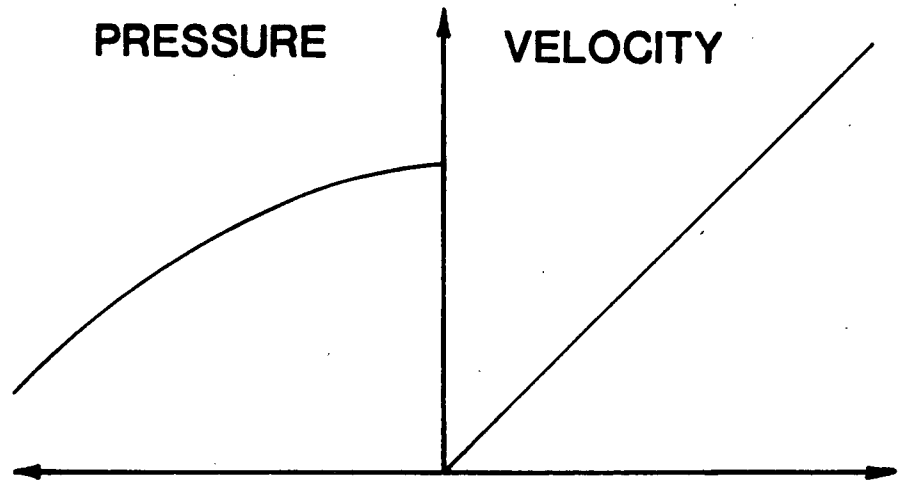

(b)

Figure 4-8. Stagnation point flow: (a) streamlines; (b) velocity (outside the boundary layer) and pressure profiles along the wall.

This formula can be derived by considering the energy balance for a jet in which the enthalpy difference is much larger than the kinetic energy.

Combining Eqs. (4-2) through (4-3) and utilizing the scaling relations of Table 1-1 we obtain

$$q = \frac{C}{R^{1/2}} \frac{Q}{x^2} \qquad (4-5)$$

where R is the cold (jet exit) Reynolds number and C is a constant that depends on the technique used to evaluate the various property ratios that appear in Eq. (4-2). Q is the effective heat release rate of the flame,

$$Q = \pi D^2 \rho U_o (h'_o - h_a) \qquad (4-6)$$

where h'_o is the enthalpy of a unit mass of jet fluid combusted with a stoichiometric amount of atmosphere under adiabatic, constant-pressure conditions. For undiluted jets, Q is the same as the heat released by the hydrogen combustion, 0.177 kW per slpm of H_2. Dilution reduces this value by an amount linear in the mass fraction of diluent.

Equation 4-5 reproduces the general features of the experimental data as represented by Eq. (4-1). The reduction in Q with dilution agrees with the trends shown for both steam and nitrogen dilution in Figures 4-4 and 4-5. The exponent in the downstream distance dependence is slightly different in the experiment, 2.2 *vs* 2.0 from this simple argument. The discrepancy is probably due to neglecting the dependence of fluid properties (viscosity, Prandtl number, *etc.*) on temperature in the steps leading to Eq. (4-5).

The comparison between the experimental data and Eq. (4-5) is also quantitatively favorable. For example, if we use the data of case 4S, we find that the coefficient A of Eq. (4-1) is in the range of 1.3-1.4. The value determined from Eq. (4-5) is in the range of 0.6-0.7. The factor of two difference is comparable to that found by Donaldson, *et al.*, for noncombusting jets.

4.2 Plumes and Intermediate Flows

Two recent investigations of the heat transfer to a ceiling above a fire plume were reported by Zukoski, *et al.*[16] and You and Faeth.[15] Zukoski, *et*

al., used a 1-1.5 kW propane burner and deduced heat transfer from transient temperature measurements on a thin metal ceiling. They correlated the data with a dimensionless heat release parameter, a functional dependence determined from a Stanton number, and turbulent plume scaling. However, the final result for the heat flux at the stagnation point can be simply expressed as:

$$q = C\frac{Q}{H^2} \qquad (4-7)$$

where Q is the heat release rate of the fire, H is the height from the fire source to the ceiling and C is an experimentally determined constant of order 1.

You and Faeth used a liquid-fuel wick burner (fuels used included methanol, ethanol, 1-propanol and n-pentane) and transient calorimeter measurements to determine the ceiling heat flux. They correlated their data using a theory similar to that outlined in the previous section. Their final result is similar to Eq. (4-7), but the constant has a weak dependence on the plume Rayleigh number. The theoretically computed values of C vary from 0.7 for Q equal to 50 W to 0.35 for Q equal to 3 kW. The experimental results follow this trend with the usual scatter and are consistent with Zukoski's range of C values, 0.5-1.0.

The form of Eq. (4-7) is quite similar to our results for forced jet flames. Common factors in both flows are: the power available for heat transfer is Q; and, the width of both turbulent jets and plumes increases linearly downstream. Therefore, by simple dimensional analysis, the characteristic stagnation heat flux must be proportional to the power available divided by the flow area. This leads immediately to a relationship of the form given by Eq. (4-7). The only remaining question is: How does the constant C vary with the scale of the experiment? In particular, does it reach a lower limit as the fire power Q is increased or does it continuously decrease as predicted by You and Faeth?

In order to investigate plume fires in the present facility, experiments were carried out with several large-diameter burners. Our interest was to investigate the scaling of stagnation heat transfer in the parameter region intermediate to plumes and jets. As indicated in Figure 1-9, many reactor accident scenarios could lead to fires in this regime.

The burners were constructed of pipe nipples of various diameters, see Figure 4-9. In order to distribute the hydrogen flow uniformly, a 2.5 cm layer of 4-mm-diameter glass beads was poured on top of a coarse mesh brass screen inserted inside the pipe. These burners were simply placed over the existing nozzles and sealed to the flange surface with Apiezon putty. Burner diameters of 10, 5 and 2.5 cm diameter were constructed by this method.

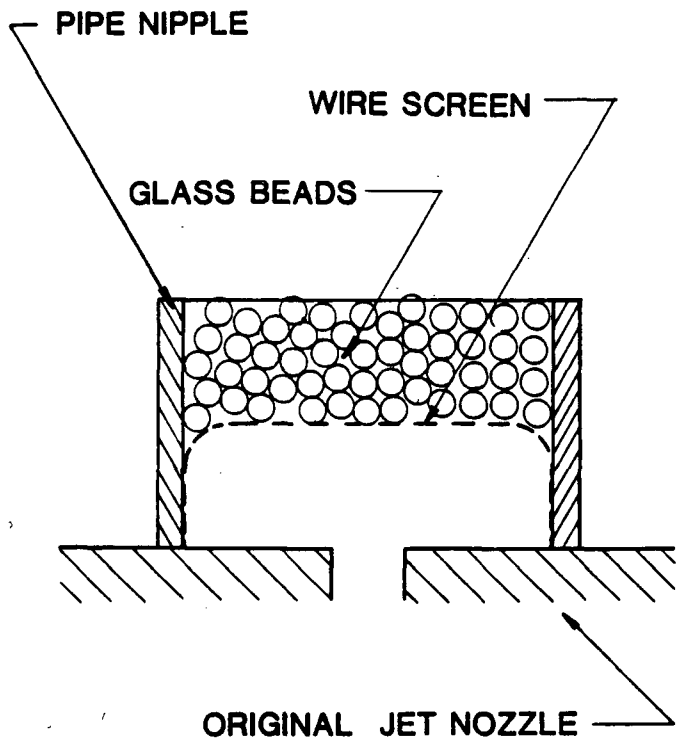

Figure 4-9. Large-diameter burners constructed for plume fire studies.

The hydrogen was supplied at room temperature, nominally 20°C. Initially, the burners were also at this temperature but thermal feedback from the flame raises the temperature to 50 – 100°C after 30 minutes of operation. The stagnation heat flux instrumentation was the same as used in the jet flame experiments.

A test of the scaling law implicit in Eq. (4-7) is shown in Figure 4-10. These data were measured at three different flow rates, 7.9, 15.8 and 31.6 slpm, in the 10 cm diameter burner. Parameters for these and other flows discussed below are given in Table 4-2. Heat fluxes for the 7.9 slpm case shown in Figure 4-10 were multiplied by two before plotting; the data for the 31.6 slpm case were divided by two. Also plotted is Eq. (4-7) with a value of the constant C equal to 0.7 and a value of Q appropirate for a 15.8 slpm flow (2.8 kW). The good agreement between the scaled experimental data and also with Eq. (4-7) indicate the validity of the approach for buoyancy-dominated flames.

The cases discussed in Figure 4-10 have exit Froude numbers in the range of 6×10^{-4} to 4×10^{-5}. For these values, the flow is completely buoyancy dominated and the results merely confirm the measurements of previous investigators. A

more interesting and less well understood problem is the variation of the stagnation heat flux with burner diameter at a fixed flow rate.

Table 4-2. Parameters for Plume Fire Heat Transfer Measurements

Case	Q_{H_2} (slpm)	D (cm)	U (cm/s)	R	F
1P	7.9	10.	2.1	17.0	3.7×10^{-5}
2P	15.8	10.	4.2	33.9	1.5×10^{-4}
3P	31.6	10.	8.4	67.9	6.0×10^{-4}
4P	15.8	5.	16.8	67.9	4.8×10^{-3}
5P	15.8	2.5	67.3	136.	0.15
6P	15.8	0.635	1077.	543.	157.
7P	15.8	0.159	1.7×10^4	2173.	1.6×10^5

This is shown in Figure 4-11 for burner diameters of 10, 5, 2.5, 0.635, and 0.159 cm diameter and a fixed hydrogen flow rate of 15.8 slpm (Q = 2.8 kW). Except for the smallest diameter case, the fluxes at a given height show a smooth increase with decreasing burner diameter. A range of Froude numbers from 1.5×10^{-4} to 1.6×10^5 is covered in the data of Figure 4-11.

A partial explanation of the variation with burner diameter can be obtained with arguments similar to those used above to derive Eq. (4-5). If the intermediate-Froude number buoyant jet scaling laws[17] are used in Eq. (4-2), the result is:

$$q = C \frac{F^{0.075}}{R^{0.5}} D^{0.15} \frac{Q}{x^{2.15}} \qquad (4-8)$$

For a fixed flow rate, the Froude number varies like D^{-5} and the Reynolds number like D^{-1}, where D is the jet burner diameter.

The net result is that,

$$q = \frac{C}{D^{0.725}} \frac{Q}{x^{2.15}} \qquad (4-9)$$

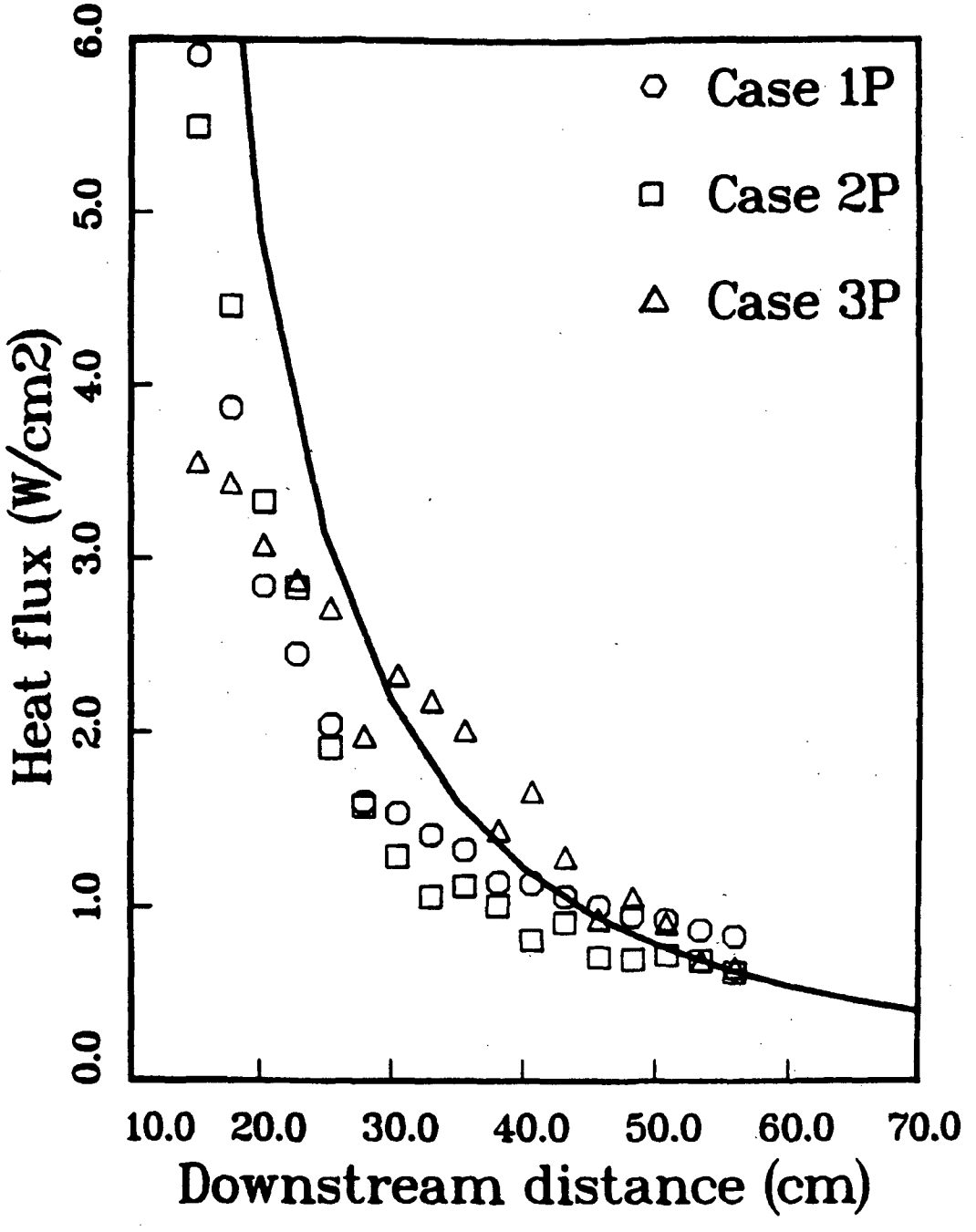

Figure 4-10. Comparison of scaled fluxes from three fires (7.9 slpm, 15.8 slpm and 31.6 slpm) on a 10-cm diameter burner. Solid line is Eq. (4-7) with C=0.7.

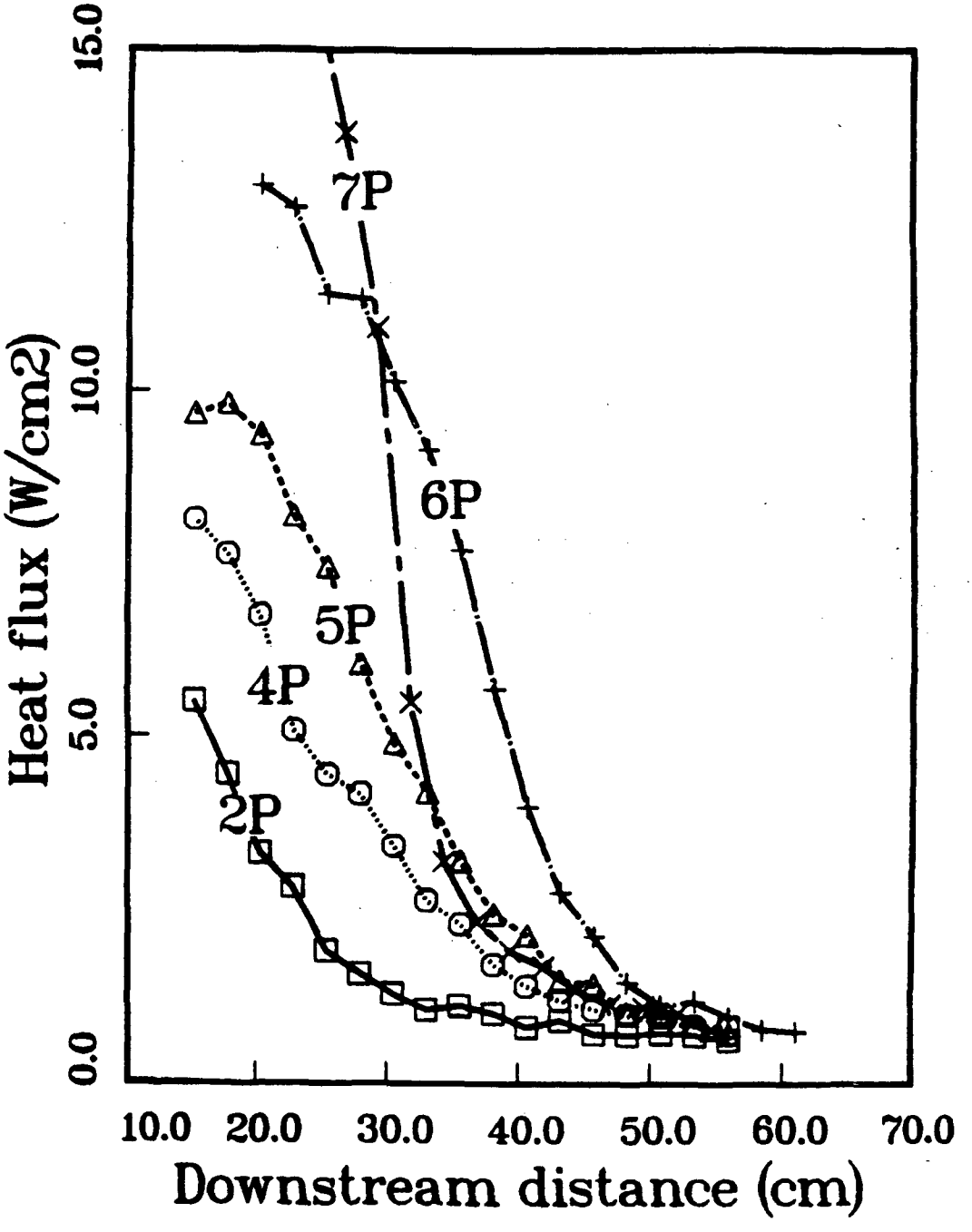

Figure 4-11. Stagnation-point heat fluxes *vs* downstream distance for five different burner diameters and 15.8 slpm hydrogen flow rate. Conditions for the cases shown are given in Table 4-2.

Numerical experiments with the data of Figure 4-11 (omitting the smallest diameter case) suggest that the data can be represented by:

$$q = \frac{C}{D^{0.5}} \frac{Q}{x^2} \qquad (4-10)$$

The result of scaling the data according to Eq. (4-10) is shown in Figure 4-12. Moderate agreement is indicated; evaluation of the accuracy of Eq. (4-10) is complicated by the intrinsic unsteadiness of fire plumes. Even though 1000 individual measurements were averaged at each vertical station, there was a great deal of scatter between two different runs with ostensibly the same fire. This is indicative of the extreme sensitivity of these flows to external disturbances.

Relocating the experiment in a controlled environment would result in a major improvement in the quality of the data. Some form of conditional sampling may also be needed; clearly, adding more points to the average would not be productive. By comparison, the flame jet data were very repeatable and only 100-200 data points were averaged at each vertical location.

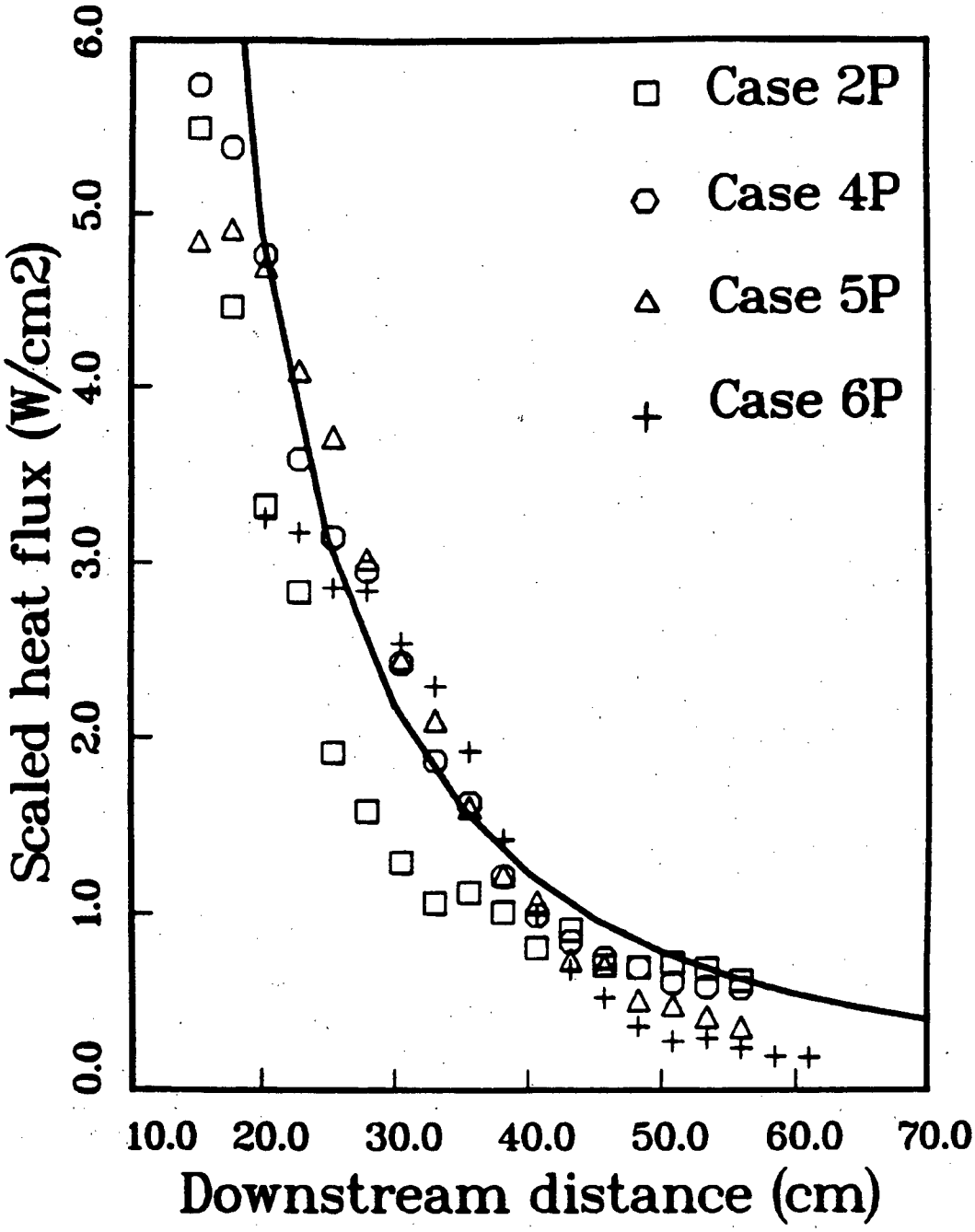

Figure 4-12. Data of Figure 11 (except case 7P) scaled according to Eq. (4-10); individual fluxes were multiplied by $(D/10.2)^{1/2}$, *i.e.*, scaled to the largest diameter. The solid line is equation 4-7 with C = 0.7.

References

1. Personal communication from D. W. Larson, Sandia National Laboratories, Albuquerque, NM.

2. A. L. Berlad, R. Jaung, and W. T. Pratt, *Electrical Cable Insulation Pyrolysis and Ignition resulting from Potential Hydrogen Burn Scenarios for Nuclear Containment Buildings,* **Proceedings of the Second International Conference on the Impact of Hydrogen on Water Reactor Safety,** M. Berman and L. Thompson (eds.), Sandia National Laboratories Report SAND82-2456 (1982).

3. The FITS tank is an experimental vessel 5.6 m^3 in volume which has been used for a number of premixed hydrogen combustion experiments.

4. An experimental program jointly sponsored by EPRI and the NRC has been conducted at the NTS in an abandoned hydrogen dewar 2085 m^3 in volume. Both continuous injection (diffusion flame) and premixed combustion tests have been carried out.

5. J. E. Anderson and E. F. Stresino, *Heat Transfer from Flames Impinging on Flat and Cylindrical Surfaces,* Journal of Heat Transfer **85,** 49-54 (1963).

6. R. Connolly and R. M. Davies, *A Study of Convective Heat Transfer from Flames,* International Journal of Heat and Mass Transfer **15,** 2155-2172 (1972).

7. J. K. Kilham and M. R. I. Purvis *Heat Transfer from Normally Impinging Flames, rm Combustion Science and Technology* **18,** 81-90 (1978).

8. R. Gardon and J. Cobonpue, *Heat Transfer Between a Flat Plate and Jets of Air Impinging on It,* **Proceedings of the 1961 International Heat Transfer Conference,** 454-460 (1961).

9. R. Gardon and J. C. Akfirat, *The Role of Turbulence in Determining the Heat-Transfer Characteristics of Impinging Jets,* International Journal of Heat and Mass Transfer **8,** 1261-1272 (1965).

10. R. Gardon and J. C. Akfirat, *Heat Transfer Characteristics of Two-Dimensional Impinging Jets,* Journal of Heat Transfer **88,** 101-108 (1966).

11. G. C. Huang, *Investigations of Heat-Transfer Coefficients for Air Flow Through Round Jets Impinging Normal to a Heat-Transfer Surface,* Journal of Heat Transfer **85,** 237-245 (1963).

12. C. Dup. Donaldson, R. S. Snedeker, and D. P. Margolis, *A Study of Free Jet Impingement. Part 2. Free Jet Turbulent Structure and Impingement Heat Transfer,* Journal Mechanics **45,** 477-512 (1971).

13. R. Gardon, *A New Transducer for the Measurement of Heat Flow Rate,* Journal of Heat Transfer **82,** 396-398 (1960).

14. R. C. Reid, J. M. Prausnitz, and T. K. Sherwood, **The Properties of Gases and Liquids, Third Edition,** McGraw-Hill, NY (1977).

15. H. Z. You and G. M. Faeth, *Ceiling Heat Transfer during Fire and Fire Plume Impingement,* Fire and Materials **3,** 140-147 (1979).

16. E. E. Zukoski, T. Kubota, and C. C. Veldman, **An Experimental Investigation of the Heat Transfer from a Buoyant Gas Plume to a Horizontal Ceiling,** California Institute of Technology Report (1975).

17. C. J. Chen and W. Rodi, **Vertical Turbulent Buoyant Jets,** Pergammon Press, New York, NY, (1980).

5 Discussion

This document reports work in progress and the results should be considered with that in mind. One major accomplishment of this project has been the identification of areas in which research is needed and in which a contribution could be made. The original scope of this project was the entire field of diffusion flame phenomena as applied to light-water reactor safety. Clearly, this was much too ambitious a goal, especially when we consider the undeveloped state of scientific knowledge on diffusion flames. A more restricted and well-focused effort will be needed to make further progress of a substantial nature.

Toward this end, we list below a number of areas of ignorance which represent specific research problems. This list is by no means comprehensive and as much reflects the author's prejudices as its does the needs of the reactor safety community and the NRC staff.

The issue of using intentionally produced diffusion flames (*i.e.*, deliberate flaring) to rid the primary system of hydrogen is separately addressed below. As discussed below, the primary difficulty is in disposing of the energy produced by the combustion. If a commitment is made to use deliberate flaring, we feel that this problem could be readily solved by standard engineering methods.

5.1 The Threat from Accidental Breaks

A. Heat Transfer to the Containment

An obvious problem that was pointed out in the heat transfer section is that all tests of the type described here are unconfined. A major mechanism for the removal of the combustion-generated heat will be large-scale convection to the containment interior surfaces in an actual reactor accident. A limited number of diffusion-flame tests have been carried out at the EPRI/NRC experiment at NTS. A concerted effort must now be made to interpret that data and try to understand the heat transfer mechanisms. A program is underway at Sandia to apply to this problem the methods used to analyze room fires.[1] This effort must ultimately be linked to the existing reactor safety codes such as HECTR in order to apply these methods to postulated reactor accidents.

B. Supersonic Jet Stability

The results of a few preliminary experiments on supersonic flame-jets indicate that the stability limits are much narrower than for subsonic jets. These results have been confirmed in a general way by experiments at NTS.[2] However, some very sketchy results by Soviet workers indicate that for extremely high pressure ratios (see References 13 and 14 of Chapter 3), the flame recovers its stability. In addition, they hypothesize that the flame is unconditionally stable for all flow rates when the burner is larger than a critical diameter.

Such a result would have extremely important ramifications for reactor safety analyses. However, there does not exist a rigorous theory or good experimental data on supersonic flame-jet stability. Experiments that have been done to date are also at very low pressure ratios compared to what one might expect in PWR accidents. Without a verified theory or scaling analysis, the extrapolation of these results to reactor situations is of dubious validity.

C. Influence of Steam in the Containment Atmosphere

Experiments on diffusion flame characteristics have almost always been conducted in air. To analyze the effect of ambient steam, extensions to empirical flame length and stability theories have been proposed but are untested. A limited amount of information could be gained by examining the results of the NTS experiments, but a systematic investigation of this effect should be carried out.

D. Scaling of the Radiant Heat Flux from Jet Flames

Even though the radiant flux from hydrogen flames is estimated to be only 5-15% of the total power output, it can be an important source of heat for those surfaces which are not in the main convection paths. Radiant flux from plume fires can be adequately characterized (for engineering purposes) as a fixed fraction of the total flame power output.

Very little work has been done to establish the corresponding relationship for jet flames. The situation is particularly uncertain due to the large and correlated fluctuations of temperature and concentration in a turbulent diffusion flame. An enormous amount of effort has gone into characterizing the radiation from rocket plumes, where the difficulties are comparable.

E. Modelling of Entrainment for Jet Flames

Further progress in evaluating the threat of diffusion flames to containment integrity will certainly require modelling of diffusion flames in some fashion. Even the most elementary integral model requires the entrainment and burning rate

as a function of position or momentum flux. Presently, the models use some variation of the noncombusting entrainment law first proposed by Ricou and Spalding[3] or the differential form introduced by Taylor, *et al.*[4]

Application of this law to combusting flows is a leap of faith which many are willing to make. To place the modelling on a firm basis, an experimental investigation similar to that made by Zukoski, *et al.*[5] for plumes should be undertaken for jets. With such an experimental underpinning, a simple integral model like that proposed by Tamanini[6] would be an extremely useful tool.

F. Large-scale Plume Fires

The limiting behavior of very large plume fires is an unsolved problem. The largest laboratory plume fires that have been investigated to date had heat release rates of several hundred kilowatts. It is a large step up to the 10-100 MW range postulated for reactor accidents. In particular, do the stagnation heat flux and centerline temperature follow strict Froude scaling? The alternative is a more complex behavior that will make the interpretation of the upcoming experiments[7] on burning in the wetwell of BWR Mark III nuclear plants more difficult.

G. Plume Fires above Distributed Sources

In a hydrogen-producing accident for a BWR Mark III nuclear plant, hydrogen will probably be released to the containment atmosphere through spargers located under the surface of the suppression pool. The gas flow will come up in a cloud of bubbles which burst at the surface and cause a great deal of motion at the pool free surface. This highly unsteady, distributed source is very different from the spatially continuous sources used in laboratory plume-fire experiments.

Entrainment may be greatly enhanced by the bubbly gas flow. Since almost all features of plume fires are dominated by the entrainment, the usual scaling laws may not apply. While some questions relating to this problem will be answered in the upcoming tests to be conducted by Factory Mutual Research Coporation, it may be desirable to separately investigate this question.

5.2 Practicability of Deliberate Flaring

In order to make deliberate flaring inside reactor containments practical, several conditions must be met. The concept itself is sound, the technique has been used for many years in the petrochemical industry both as a routine method for eliminating waste by-products and as an emergency measure for relieving

dangerous pressure build-up in storage vessels. A comprehensive review of the practical aspects of flaring can be found in the recent article by Brzustowski.[8]

Typical flow rates for process (routine) flaring are 10 to 100 kg/s and the flame power output is on the order of 1 to 10 MW. During emergency flaring, flow rates can reach 10^4kg/s with peak flame power outputs of 1000 MW for a duration of several minutes. Flare stacks are 0.5 to 1.5 m in diameter and from 20 to 50 m high. There are three principal commercial vendors in the USA and several design guides available for aid in choosing the proper design.[8]

From the information given above, it would appear that there are no major obstacles to employ flaring inside the reactor other than the thermal load that the flame would impose. Even the presence of steam in the flow does not appear to be a problem. In order to reduce sooting, steam is routinely mixed (in mass fractions of up to 0.5) into hydrocarbon gases before being flared. However, there are some important factors that should be considered when assessing the feasibility of deliberate flaring inside reactor containments; these are listed below.

A. Specific Situations in Which Flaring Could Be Used

The accident situations in which flaring would be useful are somewhat limited. In order to vent the hydrogen through the flare, some recovery must have taken place and control over the reactor's cooling system re-established. The flare stack will probably be equipped with a pilot burner to assure the continuous combustion of the deliberately released hydrogen. Operation of this pilot light could result in the initiation of a deflagration inside the containment if a combustible mixture was present. This is real concern, since the reactor has obviously been through some kind of a LOCA and possibly has a degraded core if deliberate flaring is being considered. Deliberate ignition systems have been installed in some reactors; these could eliminate this problem if they are operational throughout the accident. If a pipe break has occurred, only partial mitigation will be possible through flaring since some hydrogen will enter the containment through the break.

B. Heat Removal

The success of deliberate flaring will depend on the ability to remove the heat generated by the combustion of the hydrogen. A simple solution to this problem is to limit the flow rate of hydrogen and utilize the existing sprays and fan coolers present in most reactor containment buildings. If necessary, these systems could be augmented by a special cooling system (*e.g.*, water sprays immediately downstream of the flame) attached to the burner.

C. Flame Stability

The mixture being deliberately released from the primary system will contain a large amount of steam. As discussed in Chapter 3 of this report, hydrogen-steam jets with steam/hydrogen ratios (molar) much greater than 9 are difficult to burn as a stable diffusion flame. The presence of accident-generated steam in the containment atmosphere will only exacerbate this problem. Reducing the steam mole fraction in the flow going to the burner and supplying a continuous ignition source (pilot light) are two techniques for circumventing this problem. The steam mole fraction could be drastically reduced by simply bubbling the gas from the primary system through a cool pool of water. If the flow rate was low enough, the steam partial pressure would be limited to that given by the pool temperature.

References

1. E. E. Zukoski and T. Kubota, **A Computer Model for Fluid Dynamic Aspects of a Transient Fire in A Two Room Structure,** California Institute of Technology Report, (1978).

2. Personal communication from L. Thompson, EPRI.

3. J. P. Ricou and D. B. Spalding, *Measurements of Entrainment by Axisymmetrical Turbulent Jets,* Journal of Fluid Mechanics **9,** 21, (1961).

4. B. L. Morton, G. I. Taylor, and J. S. Turner, *Turbulent Gravitational Convection from Maintained and Instantaneous Sources,* **Proceedings of the Royal Society of London A234,** 1-23 (1956).

5. E. E. Zukoski, T. Kubota, and B. Cetegen, *Entrainment in Fire Plumes,* Fire Safety Journal, **3,** 107-121 (1980).

6. F. Tamanini, *An Integral Model of Turbulent Fire Plumes,* **Eighteenth Symposium (International) on Combustion,** 1081-1091 (1981).

7. A 1/4-scale model of a BWR Mark III nuclear plant is being constructed by Factory Mutual Research Corp. for the Hydrogen Control Owner's Group (HCOG) and EPRI. Experiments on hydrogen diffusion flames in the wetwell will be carried out under the direction of Dr. F. Tamanini of Factory Mutual Research Corp.

8. T. A. Brzustowski, *Flaring in the Energy Industry,* **Progress in Energy and Combustion Science 2,** 129-141 (1976).

Appendix A

Laminar Burning Velocity Computations

In this appendix, we give the results of laminar flame speed computations for premixed hydrogen-air-steam mixtures. These calculations were done with the computer code written by Smooke.[1] This code determines the laminar flame speed as an eigenvalue of the one-dimensional, steady-state reacting-flow equations. Diffusion of species, momentum and heat are incorporated in the code and a comprehensive reaction scheme is used. The only approximations are the neglect of radiative heat transfer and the assumption of constant pressure throughout the flow. An iterative, two-point boundary value scheme with adaptive gridding is the numerical technique used to solve the equations; details are given in Reference 1.

The reaction mechanism is the hydrogen-air portion of the acetylene oxidation mechanism proposed by Miller, *et al.*[2] The mechanism and reaction rate constants have been validated by numerous other investigations. A temperature profile and major species profiles are shown in Figure A-1 and Figure A-2 for 30% hydrogen in air at 300 K. These profiles are typical of those for all the flame calculations we have done.

We have carried out a large number of calculations to determine the sensitivity of burning velocity to initial temperature, steam mole fraction and hydrogen concentration. The results of some of these calculations are shown in Figures A-3, A-4, and A-5. Calculated burning velocities are compared to the correlation developed by Liu and MacFarlane[3] from their experimental data.

In Figure A-3, the variation of burning velocity with hydrogen concentration is shown for dry hydrogen-air mixtures at 300 K. In Figure A-4, the variation of burning velocity with steam dilution is shown for a stoichiometric hydrogen-air mixture. The mixture is at a temperature of 400 K and the equivalence ratio is fixed (*i.e.*, does not depend on the diluent fraction). In Figure A-5, the variation of burning velocity with initial temperature is shown for a stoichiometric mixture of dry hydrogen-air.

Note that the correlation obtained by Liu and MacFarlane was developed from a very limited data base (steam concentrations less than 15% and temperatures between 300 and 520 K) and our use of their results involves a large extrapolation. However, the comparison between the correlation and the present

calculations is favorable; the "data" are consistently higher than the calculations. This is typical of practically all experimental results on hydrogen-air flames and Dixon-Lewis[4] has suggested that this is due to systematic errors in the data reduction process.

The most comprehensive set of calculations were done for hydrogen-air-steam mixtures with 30 and 42% hydrogen in air, steam fractions ranging from 0-50% and initial temperatures from 400 to 900 K. Calculations were done at 42% hydrogen since that is where the maximum in burning velocity occurs for room temperature mixtures. In both sets of calculations, the hydrogen-air ratio (equivalence ratio) was held fixed as the steam fraction was varied. Results are shown in Figures A-6 and A-7 .

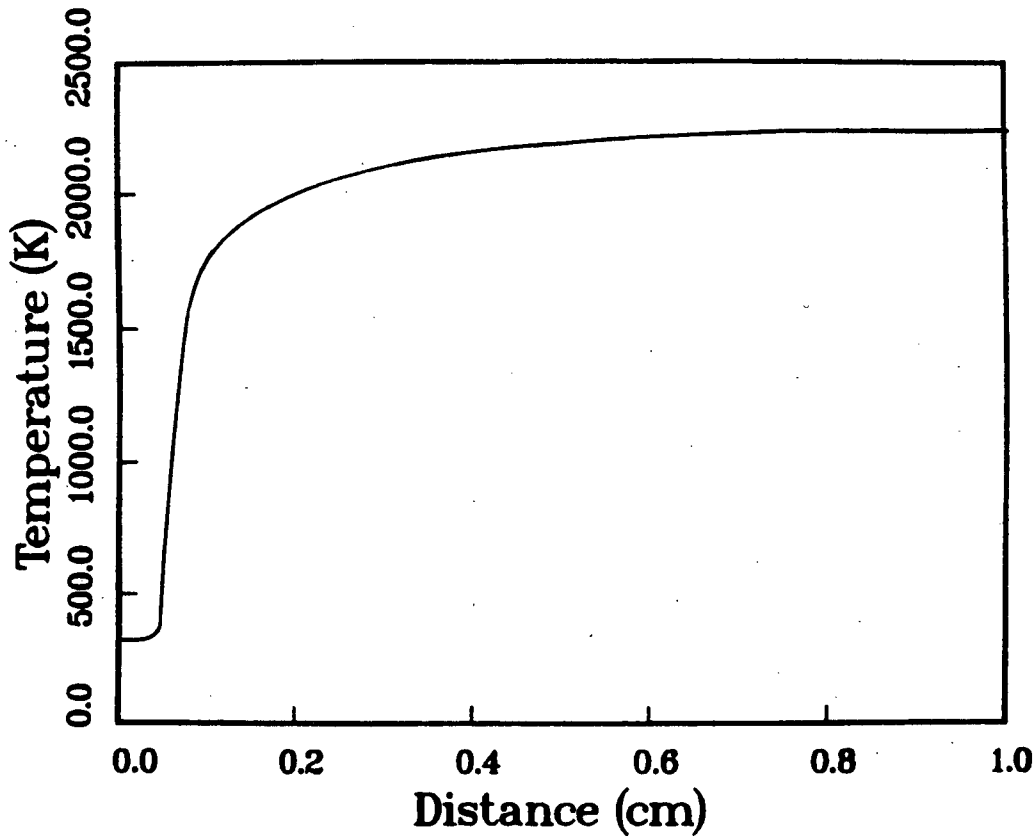

Figure A-1. Calculated reaction zone temperature profile for a stoichiometric hydrogen-air mixture initially at 300 K.

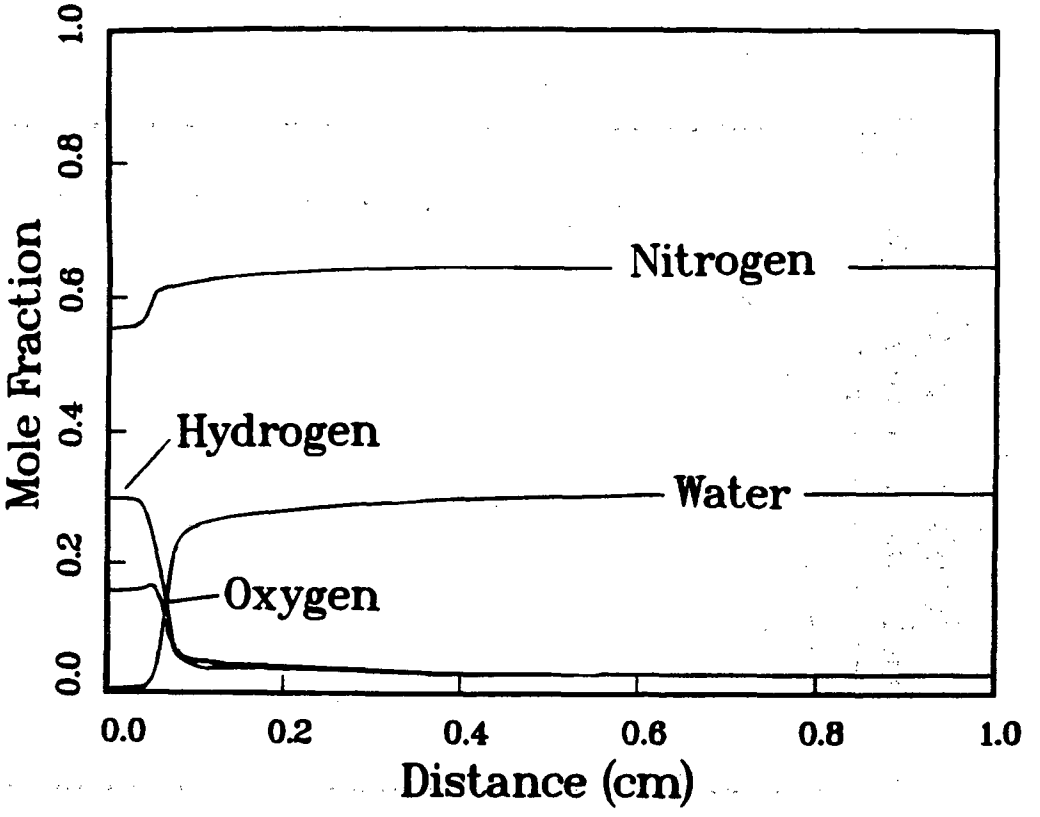

Figure A-2. Calculated reaction zone major species profiles for a stoichiometric hydrogen-air mixture initially at 300 K.

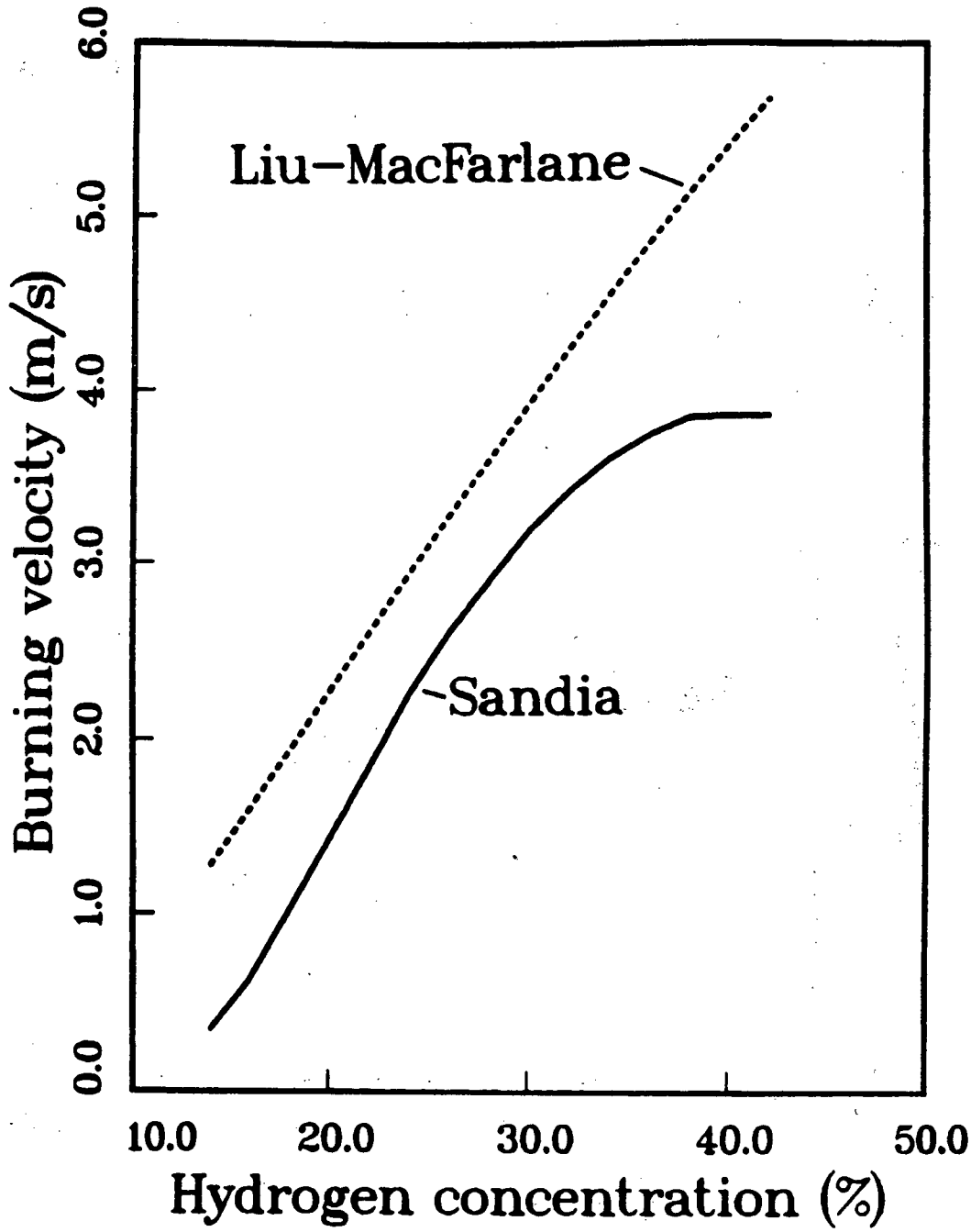

Figure A-3. Comparison between calculated (Sandia) burning velocities and extrapolated (Liu-MacFarlane) experimental data. Dry hydrogen-air mixtures initially at 300 K.

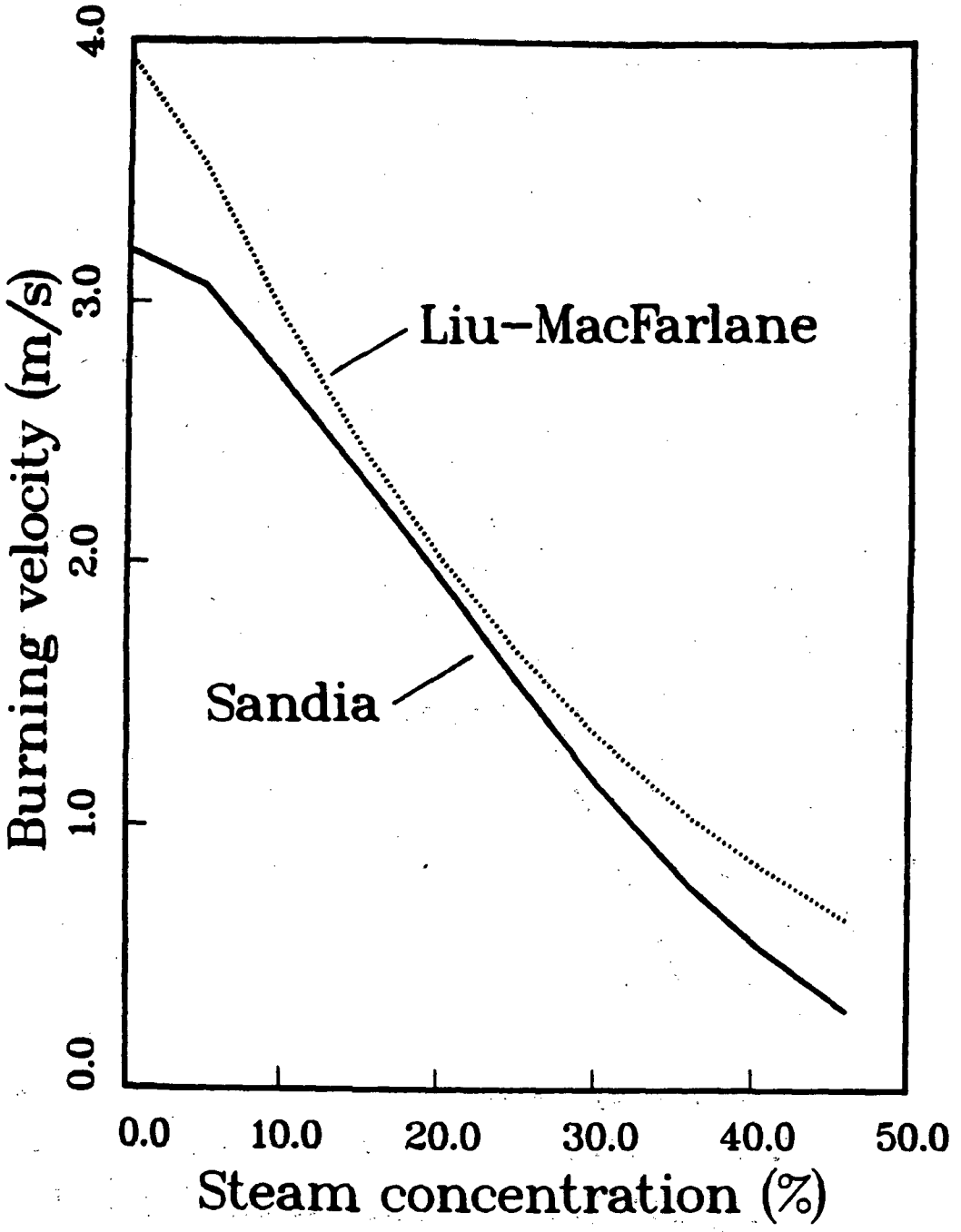

Figure A-4. Comparison between calculated (Sandia) burning velocities and extrapolated (Liu-MacFarlane) experimental data. Hydrogen-air mixtures initially at 400 K diluted with steam; the equivalence ratio is held fixed at stoichiometric.

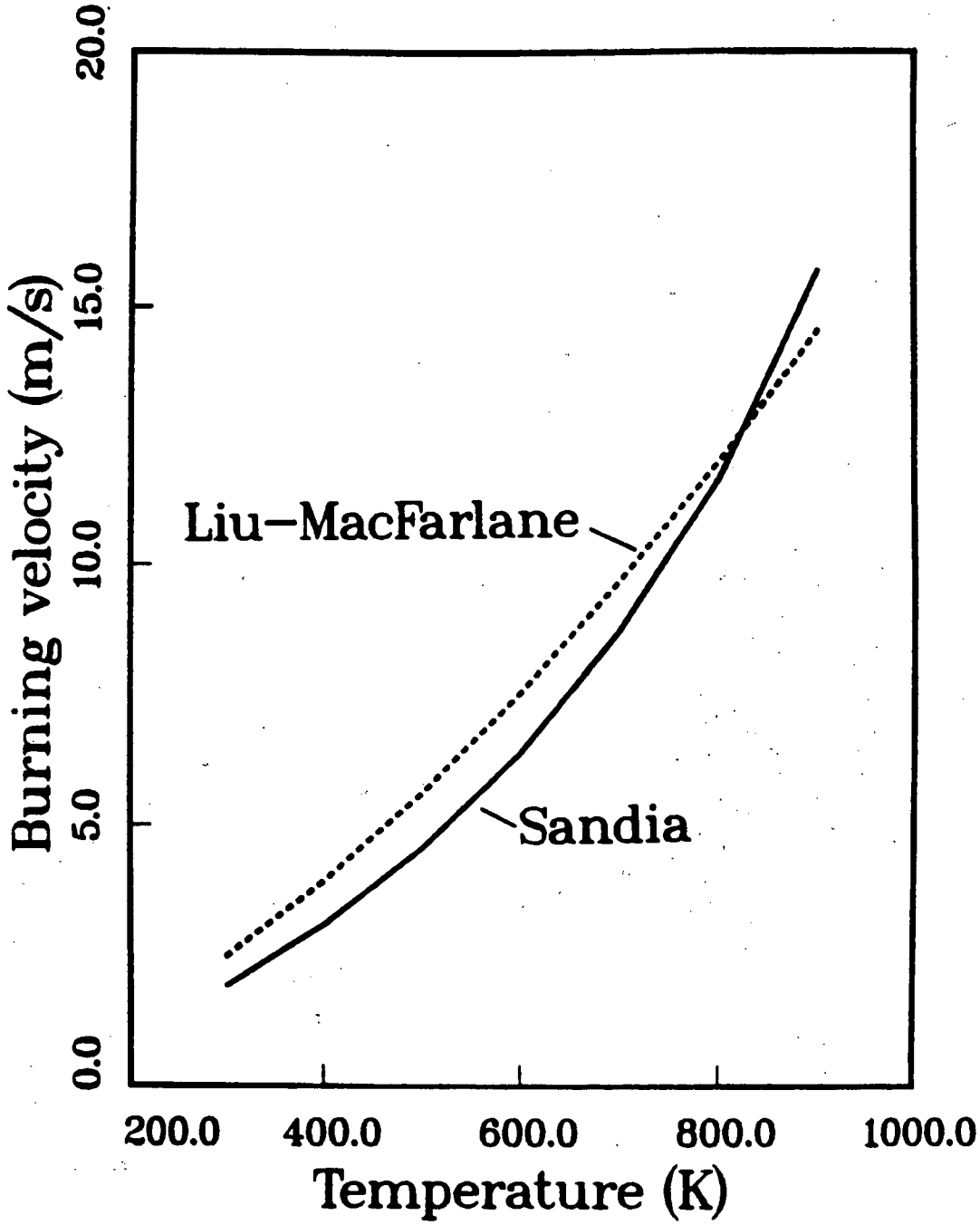

Figure A-5. Comparison between calculated (Sandia) burning velocities and extrapolated (Liu-MacFarlane) experimental data. Dry hydrogen-air mixtures (stoichiometric).

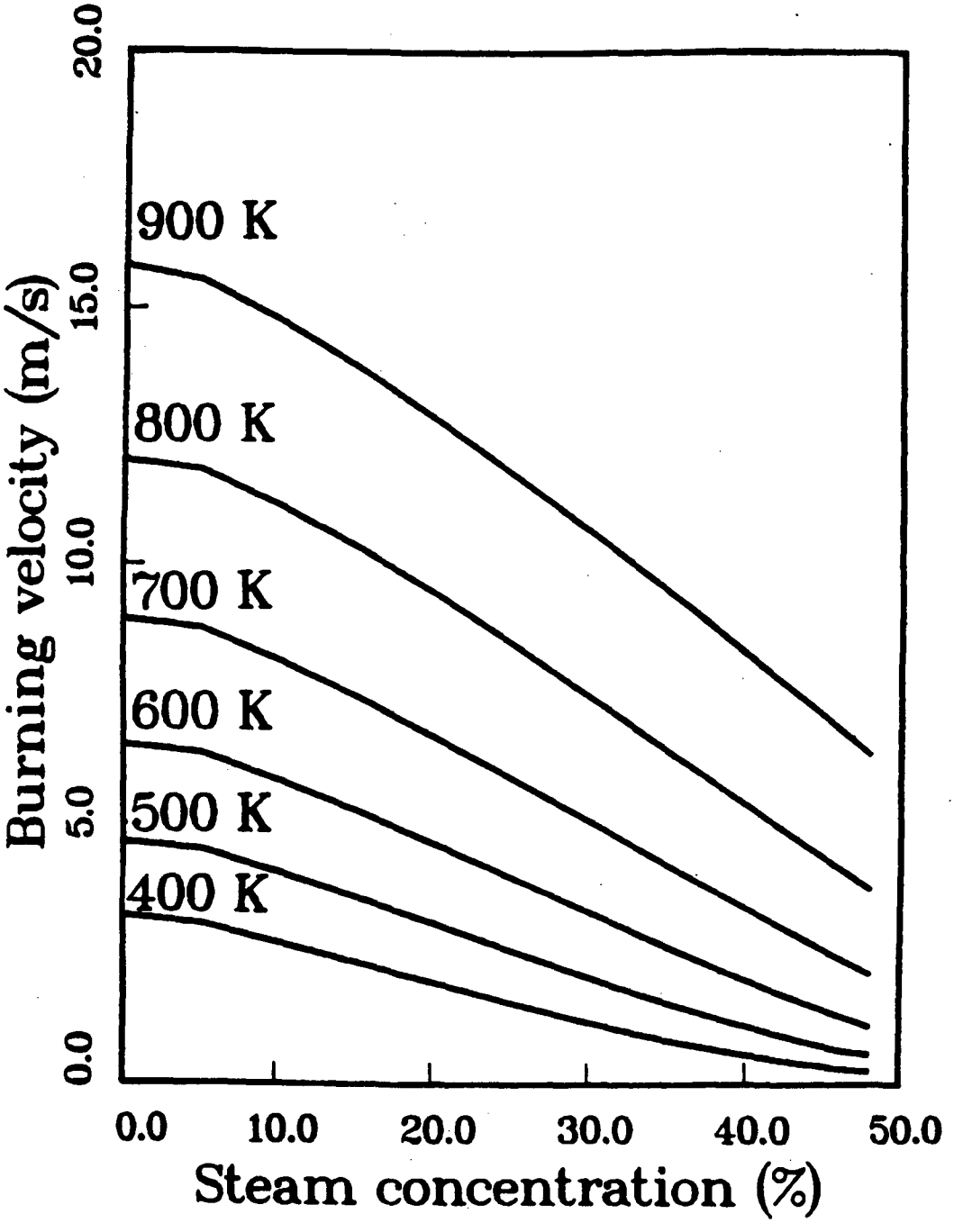

Figure A-6. Calculated burning velocities for hydrogen-air-steam mixtures. Stoichiometric ratio of hydrogen to air for all steam concentrations.

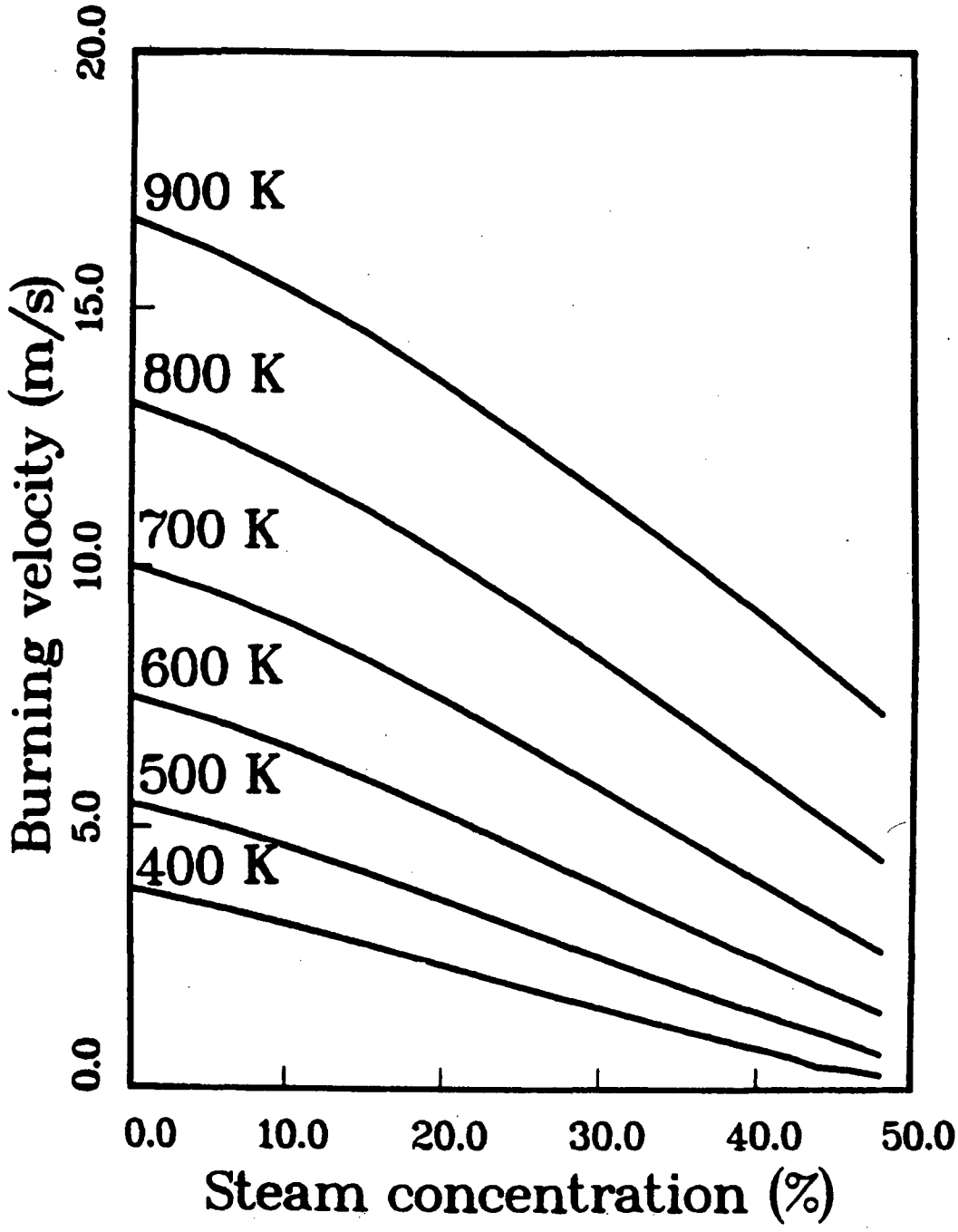

Figure A-7. Calculated burning velocities for hydrogen-air-steam mixtures. Concentration of hydrogen in air is 42% for all steam concentrations.

References

1. M. D. Smooke, *Solution of Burner-Stabilized Pre-Mixed Flames by Boundary Value Methods*, Journal of Computational Physics **48,** 72 (1982).

2. J. A. Miller, R. E. Mitchell, M. D. Smooke, and R. J. Kee, *Towards a Comprehensive Chemical Kinetic Mechanism for the Oxidation of Acetylene: Comparison of Model Predictions with Results from Flame and Shock Tube Experiments.* Nineteenth Symposium (International) on Combustion, The Combustion Institute, Pittsburgh, PA (1982).

3. D. D. S. Liu and R. MacFarlane, *Laminar Burning Velocities of Hydrogen-Air and Hydrogen-Air-Steam Flames*, Combustion and Flame **49,** 59-72 (1983).

4. G. Dixon-Lewis, *Kinetic Mechanism, Structure and Properties of Premixed Flames in Hydrogen-Oxygen-Nitrogen Mixtures*, Philos Trans R Soc London, Ser A **292,** 6 (1979).

Appendix B

Autoignition

In degraded core accidents, the vaporized coolant present in the primary system will be at a high temperature, from 500-1000 K. A hydrogen-steam mixture at these temperatures could spontaneously ignite when released into the containment atmosphere. This phenomena is referred to as "autoignition" and the conditions under which it occurs are the subject of this appendix.

Autoignition of diffusion flames is not an extensively researched subject. Other than some early work by Zebetakis,[1] the only discussions we are aware of are by Soviet scientists. The basic result is that the jet temperature must exceed a certain limiting value for autoignition to occur. This critical temperature is found to be a function of the jet velocity and composition as well as the containment atmosphere composition and temperature. For dry hydrogen jets in air, Zebetakis measured a minimum autoignition temperature of 930 K.

We have attempted to measure the autoignition temperature for hydrogen-steam jets in our small-scale facility. Unfortunately, there was a large amount of scatter in our results and a definite limit could not be established. This failure is probably due to deficiencies in our apparatus. Specifically, the nozzle of the jet was not maintained at a constant temperature. We were able to verify that hydrogen jets at temperatures above 900 - 1000 K would spontaneously ignite.

Heat transfer from the diffusion flame would raise the temperature of the nozzle, making it difficult to fix the jet temperature at a known value. In addition, the facility was designed for steady-state operation and the flow rates would undergo large excursions during startup. With an improved apparatus, we believe that the autoignition limit could be experimentally determined as a function of jet steam concentration over a range of jet velocities.

The most important parameter for autoignition studies oriented toward reactor safety is the pressure ratio (jet stagnation pressure/atmosphere pressure). This parameter determines the overall structure of the flow, and as discussed below, the characteristic mixing time of the jet fluid. A complete study should examine pressure ratios from 1 to 200, with the upper end of this range being more applicable to most degraded core accidents.

A simple theory of autoignition can be developed along the lines of the blowoff correlation discussion in Chapter 3. The fundamental idea is the same:

the autoignition limit is determined by the competing effects of mixing and chemical reaction.

There is a characteristic time for chemical reaction, T_r, and a characteristic time for the jet fluid to mix with the atmosphere, T_m. The autoignition limit is determined by a fixed ratio of these characteristic times; the value of this ratio is an empirically determined constant. The reaction time can be estimated by the methods of Chapter 3 or by calculating the time required for a stoichiometric mixture of jet and atmosphere fluid to react at constant pressure. An example of the results of such a calculation are shown in Figure B-1; the characteristic reaction time is plotted against mixture temperature for various steam fractions.

Note that both decreasing mixture temperature and increasing steam fraction result in increasing the reaction time. The longer the reaction time is for given mixing time, the less likely the jet is to autoignite. The predicted trend agrees with our intuition and suggests the effect of steam is important. Zebetakis measured the minimum jet temperature for autoignition as a function of steam concentration in subsonic jets. He found that the minimum temperature increased from 930 to 1090 K as the steam concentration was varied from 0 to 60 %. This is in quantitative agreement with Figure B-1 if the critical reaction time scale is equal to 5×10^{-6} second.

The characteristic mixing time of the jet fluid will depend on the jet structure. For turbulent subsonic jets, the characteristic time will be given by the ratio of the jet diameter to the exit velocity. This value can be estimated by the jet scaling rules discussed in Chapter 1. If the jet velocity is low enough at the exit, the mixing process may be dominated by molecular diffusion and the autoignition temperature will depend on steam concentration alone. This appears to be the situation in the experiments of Zebetakis. For sonic and supersonic jets, the characterisitic time will be determined by the ratio of the mixing layer thickness to the velocity difference across the mixing layer, see Figure 1-5. These parameters can also be estimated (some calculation is required for each individual case but the methods are straightfoward).

A combination of experimental and theoretical investigation as outlined above should help resolve this issue and enable prediction of autoignition limits for steam-hydrogen jets. Some consideration should also be made as to the influence of the atmosphere composition and temperature on the autoignition limits. Experimentally, this could be accomplished by surrounding the jet with an artificial atmosphere composed of air and diluent (nitrogen or steam).

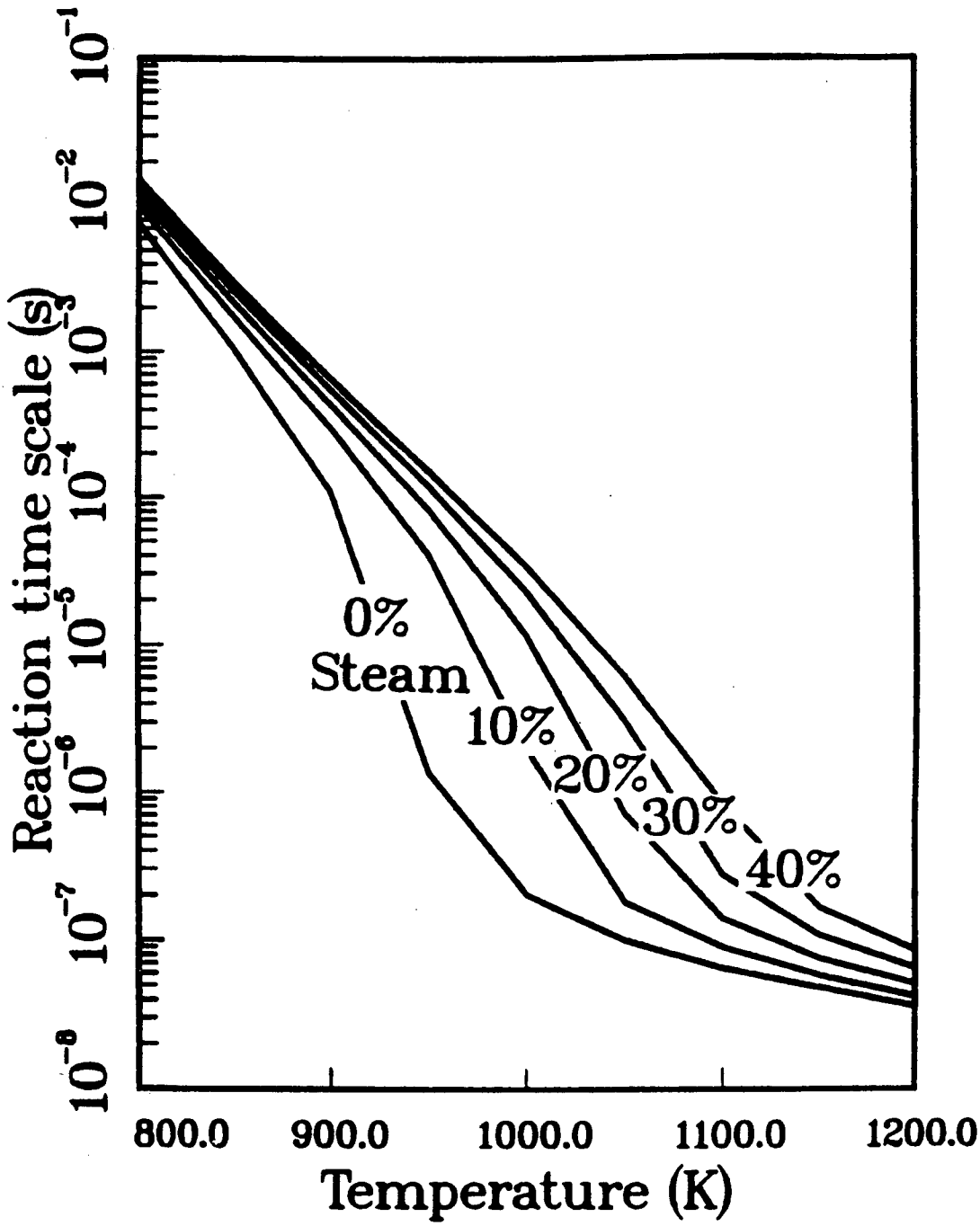

Figure B-1. Characteristic reaction times for stoichiometric hydrogen-air mixtures diluted with steam. Calculation was carried out at constant pressure and the characteristic time was determined by a 10% rise in temperature.

References

1. M. G. Zebetakis, **Research on the Combustion and Explosion Hazards of Hydrogen-Water vapor-Air Mixtures,** AECU Report 3347 (1956).

Distribution:

Division of Technical Information
and Document Control
NRC Distribution Contractor
U.S. Nuclear Regulatory Commission
15700 Crabbs Branch Way
Rockville, MD 20850
275 copies for R3

U. S. Bureau of Mines
Pittsburgh Research Center
P. O. Box 18070
Pittsburgh, PA 15236
Attn: M. Hertzberg

U. S. Nuclear Regulatory Commission (6)
Office of Nuclear Regulatory Research
Washington, DC 20555
Attn: G. A. Arlotto
R. T. Curtis
J. T. Larkins
L. C. Shao
K. G. Steyer
P. Worthington

U. S. Nuclear Regulatory Commission (5)
Office of Nuclear Regulatory Research
Washington, DC 20555
Attn: B. S. Burson
M. Silberberg
J. L. Telford
T. J. Walker
R. W. Wright

U. S. Nuclear Regulatory Commission (6)
Office of Nuclear Reactor Regulation
Washington, DC 20555
Attn: J. K. Long
J. F. Meyer
R. Palla
K. I. Parczewski
G. Quittschreiber
D. D. Yue

U. S. Nuclear Regulatory Commission (6)
Office of Nuclear Reactor Regulation
Washington, DC 20555
Attn: V. Benaroya
W. R. Butler
G. W. Knighton
T. M. Su
Z. Rosztoczy
C. G. Tinkler

U. S. Department of Energy
Operational Safety Division
Albuquerque Operations Office
P.O. Box 5400
Albuquerque, NM 87185
Attn: J. R. Roeder, Director
Dr. M. Peehs

Acurex Corporation
485 Clyde Avenue
Mountain View, CA 94042

Applied Sciences Association, Inc.
P. O. Box 2687
Palos Verdes Pen., CA 90274
Attn: D. Swanson

Argonne National Laboratory
9700 South Cass Avenue
Argonne, IL 60439
Attn: H. M. Chung

Astron
2028 Old Middlefield Way
Mountainview, CA 94043
Attn: Ray Torok

Battelle Columbus Laboratory
505 King Avenue
Columbus, OH 43201
Attn: P. Cybulskis (2)
R. Denning

Bechtel Power Corporation
P. O. Box 3965
San Francisco, CA 94119
Attn: R. Tosetti

Bechtel Power Corporation
15740 Shady Grove Road
Gaithersburg, MD 20877
Attn: D. Ashton

Brookhaven National Laboratory
Upton, NY 11973
Attn: R. A. Bari (2)
T. Pratt

Duke Power Co.
P. O. Box 33189
Charlotte, NC 28242
Attn: F. G. Hudson (2)
A. L. Sudduth

EG&G Idaho
Willow Creek Building, W-3
P. O. Box 1625
Idaho Falls, ID 83415
Attn: Server Sadik

Electric Power Research Institute
3412 Hillview Avenue
Palo Alto, CA 94303
Attn: J. J. Haugh (3)
K. A. Nilsson
G. Thomas

Factory Mutual Research Corporation
P. O. Box 688
Norwood, MA 02062
Attn: R. Zalosh

Fauske & Associates
627 Executive Drive
Willowbrook, IL 60521
Attn: R. Henry

General Electric Co.
175 Curtner Avenue
Mail Code N 1C157
San Jose, CA 95125
Attn: K. W. Holtzclaw

General Physics Corporation
1000 Century Plaza
Columbia, MD 21044
Attn: Chester Kupiec

Los Alamos National Laboratory
P. O. Box 1663
Los Alamos, NM 87545
Attn: H. S. Cullingford (4)
R. Gido
G. Schott
J. Travis

University of Michigan
Department of Aerospace Engineering
Ann Arbor, MI 47109
Attn: Martin Sichel

Mississippi Power & Light
P. O. Box 1640
Jackson, MS 39205
Attn: S. H. Hobbs

Northwestern University
Chemical Engineering Department
Evanston, IL 60201
Attn: S. G. Bankoff

NUS Corporation
4 Research Place
Rockville, MD 20850
Attn: R. Sherry

Offshore Power System (2)
8000 Arlington Expressway
Box 8000
Jacksonville, FL 32211
Attn: G. M. Fuls
D. H. Walker

Power Authority State of NY
10 Columbus Circle
New York, NY 10019
Attn: R. E. Deem (2)
S. S. Iyer

Purdue University
School of Nuclear Engineering
West Lafayette, IN 47907
Attn: T. G. Theofanous

Sandia National Laboratories
Directorate 6400
P. O. Box 5800
Albuquerque, NM 87185
Attn: R. Cochrell (20)

Sandia National Laboratories
Organization 6427
P. O. Box 5800
Albuquerque, NM 87185
Attn: G. Shaw (20)

Dr. Roger Strehlow
505 South Pine Street
Champaign, IL 61820

TVA
400 Commerce
W9C157-CD
Knoxville, TN 37902
Attn: Wang Lau

Thompson Associates
639 Massachusetts Avenue
Third Floor
Cambridge, MA 02139
Attn: Timothy Woolf

UCLA
Nuclear Energy Laboratory
405 Hilgard Avenue
Los Angeles, CA 90024
Attn: I. Catton

Westinghouse Corporation
P. O. Box 355
Pittsburgh, PA 15230
Attn: N. Liparulo (3)
J. Olhoeft
V. Srinivas

Westinghouse Hanford Company
P. O. Box 1970
Richland, WA 99352
Attn: G. R. Bloom (3)
L. Muhlstein
R. D. Peak

University of Wisconsin
Nuclear Engineering Department
1500 Johnson Drive
Madison, WI 53706
Attn: M. L. Corradini

Australian Atomic Energy Commission
Private Mail Bag
Sutherland, NSW 2232
AUSTRALIA
Attn: John W. Connolly

Director of Research, Science & Education
CEC
Rue De La Loi 200
1049 Brussels
BELGIUM
Attn: B. Tolley

AEC, Ltd.
Whiteshell Nuclear Research Establishment
Pinawa, Manitoba, CANADA
Attn: D. Liu (2)
H. Tamm

McGill University
315 Querbes
Outremont, Quebec
CANADA H2V 3W1
Attn: John H. S. Lee (3)

CNEN NUCLIT
Rome, ITALY
Attn: A. Morici

Battelle Institut E. V.
Am Roemerhof 35
6000 Frankfurt am Main 90
FEDERAL REPUBLIC OF GERMANY
Attn: Dr. Werner Baukal

Gesellschaft fur Reakforsicherheit (GRS)
Postfach 101650
Glockengasse 2
5000 Koeln 1
FEDERAL REPUBLIC OF GERMANY
Attn: Dr. M. V. Banaschik

Gesellschaft fur Reaktorsickerheit (GRS mbH)
8046 Garching
FEDERAL REPUBLIC OF GERMANY
Attn: E. F. Hicken (2)
H. L. Jahn

Institute fur Kernenergetik
und Energiesysteme
University of Stuttgart
Stuttgart
FEDERAL REPUBLIC OF GERMANY
Attn: G. Froehlich (2)
M. Buerger

Kernforschungszentrum Karlsruhe
Postfach 3640
75 Karlsruhe
FEDERAL REPUBLIC OF GERMANY
Attn: Dr. S. Hagen (3)
Dr. J. P. Hosemann
Dr. M. Reimann

Kraftwerk Union
Hammerbacherstrasse 12 & 14
Postfach 3220
D-8520 Erlangen 2
FEDERAL REPUBLIC OF GERMANY
Attn: Dr. K. Hassman (2)

Technische Universitaet Muenchen
D-8046 Garching
FEDERAL REPUBLIC OF GERMANY
Attn: Dr. H. Karwat

Swedish State Power Board
El-Och Vaermeteknik
SWEDEN
Attn: Eric Ahlstroem

AERE Harwell
Didcot
Oxfordshire OX11 ORA
UNITED KINGDOM
Attn: J. Gittus, AETB (2)
J. R. Matthews, TPD

Berkeley Nuclear Laboratory
Berkeley GL 139PB
Gloucestershire
UNITED KINGDOM
Attn: J. E. Antill

British Nuclear Fuels, Ltd.
Building 396
Springfield Works
Salwick, Preston
Lancs
UNITED KINGDOM
Attn: W. G. Cunliffe

National Nuclear Corp. Ltd.
Cambridge Road
Whetestone, Leicester, LE83LH
UNITED KINGDOM
Attn: R. May

Simon Engineering Laboratory
University of Manchester
M139PL,
UNITED KINGDOM
Attn: Prof. W. B. Hall

UKAEA Safety & Reliability Directorate
Wigshaw Lane, Culcheth
Warrington WA34NE
Cheshire
UNITED KINGDOM
Attn: J. G. Collier (3)
S. F. Hall
A. J. Wickett

Sandia Internal:

1131 W. B. Benedick
1131 J. Fisk
1510 J. W. Nunziato
1512 J. C. Cummings
1512 J. E. Shepherd (5)
1513 S. N. Kempka
1513 A. C. Ratzel
1520 D. J. McCloskey
1530 L. W. Davison
1540 W. C. Luth
2513 O. B. Crump, Jr
2513 J. E. Kennedy
6400 A. W. Snyder
6410 J. W. Hickman
6411 V. L. Behr
6411 S. E. Dingman
6411 F. E. Haskin
6412 A. L. Camp
6420 J. V. Walker
6421 J. B. Rivard
6422 D. A. Powers
6423 K. Muramatsu
6425 W. J. Camp
6425 W. Frid
6425 K. Schoenefeld
6425 S. Unwin
6427 M. Berman
6427 K. P. Guay
6427 J. T. Hitchcock
6427 J. Kotas
6427 M. S. Krein
6427 B. W. Marshall, Jr.
6427 L. S. Nelson
6427 O. Seebold
6427 M. P. Sherman
6427 S. R. Tieszen
6427 G. Valdez
6427 M. J. Wester
6427 C. C. Wong
6440 D. A. Dahlgren

6442 W. A. von Riesemann
6445 E. H. Richards
6449 K. D. Bergeron
8424 M. A. Pound
8513 W. J. McClean
8523 P. M. Barr
8523 K. D. Marx
8523 B. R. Sanders
3141 C. M. Ostrander (5)
3151 W. L. Garner

NRC FORM 335 (2-84) NRCM 1102, 3201, 3202

U.S. NUCLEAR REGULATORY COMMISSION

BIBLIOGRAPHIC DATA SHEET

SEE INSTRUCTIONS ON THE REVERSE.

1 REPORT NUMBER (Assigned by TIDC, add Vol No., if any)

NUREG/CR-3638
SAND84-0060
R-3

2. TITLE AND SUBTITLE

HYDROGEN-STEAM JET-FLAME FACILITY AND EXPERIMENTS

3. LEAVE BLANK

4. DATE REPORT COMPLETED

MONTH	YEAR
OCTOBER	1984

5. AUTHOR(S)

JOSEPH E. SHEPHERD

6 DATE REPORT ISSUED

MONTH	YEAR
MAY	1985

7. PERFORMING ORGANIZATION NAME AND MAILING ADDRESS (Include Zip Code)

Fluid Mechanics and Heat Transfer
Division 1512
Sandia National Laboratories
Albuquerque, NM 87185

8. PROJECT/TASK/WORK UNIT NUMBER

9. FIN OR GRANT NUMBER

A1246, A1336

10. SPONSORING ORGANIZATION NAME AND MAILING ADDRESS (Include Zip Code)

Office of Nuclear Regulatory Research
U. S. Nuclear Regulatory Commission
Washington, DC 20555

11a. TYPE OF REPORT

FINAL REPORT

b. PERIOD COVERED (Inclusive dates)

12 SUPPLEMENTARY NOTES

13. ABSTRACT (200 words or less)

As part of NRC-sponsored research on light-water reactor safety, the high-temperature combustion of steam-hydrogen jets in an air atmosphere is being investigated at Sandia. This research is oriented at understanding the generic issues involved in accident-generated jets and the specific problems of using deliberate flaring from high-point vents to eliminate hydrogen from the primary system. In this report we give some background on diffusion-flame combustion, describe the experimental facility constructed at Sandia to study high-temperature, steam-hydrogen jets and discuss our results.

14. DOCUMENT ANALYSIS – a. KEYWORDS/DESCRIPTORS

b. IDENTIFIERS/OPEN-ENDED TERMS

15 AVAILABILITY STATEMENT

UNLIMITED

16. SECURITY CLASSIFICATION

(This page) UNCLASSIFIED

(This report) UNCLASSIFIED

17 NUMBER OF PAGES

117

18 PRICE

*U.S. GOVERNMENT PRINTING OFFICE: 1985-0-576-037/20,025